Optogenetic manipulation of the macaque primary visual cortex

Beshoy Agayby

A thesis submitted for the degree of Doctor of Philosophy

Biosciences Institute, Newcastle University

November 2022

Abstract

Globally, about 100 million people suffer from total or severe vision loss and visual prostheses offer the potential to restore some visual function. One key target for visual prosthesis has been the primary visual cortex (V1). Such prostheses typically use electricity to stimulate V1 neurons to artificially induce patterns of spots called phosphenes. Visual prostheses relying on electrical stimulation, however, face challenges such as low visual resolution, lack of activation selectivity, long-term stability due to gliosis and possible painful side effects like headaches.

Optogenetics enables the stimulation of neurons using light via light-sensitive ion channels called opsins. Optogenetic stimulation of V1 offers an attractive alternative to electrical stimulation because of its ability to selectively target specific neural populations. Examining the effects of optogenetics in animal models such as nonhuman primates (NHPs) is a vital step before its translation and use in human clinical trials. However, optogenetics use in NHPs has been relatively limited with significant knowledge gaps. In this thesis, I aim to address some of those gaps by studying the effects of optogenetically stimulating the macaque V1.

To accomplish this, I first verified the efficacy of V1 optogenetic stimulation and its effect on neural activity recorded by multi-contact laminar probes and characterised the effects of different stimulation parameters. Results showed that light successfully modulated neural activity with the observed effects depending on the light wavelength and stimulation parameters. I followed by examining the effects of stimulation across the different layers of the cortex which revealed very strong modulation of neural activity across the cortical layers as well as stimulation intensity- and frequency-specific effects. Furthermore, I show similarities between V1 responses to optogenetic responses and the well-established visually evoked responses.

Finally, I found that with the appropriate testing paradigm, I could confirm that one animal could indeed perceive a phosphene. Not only this, but my paradigm enabled the inference of some of the phosphene's characteristics.

While my results show the challenges of using optogenetics in the macaque brain, they also show its potential. I report that optogenetics can result in neural activity modulation that is sufficient to generate a phosphene opening the way for future studies developing the use of optogenetics for visual prostheses.

Acknowledgements

I would like to thank many people who helped me during this journey. I would like to first thank my supervisor, Michael, for his support, guidance, and the opportunity to work in such an exciting and novel field. I would like also to thank my co-supervisor, Alex, for his valuable insight and help.

I would like also to thank Marcus for all the help and support both scientific, and personal. He taught me the ways of life in Britain and cinema sweet Sundays. I would like to thank Michael Ortiz for the comradery and partnership in the optogenetic project as well as for advice and feedback. Also, I can't forget the excellent BBQs! I would like to thank Tenri for being a real-life reference manager and humouring all my non-sensical scientific ideas with extensive discussions. I would like also to thank Alwin who helped me with my first steps undertaking electrophysiological recordings and answering all my questions later.

I would like to thank Chris for the great support while I finish my PhD and for providing an opportunity to further explore the use of optogenetics. I would like to thank the rest of Chris' lab members, especially Yuki and Jen, for being helpful and accommodating and for making long recording sessions less arduous.

The last couple of years has been a challenging time on a global and personal level. It would have been a lot harder without all the people who provided support and company so thanks to Matthew, Maria, Maydel, Jen, Rachael, and Theo for keeping my sanity. A special thank you to Janire, or eskerrik asko as they say in your part of the world, for supporting me and tolerating all the extra-long workdays/weeks; I am grateful for having you in my life. Finally, I would like to thank my parents for giving me the opportunity to be on that path and for the remote support while nobody was able to travel.

Table of Contents

List of Figures

List of Tables

List of Abbreviations

1/2P	One/two photon
2AFC	Two-alternative forced-choice
AAV	Adeno-associated virus
ANOVA	Analysis of variance
ArchT	Archaerhodopsin
BIC	Bayesian information criterion
CaMKII	Calmodulin-dependent protein kinase II
BOLD	Blood-oxygen-level-dependent
CBC	Comparative biology centre
ChR2	Channelrhodopsin-2
CRT	Cathode-ray tube
CSD	Current source density
DAPI	4’,6-diamidino-2-phenylindole
DAQ	Data acquisition
DBS	Deep brain stimulation
DPSS	Diode-pumped solid-state
EEG	Electroencephalogram
eYFP	Enhanced yellow fluorescent protein
FEF	Frontal eye fields
FFT	Fast Fourier transform
fMRI	Functional magnetic resonance imaging
FP	Fluorescent protein
GABA	Gamma-Aminobutyric Acid
GC	Granger causality
GCI	Granger causality index
GFP	Green fluorescent protein
HA	Hydroxyapatite
hSyn	Human Synapsin
IT	Inferior temporal
LED	Light emitting diode
LFP	Local field potential
LGN	Lateral geniculate nucleus
MLR	Multiple linear regression
mRF	Minimum receptive field
MRI	Magnetic resonance imaging
MST	Medial superior temporal
MT/V5	Middle temporal area
MUA	Multiunit activity
MUAe	Multiunit activity envelope
MVGC	Multivariate Granger causality
MWEL	Mworks experimental language
NHP	Nonhuman primate
NHS	National Health Service
NI	National Instruments
NSP	Neural signal processing system
PCA	Principle component analysis
PEEK	Polyether ether ketone
PEG	Polyethylene glycol
PFA	Paraformaldehyde
PL	Plexon
PLR	Pupillary light reflex
PSTH	Peristimulus time histogram
RF	Receptive field
RGC	Retinal ganglion cells

RMS	Root mean square	**RGT**	Reverse Granger test
ROI	Region of interest	**SUA**	Single unit activity
RT	Reaction time	**V1**	Primary visual cortex
SC	Superior colliculus	**VAR**	Vector autoregressive model
SEM	Standard error of means	**vGlut2**	Vesicular-glutamate transporter 2

Chapter 1: Introduction & Background

1.1 The need for visual prothesis

Total vision loss or complete blindness affects more than 34 million individuals around the world with an additional 86 million people suffering from severe vision impairment (Bourne et al., 2017, 2021). Those numbers are also increasing for a variety of reasons (Bourne et al., 2021) which makes addressing it of increasing importance. While there are a variety of efforts and medical interventions aimed at reducing the loss of vision, it is important to, in parallel, work on solutions that can restore some form of visual function to those who lost it.

The development of cochlear implants is a great success story showing the potential of neural prostheses in restoring auditory function with thousands of people receiving the implant in the UK alone (Raine, 2013). After decades of efforts, the first cochlear implants were approved in the early 1980s (Raine, 2013) and are nowadays part of a standardised procedure that can be supplied by many healthcare providers such as the National Health Service (NHS). Similar interest has been directed towards visual neural prostheses and an increasing commercial development has been underway for the past 15 years (Shepherd et al., 2013) with some prototypes already being tested in clinical trials with mixed results and poor visual acuity in general.

The Argus II (SecondSight Medical Products, Sylmar, California, USA) and Alpha AMS (Retina Implant AG, Reutlingen, Germany) are examples of visual prostheses prototypes developed for patients who lost visual function due to retinitis pigmentosa (Iuliano et al., 2021; Mills et al., 2017). Both systems made their way to the market after the appropriate clinical trials in 2013 offering patients an improved quality of life with improved environmental navigation as an example (Edwards et al., 2018; Geruschat et al., 2016; Mills et al., 2017). However, the visual acuity of those devices is limited to recognising few shapes and words (Mills et al., 2017).

In addition to prostheses, other more biological approaches are being investigated. For example, gene therapy aims at addressing the pathogenic retinal genetic mutations by replacement or augmentation to avoid or limit vision loss; however, success has been limited and the solution is mainly preventative (Gupta & Huckfeldt, 2017). Another approach is to use stem cells to replace the damaged retinal cells; although it has had some success in animal models, extensive work is still needed to ensure long term function (Santos-Ferreira et al., 2017).

1.2 The visual pathway and targets of prostheses from the retina to the cortex

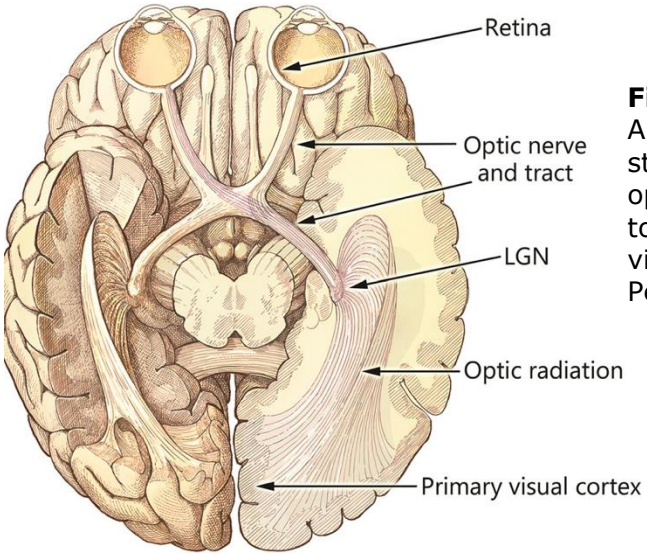

Figure 1.1 Early human visual system. A ventral view of the visual pathway starting from the retina and followed by the optic nerve crossing the optic chiasm towards the LGN and finally the primary visual cortex. Figure from Mirochnik & Pezaris, 2019.

Visual prostheses can be targeted at different parts of the visual pathway from the retina to the cortex. The visual pathway (Figure 1.1) starts with light going through the eye and transformed into neural signals by photosensitive cells, rods and cons, then conveyed by the retinal ganglion cells; those signals are then carried via the optic nerve to the lateral geniculate nucleus (LGN) before being passed on to the primary visual cortex (V1) and then to other areas of the brain for further processing and extraction of visual information (Mirochnik & Pezaris, 2019; Schiller & Tehovnik, 2015). Vision loss can happen due to damage to various parts of

that pathway and therefore visual prostheses have different potential targets.

1.2.1 Retinal prostheses

Some disorders such as retinal pigmentosa cause degradation of the photosensitive cells but leave the retinal ganglion cells (RGCs) intact (Hartong et al., 2006) providing potential for vision restoration by delivering electrical stimulation via microelectrode arrays implanted in the retina (da Cruz et al., 2013; Shepherd et al., 2013). One type of retinal prosthesis is subretinal prostheses; they can act as a replacement of the photosensitive cells and transduce light to electrical signals via photodiodes arrays replacing the damaged rods and cones (Sachs et al., 2005). This type of retinal prosthesis does not require additional hardware and shifting the gaze and locating objects can be done by eye movement like normal vision. Furthermore, no additional image processing is needed, and the retinal network of neurons is used instead; however, it has its downsides such as the limited activation by ambient light. Another type of retinal prostheses is epiretinal prostheses; they rely on direct stimulation of RGCs with stimulation patterns generated according to an external camera system (da Cruz et al., 2013; Zrenner et al., 2011). While an epiretinal prosthesis can overcome the low light constraints of its subretinal counterpart, the user's head must move so that the camera can move for a gaze shift which creates a difficulty in coordination (Ayton et al., 2020). Even though retinal prostheses are the closest to being approved and used clinically, they suffer from low resolution and acuity (Shepherd et al., 2013; Zrenner, 2002). Furthermore, the development of visual prostheses targeting the retina limits the potential market to patients with intact RGCs or optic nerve; that was a major contributing factor for the companies Second Sight and Retina Implant AG to go out of business few years, in 2019, after their first commercial use in 2013 (Mills et al., 2017; Strickl & Harris, 2022). Those companies targeted patients with retinitis pigmentosa since it is one of the most prevalent inherited diseases affecting the retina,

1 in 3500 to 4000 people in the western world (MedlinePlus.gov). However, the complete vision loss resulting from retinitis pigmentosa constitutes only a little above 2%, 2 million people (Sahel et al., 2021) of those affected by total vision loss. This limits the main target group for those retinal prostheses significantly. That group is even more limited considering the willingness of patients to undergo such an invasive procedure. On the other hand, a key factor for the cochlear implant success was the larger number of people who can use it and the relatively less invasive nature of it; that lead to improved surgical techniques and lower costs. The limited number of people suitable for retinal implants increases the cost of the implant making it less commercially viable. Additionally, the visual acuity is limited by the number of stimulation electrodes that can be placed in the retina which is limited due to the nature of electrical stimulation that is explored later.

1.2.2 Optical tract prostheses

Retinal prostheses are suitable for intact RGCs; after photoreceptors death, RGCs would suffer from degeneration with the lack of visual input (Humayun et al., 1999; Palmhof et al., 2019). Additionally, retinal approaches are not appropriate for disorders affecting other parts downstream from photoreceptors such as RGCs loss due to glaucoma (Gupta et al., 2006; Pezaris & Eskandar, 2009). Glaucoma is the cause of almost 50% of vision loss instances (Bourne et al., 2021). Optical tract stimulation targets the next step in the visual pathway instead. Optical tract prostheses use multielectrode array cuff to stimulate the axons on their way to LGN. The current resolution and specificity of the generated patterns are still limited due to a lack of a clear visuotopic mapping of the optical tract (Lu et al., 2013). Unlike retinal prostheses, the electrodes are not restricted to limited 2-D space but can be spaced both horizontally and along the tract allowing potential higher acuity (Veraart et al., 2003); however, the spatial resolution and consistency remain limited for now (Sakaguchi et al., 2009; Veraart et al., 2003).

1.2.3 Lateral geniculate nucleus (LGN) prostheses

Following the optical tract, the subsequent target for a visual prosthesis is LGN. LGN is the thalamic visual relay hub that receives input from the optical tract and forwards it to V1. The retinotopic organisation of LGN has been studied extensively (Jeffries et al., 2014) and electrical stimulation can reliably generate a visual percept at the stimulated neurons' receptive field (Pezaris & Reid, 2007). Furthermore, LGN is divided into well-defined parvocellular and magnocellular layers. Parvocellular cells convey colour information from the retinal cones while magnocellular cells convey luminance information from the retinal rods. Selective stimulation of each type of cells could potentially convey colour information as well (Panetsos et al., 2011; Pezaris & Reid, 2009). Not only this, but the fovea is overrepresented by a larger proportion of LGN neurons potentially enabling higher acuity at the centre of the visual field (Pezaris & Reid, 2009). Despite the many attractive qualities of LGN as a target for visual prostheses, its location presents a surgical challenge; LGN is located about 8cm below the surface of the cortex maki ng placing electrodes a challenge for a wider implementation (Nguyen et al., 2016; Yagi et al., 2005). Furthermore, the compact area and layered nature of LGN allows for limited space for the stimulating electrodes.

1.2.4 Visual cortical prostheses

The primary visual cortex (V1), or the striate cortex, represents the last stage of the main visual pathway before higher cortical areas and a main target for visual prostheses in addition to the retina. In primates, V1 is the main cortical destination for LGN projections with some minor projections to the middle temporal area (MT), or V5 (Sincich et al., 2004). It also represents the first stage of cortical processing and integration of visual signals (Hubel & Wiesel, 1977). The location of V1 makes it a good candidate for prostheses; V1 is located on the surface of the posterior portion of the occipital cortex (macaque example, Figure 2.1) (Gattass et

al., 2005) allowing easier access compared to the much deeper LGN. Like LGN and the retina, V1 is visuotopically organised with an ordered representation of the visual field. That representation is magnified for the fovea with a larger neuronal population dedicated for the central 6-8 degrees (the macaque V1 as an example in Figure 2.1) (Schiller et al., 2011). The foveal magnification coupled with the much larger size and neuronal density of V1 (Barlow, 1981; O'Kusky & Colonnier, 1982) makes it an attractive target for visual prostheses with potentially higher foveal resolution than currently possible with the smaller retina and LGN. Furthermore, compared to RGCs and the optic tract, V1 survives long, even for decades, after signals cease to come from the retina (Dobelle, 2000).

In addition to its importance in visual processing, the accessibility of V1 has made it one of the most extensively studied areas of the brain whether to examine its function and/or to elicit phosphenes. A phosphene is an artificially generated sensation of light resulting from nontypical stimulation of the visual system; for example, applying pressure to the closed eye creates mechanical stimulation to the retinal cells creating a sense of light spots. Electrical stimulation of the visual pathway also elicits phosphenes with most of those phosphenes being of white colour and non-specific shape. The white colour of the electrically generated phosphene is likely resulting from an overstimulation resulting in the activation of many neurons with different colour preferences (Towle et al., 2021). Phosphene generation by electrical stimulation of V1 in humans has been reported as early 1929 by Foerster; during surgeries for epilepsy, patients reported static bright spots when V1 was electrically stimulated with the location of the spot changing depending on the stimulation site in the cortex (Bloch et al., 2019; Lewis & Rosenfeld, 2016). In 1950s, Button and Putnam made the first attempts for a visual cortical prosthesis by using 4 stainless steel wires to stimulate a blind patient's V1 (Lewis & Rosenfeld, 2016; Mirochnik & Pezaris, 2019); the patient was able to get a sense of external brightness but nothing more precise. Not long after, Brindley and Lewis demonstrated

the ability to generate patterns via cortical stimulation by using an array of 80 microelectrodes to electrically induce patterns of phosphenes (Brindley, 1971; Brindley & Lewin, 1968). Visual cortical prostheses have been further developed in the following decades with Dobelle testing one of the first complete prostheses in a blind patient with moderate success in identifying some shapes and letters (Dobelle, 2000).

Since then, great strides have been made towards a practical visual cortical prosthesis like current cochlear implants. For example, several research groups are working on devices delivering intracortical microstimulation and powered wirelessly via external coils (Farnum & Pelled, 2020; Fernández & Normann, 2017; Lowery et al., 2017). Such devices have much bigger microelectrode density than those used by Brindley, but they use the same concept of producing patterns of small phosphenes to create shapes akin to pixels on a screen. A recent more interesting study by Beauchamp and colleagues (2020) have used dynamic stimulation to create shapes and patterns recognised 3 times faster than achieved earlier by Dobelle. Dynamic stimulation uses current steering between pairs of electrodes to create a virtual stimulation electrode the location of which can be precisely controlled. Traditional cortical stimulation methods would generate multiple phosphenes simultaneously to create a particular shape; however, those phosphenes can merge hindering accurate shape generation. However, by using dynamic stimulation and controlling the virtual stimulation site, phosphene sites are not limited by the resolution achieved by electrode spacing (Beauchamp et al., 2020).

Table 1.1 Summary of prostheses targets. The table shows a summary of the diseases that can be addressed by each prostheses targets (information adapted from Mirochnik & Pezaris, 2019) as well as the ease of access to place stimulating electrodes.

Prostheses targets	Examples of addressable diseases	Surgical Accessibility
Retina	Age-related macular degeneration (AMD), Cone Rod Dystrophy (CRD), Retinitis pigmentosa (RP), Outer	High

	Retinal Degeneration (oRD), Inherited Retinal Dystrophy (RD), Choroidermia	
Optical tract	Glaucoma, AMD, CRD, RP, oRD, RD, Choroidermia	Low
LGN	Glaucoma, AMD, CRD, RP, oRD, RD, Choroidermia	Low
Cortex (v1)	Glaucoma, AMD, CRD, RP, oRD, RD, Choroidermia	High

1.2.5 Phosphene generation in primates

Since the early 2000s, visual prostheses have advanced rapidly and a key reason is the use of nonhuman primates (NHPs), such as macaques, as an animal model. Recently, that progress allowed Chen et al. to stimulate the macaque V1 via dense electrode arrays, 1024 channels, to generate moving phosphene patterns (2020). Prior to their experiments, Brindley and Lewis did use an animal model, a baboon, but only to test the biocompatibility of the microelectrode array. However, there were no established animal models to examine the efficacy of the stimulation patterns. The macaque V1 is a prime candidate for studying and developing visual cortical prosthesis; it is mostly lissencephalic meaning it is smooth and almost lacks any sulci or gyri (Figure 2.1). Like humans, foveal magnification is also present in the macaque V1, and the large smooth surface represents the foveal 5°-6°. A barrier to the use of animal models to develop visual prostheses is the lack of reporting what artificial precepts, if any, are reported compared to humans who can verbally describe the phosphenes in detail. Initially, it has been reported that microstimulation of the macaque V1 can affect the detection of visual stimuli (Tehovnik et al., 2002) and delays visually evoked saccadic responses (Tehovnik et al., 2004). V1 microstimulation was later found to elicit saccadic eye movements to the receptive fields of the stimulated neurons (Tehovnik, Slocum, & Carvey, 2003) and that the animals can reliably report when electrical microstimulation was delivered to V1 (Bradley et al., 2004; Murphey & Maunsell, 2007; Tehovnik, Slocum, & Schiller, 2003). However,

it was not clear whether the generated saccades were in response to a phosphene or if it was due to the recruitment of V1 projections to the superior colliculus (SC) which is involved in the oculomotor responses and saccade execution (Schiller & Tehovnik, 2015). In the primate brain, SC is connected to several brainstem regions that have projections to the ocular muscles controlling vertical and horizontal movements (Sparks & Mays, 1990). This uncertainty was addressed by introducing a gap between when visual or microstimulated takes place and the animal response (Bradley et al., 2004; Tehovnik et al., 2005, 2009); saccades were found not to start at the onset of stimulation but rather they depended on the task requirements indicating that they were not caused by activation of oculomotor circuitry. Later experiments have managed to identify the size and colour of the generated phosphenes (Schiller et al., 2011). Those advancements have paved the way to establish macaques as a useful animal model to advance and test visual prostheses before their use in humans. Since the first phosphene generation via microstimulation of the macaque V1, artificially generated phosphene have also been found via LGN stimulation (Pezaris & Reid, 2007) and retinal stimulation (Matsuo et al., 2018; Prévot et al., 2020). However, V1 remains the main target of visual prostheses development in NHPs.

1.3 Electrical stimulation of V1 and its limitations

Neural prostheses need to communicate with the brain. That communication includes either "reading" or "writing" neural activity or a combination of both. Reading would be required to control an external device while the writing would be required to receive feedback or sensory information. In systems neuroscience in general, there have been great strides in the reading part with most neural prostheses utilising electrophysiology as a reflection of neural activity. Writing or manipulating neural activity has been the more challenging process, however, and remains imprecise.

As described earlier, electrical microstimulation has been long used in V1 to generate phosphenes (Tehovnik et al., 2009), in particular, and in neuroscience, in general (Verkhratsky et al., 2006). The initial attempts of generating phosphenes by Brindley and Lewin (Brindley, 1971; Brindley & Lewin, 1968) and Dobelle and Mladejovsky (Dobelle et al., 1974; Dobelle & Mladejovsky, 1974) used surface electrodes placed below the dura but above the pia. That placement required higher currents, milliampere range, to activate the neural tissue below since the amount of current required to activate neurons is proportional to the square distance to the stimulating electrode (Tehovnik, 1996). The use of higher currents resulted in poor spatial resolution since larger portions of the visual field were stimulated simultaneously; phosphenes could be distinguished only at sites >2.4mm apart (Brindley & Lewin, 1968) which could correspond to 1° in the foveal visual field resulting in low visual acuity (Duncan & Boynton, 2003; Qiu et al., 2006). Additionally, using high currents caused pain in some cases possibly from stimulating the passing by nerve fibres (Rushton & Brindley, 1977). Later work by Schmidt et al. (1996) resolved some of those issues by using intracortical microstimulation via electrodes penetrating V1. Schmidt et al. were able to generate precepts with much lower currents (2-25μA) and therefore about 5 times better resolution (~0.5 compared to 2.4mm) with the absence of pain compared to surface stimulation. Phosphene generation in NHPs has also found comparable low current thresholds for intracortical stimulation with the lowest thresholds (~2μA) at deeper layers (Figure 1.2, Tehovnik & Slocum, 2009).

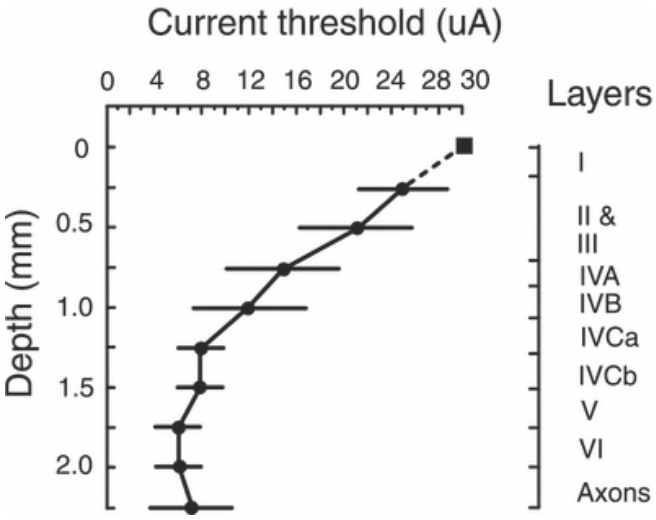

Figure 1.2 Intracortical microstimulation current thresholds as a function of depth. Current thresholds resulting in a detection rate > 50% of the trials as a function of cortical depth from the surface of the cortex. Lower currents were required for deeper sites. Figure from Tehovnik & Slocum, 2009.

Stimulation currents of 2μA spread for an estimated distance of 50μm in macaque V1 (Tehovnik & Slocum, 2007) allowing potential resolution of 100-200μm per pixel while avoiding interference that could be observed between neighbouring electrodes in earlier phosphene studies (Brindley & Lewin, 1968). Such a resolution could provide enough visual acuity of about 20/30 (Cha et al., 1992; Pio-Lopez et al., 2021). The promising work by Chen et al. (2020) provides promising results, but the resultant resolution, ~400μm (Rousche & Normann, 1992), still falls short of the desired visual acuity. It's worth noting that the spread of the stimulation current is more problematic when stimulating smaller structures such as the retina or LGN thus highlighting the promise of V1 stimulation to restore vision.

While further technical developments are likely to improve the resolution of cortical prostheses, there are still undesirable effects of electrical microstimulation. Long, and even short, term use of microstimulation has been observed to cause headaches (Dobelle & Mladejovsky, 1974; Niketeghad et al., 2020) or even seizures (Viventi et al. 2012). Microstimulation affects the tissue surrounding the electrode tip indiscriminately potentially affecting the meningeal nerve and causing pain and headaches in the case of surface stimulation (Pio-Lopez et al., 2021). Furthermore, the lack of microstimulation selectivity can recruit various

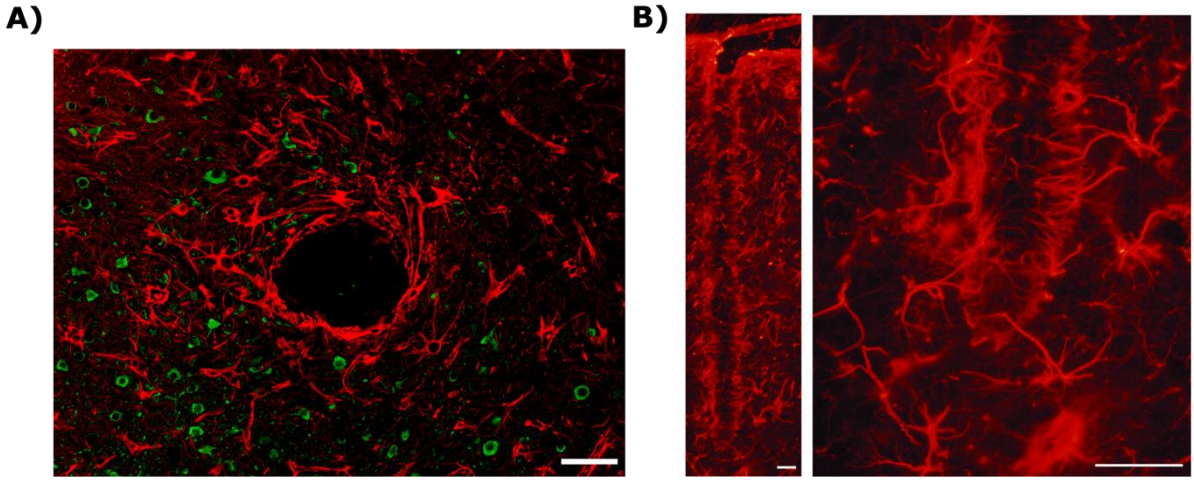

Figure 1.3 Glial encapsulation of microelectrodes. A. Example of glial cells (in red, neurons in green) encapsulating the circumference of a penetrating multielectrode probe in the rabbit brain. **B.** Another view of the glial encapsulation along the tract of the probe across the layers of the cortex (left) with a zoomed in view of the tip of the probe (right). Figure from (Marin & Fernández, 2010).

passing by neural tracts producing mixed and unclear results (Histed et al., 2009) which has been observed with deep brain stimulation (DBS) side effects (Alhourani et al., 2015; Hariz et al., 2013). In addition to the side effects, the lack of specificity of electrical stimulation has been found to produce phosphenes with varying appearance, size, and colour (Schmidt et al., 1996; Shepherd et al., 2013).

The long-term effects of implanting electrodes in the brain pose further challenges in the form of gliosis or glial encapsulation. In response to an injury in the brain, caused by an electrode, gliosis takes place with a proliferation of glial cells at the site of the injury forming a scar and forming a layer around any foreign objects (Figure 1.3, Marin & Fernández, 2010). The biocompatibility of implanted electrodes has improved since the attempts of Button and Putnam in the 1950s with the use of flexible silicon arrays (Edell et al., 1992); however, the implantation of probes is still an invasive process that would result in gliosis (Pio-Lopez et al., 2021). Gliosis could result in reduced stability of the implants due to the movement of the electrodes (Liu et al., 2006). Furthermore, electrode encapsulation would reduce the effectiveness of stimulation (McIntyre & Grill, 2002) and higher currents might be needed, possibly resulting in unwanted side effects and/or reduced resolution.

Finally, electrical stimulation complicates simultaneous electrophysiological data acquisition by introducing artefacts. While a variety of methods have been developed to dramatically reduce the impact of such artefacts to a few milliseconds post stimulation onset, such as the SALPA method (Wagenaar & Potter, 2002), it would pose a problem with more complex stimulation patterns with a dense electrode array (Gilja et al., 2011). A read-out of neural activity would be a useful addition for closed-loop solutions for more consistent phosphene generation. For example, a broad range of stimulation current thresholds has been observed to elicit phosphenes in macaques (Tehovnik, Slocum, & Carvey, 2003) depending

on the state of the animal. Monitoring of neural activity could prove useful to adjust the stimulating currents accordingly.

1.4 V1 microcircuit and connectivity

As described earlier, Tehovnik and Slocum (Tehovnik & Slocum, 2009) found different current thresholds to generate phosphenes depending on the depth of the electrode; this is due to the layered organisation and microcircuit of V1. V1 is divided into 6 layers like other sensory cortical areas (Figure 1.4A); unlike other cortical areas, some layers are further subdivided based on the source of neuronal axons from the LGN. Layer 4C is the main recipient of the thalamic input carrying visual signals from the retina. The magnocellular projections terminate in the upper section, or layer 4Cα, while the parvocellular projections terminate in the lower section, or 4Cβ (Lund, 1973).

Visual signals get distributed from layer 4C to the other layers of V1; most neurons project to layers 4A, 4B and 2/3 with less extensive projections to the deeper layers 5 & 6 (Blasdel et al., 1985; Callaway, 1998). Layers 5 & 6 send axons to subcortical areas and feedback to LGN while layers 2-4B project to higher cortical areas (Figure 1.4B) (Salin and Bullier 1995). This

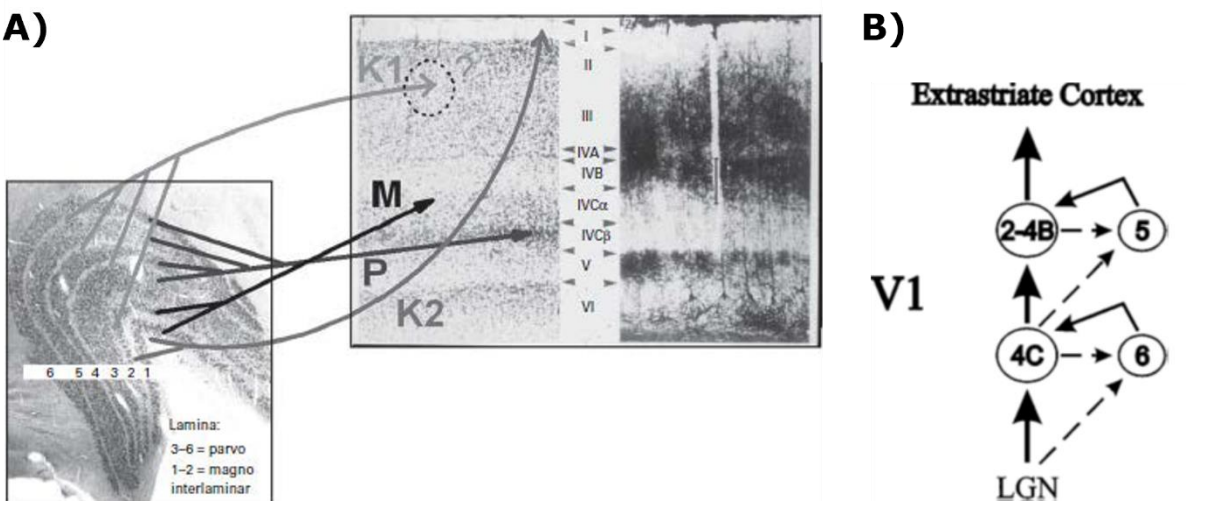

Figure 1.4 Schematic of connectivity between LGN and V1 and within V1. **A.** Arrows shows connectivity between each layer in LGN and V1. Magnocellular and parvocellular layers project to layers 4Cα & 4Cβ respectively while koniocellular projections go to layers 2/3. Figure from Schiller & Tehovnik, 2015 and based on the work by Lund, 1973. B. Schematic of V1 layer connectivity. Figure from Callaway, 1998.

could explain the lower current thresholds found by Tehovnik and Slocum; microstimulation of layer 4C could be amplified by the local circuitry and connections with other layers similar to visually evoked signals coming from LGN. Alternatively, microstimulation could be activating axons projecting from the deeper layers to the superficial output layers (Peters & Sethares, 1991) and to higher cortical areas. V1 also receives extensive feedback connections from the extrastriate cortices such as V2, V3 (Nassi, Lomber, and Born 2013), V4 (Klink et al. 2017) and MT (Salin and Bullier 1995). Those feedback connections mostly terminate in layers 2-4B; they are hypothesized to help visual perception by modulating V1 representation of visual objects by selective spatial attention for example (Desimone & Duncan, 1995).

V1 represents the first stage of cortical processing and feature extraction from incoming thalamic visual signals. As a result, V1 neurons are tuned to specific visual features such as orientation, spatial frequency (Mazer et al., 2002), direction (Gur et al., 2005) and colours (Wachtler et al., 2003). This tuning has important implications on the generation of detailed phosphenes; it is likely that stimulation of a neuron would generate a phosphene with features that neuron is selective for. Indeed, phosphenes generated via V1 microstimulation in macaques were found to have different colours that varied with the site of stimulation (Schiller et al., 2011); this is likely due to the stimulation of neurons with different colour preferences from one site to another. As described earlier, phosphenes are usually identified as bright spots likely resulting from the nonspecific electrical stimulation of a larger number of neurons surrounding the electrode tip (Tehovnik, 1996) encompassing preferences for a variety of features. A more selective stimulation method and strategy would be needed to achieve higher specificity.

1.5 Optogenetics

One method that has been rapidly adopted as an alternative to electrical microstimulation is optogenetics due to its potential to address several of its shortcomings. Optogenetics is a technique that enables the use of light to manipulate the neural activity of specific cell types; this manipulation is achieved by utilising light-sensitive ion channels called opsins. Opsins used in optogenetics are derived from microbial opsins that can be in found several types of fungi and algae (Nagel et al., 2002) helping with orientation towards light (Hegemann, 2008). In animals, G-protein coupled opsins can be found in animals instead of ion channels or pumps; for example, opsins are used by rods and cones in the retina to transduce light into electrical signals conveyed by neurons. By expressing opsins in neurons, they are rendered light-sensitive and can be manipulated with light. While opsins have been described since the early 1970s, they have only been used to manipulate neural activity in the early 2000s when they were successfully expressed in mammalian neurons (Deisseroth, 2015). There are three types of microbial opsins: bacteriorhodopsins, halorhodopsin and channelrhodopsins (Deisseroth, 2015; Zhang et al., 2011). Bacteriorhodopsins are used to inhibit neural activity by transporting positive ions, H^+, outwards causing hyperpolarisation and a decrease in the probability of an action potential. Halorhodopsins also inhibit neural activity by transporting negative ions, chloride (Cl^-), inwards causing hyperpolarisation. Channelrhodopsins (ChRs), on the other hand, increase neural activity by allowing a broad range of positive ions, NA^+, K^+, Ca^+ and K^+, inside the cell causing depolarisation and an increase in the probability of an action potential. Different opsins respond to different light wavelengths; for example, channelrhodopsin-2 (ChR2) responds only to blue light (Nagel et al., 2003) while Chronos responds to red light (Hight et al., 2015). Over the years, new opsins have been engineered to respond to different wavelengths or to be more efficient (Deisseroth, 2011, 2015).

1.5.1 Viral constructs and light delivery

The genetic material to express opsins is usually delivered via a virus such as an adeno-associated virus (AAV) or a lentivirus. Both are routinely used in human gene therapy (Gupta & Huckfeldt, 2017). Most optogenetic studies in NHPs have used AAVs; AAVs can remain in the host cells for years without much damage (Tremblay et al., 2020). AAVs also have different serotypes that can infect different cell types and can differ in their capacity to carry the opsins genetic material (Watakabe et al., 2015). The cell specificity of optogenetics comes predominantly from the promoter used in the viral vector (Zhang et al., 2007). For instance, Ca2+/calmodulin-dependent protein kinase II (CaMKII) is a commonly used promoter (Tremblay et al., 2020) and it helps target excitatory pyramidal neurons (Aravanis et al., 2007; Liu & Jones, 1996). Human Synapsin (hSyn) is another commonly used promoter that results in less restrictive expression than CaMKII (Gerits, et al., 2015). Opsins are the next part of the viral vector and were described earlier. The choice of opsins is based on the desired effect, excitatory vs inhibitory, and the light wavelength to activate it. In theory, two different opsins operating at different wavelengths could be expressed in the same neuron with one of them stimulating it and the other causing inhibition allowing precise control of neural activity (Deisseroth, 2011; Grosenick et al., 2015). For stimulation in NHPs, ChR2 is one of the more commonly used opsins; it is a blue gated ion channel that allows the flow of non-specific cations, mostly NA^+ (Nagel et al., 2003). Its variant, C1V1, has been gaining ground due to its response to more red-shifted light (Tremblay et al., 2020). For inhibition, ArchT, an outwards proton pump, and JAWS, an inwards Cl^- pump, are commonly used (Tremblay et al., 2020); however, excitatory opsins are more common in optogenetic studies. The last part of the viral vector is a reporter which is usually a fluorescence protein (FP) such as green fluorescence protein (GFP). FPs are used to visualise and quantify opsin expression in the targeted cells and the specificity of this expression as well. FP visualisation

can be useful in vivo to get an estimate of viral expression (Chen et al., 2021) or during histological analysis.

Another piece in the optogenetic manipulation toolbox is light delivery. Light can be generated by an external light source such as a light-emitting diode (LED) or laser systems and then delivered to neural tissue of interest (Andrei et al., 2019; Chernov et al., 2018) or locally via implanted micro-LED arrays (Grossman et al., 2010; Rajalingham et al., 2021). The externally generated light is usually delivered to the surface of the tissue (Ju et al., 2018) or coupled to an optical fibre that is carefully inserted in the brain (Pisanello et al., 2017).

Compared to the more traditional neural manipulation methods, optogenetics might include a more complex set of steps and components. However, it offers more tools to control the specificity and spread of modulation. That can be achieved via careful selection of viral vectors, injection sites as well as placement of the light source. The use of optogenetics can also circumvent the adverse effect of penetrating microstimulation electrodes by placing the light sources on the surface of the brain and using longer wavelengths that can travel further through the tissue. Finally, optogenetics results in fewer artefacts in simultaneously recorded signals.

1.5.2 Optogenetics in primates

Since its first use, optogenetics has been quickly and extensively adopted for use in rodents and it has been used to reliably modulate specific neuronal populations and produce behavioural changes (Aravanis et al., 2007; Kim et al., 2017; Kim et al., 2016; Mamad et al., 2019). In primates, however, the number of studies using optogenetics has been low with limited success in causing behavioural effects (Tremblay et al., 2020). Microstimulation, on the other hand, has been used extensively to induce behaviours directly, such as initiating a motor-related action (Jackson et al., 2006), or indirectly by eliciting a sensory percept (Schiller et al., 2011).

Han et al. (2009) are one of the first to successfully optogenetically stimulate the primate brain; they used ChR2 to stimulate the frontal cortex of awake macaques and illustrated the feasibility of the technique without examining any behavioural effects. Later, Diester et al. (2011) tried to elicit behavioural responses, limb movements, by optogenetically stimulating the motor and somatosensory cortices. While the optogenetic stimulation reliably modulated the targeted neurons' activity, the authors failed to observe any behavioural responses that are usually observed when microstimulation is applied. Lu et al. (2015) also did not manage to induce limb movements by optogenetic stimulation of the macaque motor despite clear modulation of neural activity using the ChR2 variant, C1V1. Recently, Watanabe et al. (2020) had more success in evoking forelimb movement by optogenetic stimulation of the motor cortex using ChR2 but with stronger optical stimulation than Diester et al. (2011). May et al. (2014) had more success than Diester and colleagues in creating an artificial tactile sensation by stimulating the somatosensory cortex using C1V1.

A greater number of studies have found success in modifying behavioural responses using optogenetic modulation instead of generating the behaviour or sensory percept. Gerits et al. (2012) found that saccade latencies can be modulated when the arcuate sulcus was optogenetically stimulated. In some of the trials, optogenetic stimulation resulted in shorter saccade latencies but optogenetic stimulation on its own failed to induce saccades. Ohayon et al. (2013) also found that optical stimulation of the frontal eye fields (FEF) failed to evoke a saccade on its own; however, optical stimulation increased the probability of microstimulation to evoke saccades. The electrically induced saccade probability decreased when the authors optically inhibited FEF activity using ArchT opsins. Acker et al. (2016) also found behavioural effects of FEF optogenetic inhibition using JAWS opsins; optogenetic inhibition resulted in a deterioration in the performance of a memory-guided saccade task. Optogenetic inhibition of

face patchers in the macaque inferior temporal (IT) cortex was also found to affect responses in a gender-discrimination task (Afraz et al., 2015).

1.5.3 Optogenetic manipulation of the macaque V1

Optogenetics has been used to manipulate the macaque V1 to elucidate its circuitry as well as explore the generation of phosphenes. Nassi et al. (2015) optogenetically stimulated, using C1V1, V1 to examine normalisation circuits; the authors found that visual and optical stimulation produced sub-additive electrophysiological responses and that their interactions were similar to those observed with multiple visual stimuli. Another study used optogenetic stimulation to examine functional connectivity in V1 via intrinsic optical imaging (Chernov et al., 2018); Chernov et al. found that stimulation of cortical columns resulted in activation of nearby columns with similar ocular dominance or orientation selectivity highlighting the local connectivity of V1. Andrei et al. (2019) used optogenetic stimulation of V1 to examine the integration of neural signals in V1. They found that optically and visually induced signals are pooled when they activate similarly tuned neural populations; that pooling was reflected in the animal's performance in detecting gratings. De et al. (De et al., 2020) found very strong neuronal and behavioural effects on visually evoked responses by stimulating the inhibitory GABAergic neurons in V1; the animals failed to detect visual stimuli in the RF of the indirectly inhibited neurons. Chen et al. (2022) found that optogenetic stimulation of V1 in the presence of visual stimuli produced sub-additive responses similar to what Nassi and colleagues found earlier. In addition, Chen and colleagues found a behavioural masking effect where optogenetic stimulation reduced the detection of visual stimuli.

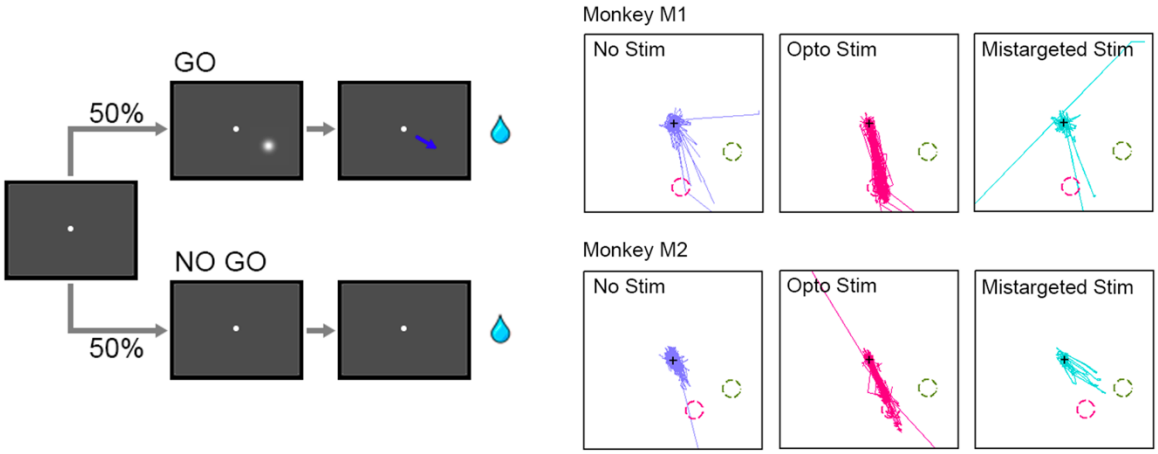

Figure 1.5 Go/No Go task reveals phosphene induction by optogenetic stimulation of V1. In the Go trials, the animals were required to make a saccade to a visual stimulus while in the No Go, the animals were required to maintain fixation. Optical stimulation of V1 neurons expressing opsins resulted in the animals making a saccade to the RF of the stimulated neurons indicating a perception of a phosphene. Mistargeting optical stimulation at neurons not expressing any opsins did not induce a similar effect indicating the absence of phosphenes. Figure from Ju et al., 2018.

Despite the neural and behavioural effects of optogenetic stimulation of the macaque V1, very few studies demonstrated phosphene generation using the new technique. Jazayeri et al. (2012) were the first to show the potential of eliciting artificial sensory precepts via optogenetic stimulation of the macaque V1 using ChR2. The monkeys were trained on a simple central fixation paradigm and received a reward upon maintaining fixation with a subset of the trials, opto trials, including optical stimulation during fixation. The post-fixation spontaneous saccadic endpoints were concentrated around the receptive field of the stimulated neurons for opto trials and were randomly distributed otherwise suggesting phosphene generation. A more recent study by Ju et al. (2018) confirmed the generation of phosphenes by optogenetic stimulation of the macaque V1 using C1V1. The authors used a Go/No GO task where the animals were required to make a saccade to a target or maintain fixation in the absence of any (Figure 1.5). When optical stimulation was applied, the animals made saccades to the RF of the stimulated neurons with a high success rate and few false alarms indicating the generation of a phosphene.

1.5.4 Primate optogenetics challenges

There are various possible reasons that can account for the lack of optogenetics success in eliciting behavioural effects. To begin with, the use of optogenetics in primates is very recent and the effects of different viral vectors are not yet well understood. With the increasing number of optogenetic studies, researchers can learn more about the expression patterns of the different viral vector combinations (Tremblay et al., 2020). Additionally, the effects of stimulation parameters, such as stimulation frequency and intensity, have not been systematically examined. Later studies evoking limb movement used higher intensity compared to the earlier ones that failed to evoke movement with continuous stimulation at a lower intensity. The frequency of stimulation also could be playing a role in better activation. Furthermore, the current optogenetically modulated responses might be too weak to evoke behavioural effects directly; on the other hand, optical stimulation of sensory areas can be more effective as signals in the sensory cortex go through a complex series of processing stages during which the effects can be amplified (Jazayeri et al., 2012; Jazayeri & Remington, 2016).

1.6 Knowledge gaps and project aims

Although there have been an increasing number of studies examining the effects of optogenetic manipulation in the macaque brain, in general, and V1, in particular, there are still gaps to be addressed. To begin with, no studies have examined the effects of optogenetic stimulation on the different layers of the cortex. Such examination would be crucial to identify the spread of activation and examine the relationship between opsin expression patterns and the optogenetically modulated activity. To achieve this, we have used multi-contact laminar probes to examine how the evoked activity across layers. Additionally, no study has systematically examined the effects of varying stimulation parameters on the modulated responses. We examined using a range of stimulation intensities and

frequencies; optimising stimulation parameters could result in more efficient and effective modulation akin to the optimisation of microstimulation parameters. Finally, we examine the possibility of generating phosphenes and the nature of such phosphenes. While previous studies have illustrated the feasibility of optogenetically induced phosphenes, the findings have not been consistent across studies and the perceptual nature of the generated phosphenes remain a mystery. In summary, this project aimed to address the following aims:

- Assess the effects of stimulation parameters (frequency and intensity) on optogenetic modulation.
- Examine the optogenetically evoked laminar activation patterns.
- Examine optogenetic phosphene generation and its characteristics

Chapter 2: General Methods

2.1 Subjects

Four female rhesus macaques (*Macaca mulatta*) were used in this project (Th and Dp: 7 years, weighing 7-9 kg; Fl and Al: 5-6 years, weighing 6-7.5 kg). Monkeys Th and Dp were previously trained for a primate chair and a fixation task prior to the start of the project. Monkeys Al and Fl were acclimatised, and chair trained by the technicians of the animal facility (CBC, Newcastle University) and for a fixation task during the project. All animals were then trained on other visual paradigms such as visual discrimination tasks. While monkeys Dp, Al and Fl were successfully trained for the different behavioural paradigms, monkey Th's training was challenging and not as successful.

2.2 Implants

Each animal was first implanted with a PEEK headpost (Figure 2.1) coated with hydroxyapatite (HA) as described by (Ortiz-Rios et al., 2018). The surgical and postoperative procedures were similar to what is described by Thiele et al (2006). All surgical procedures were approved by the UK Home Office and comply with the Animal Scientific Procedures Act (1986) on the care and use of animals in research, including the European Directive on the protection of animals used in research (2010/63/EU).

After recovery from the surgery, animals were trained to be head-fixed using the headpost implant which enabled accurate eye tracking crucial to the paradigms conducted throughout the experiments. Additionally, head stabilisation improves electrophysiological data acquisition and limits artefacts. Once the animals were successfully trained for head fixation and visual fixation tasks, HA-PEEK chambers were implanted (as described by Ortiz-Rios et al., 2018) to allow acute electrophysiological recordings. The chambers were implanted over the dorsomedial portion of V1 (Figure 2.1) targeting the portion of V1 corresponding to the foveal 5°-7° of the lower

right visual field (Brewer et al., 2002). The chambers are circular with an inner diameter of 17mm and an outer diameter of 22mm and a height of 18.6mm. For animals Th and Dp, the chamber included two screw holes in the sides of the chamber to anchor a grid for electrophysiological recordings. For animals Al and Fl, the chamber wall included an outdent that would guarantee a consistent placement of the grid. All surgeries were conducted by Prof. Michael C. Schmid and Dr Michael Ortiz-Rios with assistance from the lab members.

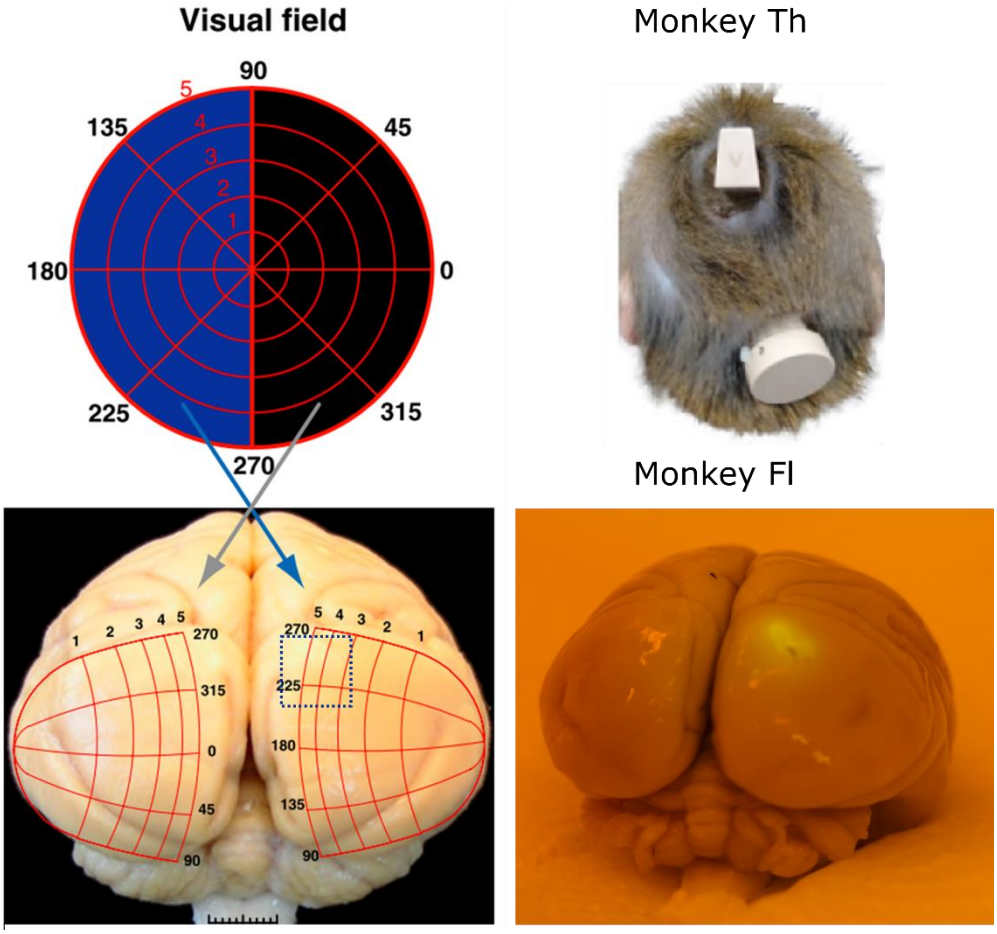

Figure 2.1 Chamber implant location (left) A posterior view of the rhesus macaque V1 with an overlay representing foveal 5° of visual representation. Visual signals from each hemifield are projected to the contralateral hemisphere. The blue square highlights the location of the chamber implants which targeted the foveal 5°-7° of the lower right visual field. Figure from Schiller et al., 2011. (top right) A posterior view of monkey Th head illustrating the headpost and chamber implants after full recovery from the surgery. (bottom right) A posterior view of monkey Fl with the green fluorescence indicating the viral injection location inside the chamber.

2.3 Injections

For optogenetic activation, humanised channelrhodopsin-2 (ChR2) with the H134R mutation was used. To deliver ChR2, adeno-associated virus (AAV) serotypes 5 and 9 were used as the viral vectors in the four animals. Human Synapsin (hSyn) was used as a promoter to target cortical neurons. The use of hSyn was motivated by requiring a non-specific widespread expression. For visualising the expression, the enhanced yellow fluorescent protein (eYFP) was used.

For monkeys Th, Dp and Al, injections were made during the chamber implant surgery. A craniotomy was first performed over the dorsomedial V1 under general anaesthesia. Then, an average volume of 24ul of the viral solution (AAV5/9-hSyn-ChR2-eYFP, UPenn Lot: CS0964 based on Addgene 26973P, titre: 1.03e13 GC/ml) was injected in each animal (see Table 2.1 for details). A Nanofil syringe (World Precision Instruments) with a 34-gauge bevelled needle (World Precision Instruments) was loaded with the viral solution. The syringe was attached to a microinjection system (UMP3-1, SYS-Micro 4; World Precision Instruments). Injections were made at 5 different locations separated by 1-2mm resulting in an estimated area of expression around 12 mm^2. To improve the expression spread across the cortex, injections were made at three depths separated by 500μm at each site; the first injection was made approximately 1500μm followed by another at 1000μm and 500μm below the surface of the dura. At each depth, the injected volume was approximately 1500nl over the course of 6 min (4nl/sec). After moving the needle to each depth, the tissue was allowed to settle for 1-2 minutes to compensate for any movement caused by the needle movement. After the injections were made, we covered the craniotomy with a custom-fit MRI compatible recording chamber (Ortiz-Rios et al., 2018). For monkey Fl, the injections were not made during the chamber implant surgery but a few weeks after to allow fMRI scans of non-transfected tissue. To compensate for any tissue growth above the dura, injections were made deeper in general with an additional deeper fourth

injection for each location; injections started 2.2mm below the tissue surface with a vertical spacing of 500um like the previous animals.

Additional injections were made in monkey Dp after a year of the first injections. We injected approximately 4mm from the first injection site using the same construct but repackaged in serotype AAV5 (AAV5-hSyn-ChR2-eYFP, UPenn Lot: CS1078 based on Addgene 26973P, titre: 3.828e13 GC/ml). Injections were performed in a cross-like pattern at 5 locations approximately 1mm apart from each other.

Table 2.1 Viral injections details. For each animal, the specific viral vector is specified alongside the injected amount. For monkey Dp, the last entry represents the additional injections made after a lack of results from the first set of injections. Viral vectors based on Addgene 26973P.

Animal	Viral Vector	Amount (µl)	Titre (GC/ml)
Dp	AAV9-hSyn-ChR2-eYFP	25	1.03e13
Th	AAV9-hSyn-ChR2-eYFP	25.5	1.03e13
Al	AAV9-hSyn-ChR2-eYFP	22	1.03e13
Fl	AAV9-hSyn-ChR2-eYFP	24.5	1.03e13
Dp	AAV5-hSyn-ChR2-eYFP	28.5	3.828e13

2.4 Electrophysiology acquisition

2.4.1 Electrode Types

To record neural activity with a laminar resolution, we used multi-contact electrode arrays. For monkey Th, we used dual-shaft Atlas electrodes (Atlas Neuroengineering BV, Leuven, Belgium) with each shaft containing 16 channels of either platinum or iridium oxide contacts. Contacts were 30um in diameter with a vertical spacing of 150um. The distance between the two shafts was 360um allowing sampling of two locations simultaneously. The electrodes included a flexible cable that was fixed before insertion into the cortex using polyethylene glycol (PEG). PEG is a biocompatible compound that is used in a variety of medical applications (Yang et al.,

2008). PEG was heated up in a microwave and applied in its liquid state to the probe cable after which it solidifies. After insertion in the brain, the chamber is filled with saline and the PEG dissolves and then it gets cleaned after the experiment. A wire submerged in saline in the chamber was used as a reference and was also connected to the recording system ground.

For monkeys Al, DP and Fl, single-shaft S-probes (Plexon Inc.) with 24 or 32 platinum/iridium contacts were used. Contacts are 15um in diameter with a vertical spacing of 100um allowing for a finer laminar resolution. A bevelled guide tube was used to aid the insertion of the electrode. For the S-probes, the shaft of the probe itself was used as a reference and connected to the recording system ground as well.

2.4.2 Data acquisition (DAQ) system

All data was recorded by the Blackrock Cerebus Neural Processing System (NSP) (Blackrock Microsystems, UT, USA). Signals were first passed, through Cereplex headstages (Blackrock Microsystems, UT, USA) to an analog hub that converted the electrical signals to an optic digital format which was transferred via an optical fibre to the NSP; this method reduced the electrical noise from the environment and kept the recording system electrically isolated from the outside world. The system was unable to record filtered signals, such as local field potentials (LFPs) or multiunit activity (MUA), as well as the raw signal. Therefore, the raw signal was recorded at a high sampling rate, 30kS/s, during experiments and processing of LFP, and MUA was done offline post recordings as described in later chapters.

The NSP also was used to record other analog signals used in the experiment such as the signal used to modulate the laser system or to operate the reward pump. Those signals were used to obtain precise timing information for data analysis. In addition to analog inputs, a 37-pin parallel digital input allowed for the recording of event markers that were sent by the experiment computer.

2.4.3 Acute recordings

The collection of the behavioural and neurophysiological data was done by the author of this thesis; this included the whole experimental procedure from moving the animal to the lab, cleaning the chamber, acute recordings and returning the animal to the colony. Recording and training sessions were conducted in a custom-built recording booth (IAC Acoustics) that was designed to act as a faraday cage; the booth walls included an inner mesh layer that was designed to reduce electromagnetic noise from contaminating the electrophysiological recordings. The inner walls of the booth were painted black to avoid light reflection from the display. The outer layer of the booth was solid metal to block any external visual stimuli from reaching the animal; it also acted to dampen auditory noise from outside the booth. In the front wall of the booth, a transparent window with an inner layer of mesh was installed such that an animal can view the display and still avoid electrical noise from the display. The back of the display was blocked with a solid black metal backplate to avoid any external visual stimuli. Inside the booth, a metal frame was installed to enable attachment of the headpost used to fix the head of the animal. Prior to the start of experiments, the animals were trained to be handled and their head fixated; the animal was brought into the booth in a primate chair followed by attachment of the implanted headpost to a metal rod and then to the metal frame attached to the booth. Once the headpost was attached to the frame, it could be manipulated so that the head of the animals were at a comparable position across sessions/animals. A tube was fixed in front of the animal's mouth to deliver juice rewards for correct trials. Once fixed, the margins of the implant were first cleaned with saline then the chamber is opened. Once opened, the chamber was flushed with an antiseptic and saline. Prior to an experiment, the electrodes were attached to a micromanipulator (Narishige International Limited) that was equipped with a custom adapter for the chamber; the micromanipulator allowed for 2d movement in addition to the vertical manipulation. The electrodes'

impedance was measured using a 1000Hz sinusoid signal (NanoZ, Whitematter LLC, WA, USA); the impedance was used to monitor the health of the electrode. Prior to electrode insertion, a grid was fitted to the chamber and the micromanipulator was adjusted according to a target site on the grid; the grid was then removed before lowering the probes.

The electrodes were lowered with the coarse manipulator till the tip(s) of the electrode touches the surface of the tissue then the fine manipulator was used to lower the electrode in micrometre increments. Since the brain region of interest is located directly beneath the chamber (Figure 2.2A & B), the electrode was lowered until neural activity was first encountered. The electrode depth was adjusted to ensure coverage of all the cortical layers of the foveal V1; this was done by lowering the electrode so that most contacts of the laminar probe are picking up neural activity. Current source density (CSD) analysis of the visually evoked responses showed response patterns and early sink latencies that are expected of V1 (Raiguel et al., 1989; Schroeder et al., 1998; Wójcik, 2014); this was confirmed by the short latencies (~40ms) of the visually evoked MUA as well (more on the laminar analysis in chapter 4). The depth was then further confirmed by mapping the receptive field of the recorded neurons. It is well known that this region of V1 represents the visual field close to the fovea (Figure 2.1A, Schiller & Tehovnik, 2015). Once the desired depth was reached, the chamber was filled with saline to dissolve the PGA if the Atlas probe was used. The brain tissue was usually pushed down with the movement of the electrode, so the tissue was allowed to settle after electrode insertion and the electrode was adjusted in case the tissue moved up.

2.4.4 Event markers calibration

The display used in the experiment was a Viewpixx (Vpixx Technologies, Saint-Bruno, QC, Canada). Viewpixx provided high temporal and spatial precision that is comparable to the traditional CRT displays typically used in visual neuroscience (Ghodrati et al., 2015). In addition to high precision, the Viewpixx offered integration with MATLAB and its settings could be

adjusted via a command prompt on the experiment computer. Furthermore, the display included a digital 24-pin output providing RGB information (8-bit/colour) for the top left pixel of the display. This pixel information was useful to provide precise temporal information about when a stimulus appeared on the screen instead of using a photodiode to detect visual signal change which provided a noisy signal. The Viewpixx monitor is designed so that the RGB values of the pixel are converted to a digital signal that is provided as an output 6 ms before the actual change of the pixel to those values. Prior to experiments, the timing of the pixel change was tested and validated against a photodiode placed on the screen and both were connected to the electrophysiological recording system. In addition to providing precise timing information for the experimental events, the pixel system can be used to provide unique RGB values that can be used to identify the different events during a trial. By assigning specific colour values for the top left pixel of the screen, we could obtain unique RGB values from the 24-pin digital output which were used as unique event codes providing information about the trial type, stimulus type as well as the trial outcome; such information was recorded by the electrophysiological acquisition system allowing robust trial extraction and analyses independent of the computer managing the experiment events. Since 16 bits only can be used with the 37-pin connector in our DAQ, the information from two colours only, 1 byte/ 8 bit each, were used from the pixel information. For each colour, the most significant 5 bits were more reliable with less chance of errors which gave a range of 32 (2^5) unique codes for each colour that can be used.

For each visual stimulus on the screen, a pixel with specific colour codes was queued to appear at the same frame and provided a precise timestamp for that event. The pixel information was updated 6ms prior to the appearance of the frame on the screen. Prior to experiments, the timing of the pixel signal was confirmed to be precise when compared to a photodiode placed on the top left corner of the screen.

In addition to the visual stimuli timing onsets, we needed timing information for optical stimulation which was controlled by a digital signal. The digital output from the NI card was fed into one of the analog inputs in the Blackrock systems in addition to being fed into the laser/led systems. The systems were voltage modulated so additional loads did not have any effect.

2.5 Optical Stimulation

2.5.1 Surface stimulation

Previous optogenetics work in macaques have used lasers as sources of light to manipulate neural activity; however, those studies either delivered light intracortically or via precise optical targeting tools that were not available to us. Due to the difficulty of targeting the recorded neural population with a precise laser beam from the surface, an LED system with a wide-aperture fibre was used instead to provide a wider spread of light to cover the region recorded by the electrode array. This stimulation approach was aimed at replicating the stimulation method used in another study examining the optogenetic effects using functional magnetic resonance imaging (fMRI) (Ortiz-Rios et al., 2021) as well as assessing V1 laminar responses to provide information about the electrophysiological signature of the observed BOLD responses. In addition, surface stimulation was used to explore the potential of surface stimulation to deliver light to different cortical layers in a larger mammalian brain. Surface stimulation, via microLED arrays, has been successfully used with smaller animal models such as rodents but not with NHPs without direct access to the brain (Rajalingham et al., 2021). A blue (451nm) LED (Prizmatix UHP System) was used for stimulating neurons expressing ChR2 opsins while a red (626nm) LED was used as a control. Both LEDs were connected to a 4.5m optical fibre (1.5mm diameter, 0.63 NA, Prizmatix) that produced a 60^0 light beam (Figure 2.2C). Surface stimulation was used during recordings that used the Atlas electrodes. The electrodes were attached to a custom

holder attached to the micromanipulator with an angled fibre holder in such a way that the light would be shining on the tissue surface near the electrodes. Power levels for the blue LED were between 40-62mW and 50mW for the red one. Optical power was measured at the tip of the 4.5m optical fibre using a digital power meter (PM100D, Thorlabs GmbH) and a photodiode power sensor (S121C, Thorlabs GmbH).

Table 2.2 Summary of the stimulation and recording combination used in all animals.. The table summarises the number of sessions where a particular combination of stimulation method (surface vs intracortical) and recording probe (Atlas vs FHC vs Plexon) was used for each animal in addition to the total number of sessions obtained from each animal. In later results, subsets of the sessions were used for different analyses depending on the experimental conditions.

Stimulation method + Probe type	Number of sessions per animal (n)			
	Th	Dp	AL	FL
Surface + Atlas	10	0	0	0
Surface + Plexon	0	35	14	0
Surface + Single electrode (FHC)	0	20	0	0
Intracortical + Plexon	0	20	37	43
Total number of sessions (n)	10	75	51	43

2.5.2 Intracortical stimulation

While surface stimulation modulated neural activity in monkey Th, it did not produce clear results in other monkeys (monkeys Al, Dp & Fl). Therefore, we moved to an intracortical stimulation approach. We used Plexon S-probes (Plexon Inc., Texas, USA) with an embedded fibre (50µm diameter, located between channels 8-9 from the top) (Figure 2.2D) delivering light in the upper third of the electrode. To deliver light, the electrode included a ceramic ferrule that was coupled via a sleeve to a 4m optical fibre (200µm diameter, 0.39 NA, FT200UMT, Thorlabs GmBH). The fibre was connected to either a blue laser (473 nm, LuxX diode laser,

Omicron Lighthub-4) for stimulation or a red (594 nm, DPSS laser, Omicron Lighthub-4) one for control. The power of the blue laser was between 38-52mW and ~42mW for the red one. Optical power was measured at the tip of optical fibre before being coupled to the probe. We were not able to measure the power out of the embedded optical fibre in the probe itself. Table 2.2 represents a summary of the stimulation method(s) and the probe type(s) used for each animal with the number of sessions for each combination. Table 2.3 represents a summary of the observed effects in all animals using different assessment methods; the details will be expanded upon in the following chapters.

All light sources were modulated externally via a TTL signal that would turn the laser on or off. Light was delivered continuously or pulsed via a train of square pulses. For the continuous stimulation, light was delivered for 1 s when using external stimulation and only for 300ms when using intracortical stimulation to avoid potential heating and tissue damage. For pulsed stimulation, the square wave was set at either 5Hz, 10Hz or 40Hz with a 50% duty cycle.

Animal	Electrophysiology	fMRI	Behaviour	Histology
Th	Strong effects	Strong effects	Not tested	Medium expression
Dp	No effects	Strong effects	Possible effects	Weak expression
Al	No effects	Strong effects	Not tested	Weak expression
Fl	Strong effects	N/A	Strong effects	Strong expression

Table 2.3 Summary of optogenetic effects in all animals .
The fMRI effects are from a related study that is not the focus of this report (for details see Ortiz-Rios et al. 2021). The electrophysiological effects are explored in chapters 3 and 4 while the behavioural effects are explored in chapter 5.

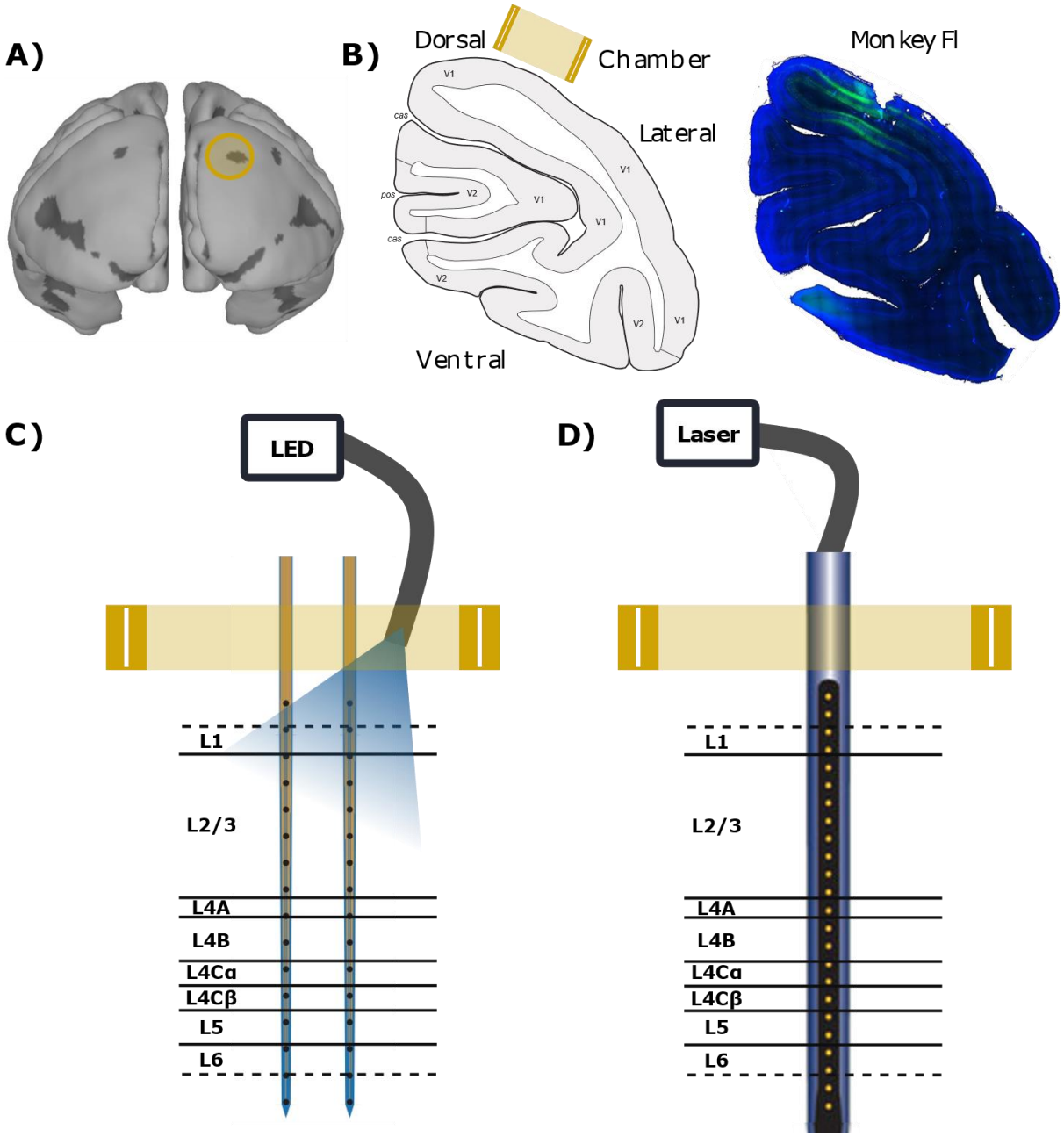

Figure 2.2 Schematic of the recording site and stimulation methods. A. Illustration of the chamber position (yellow) over a brain model. The 3D brain model was built using the anatomical scans of the four monkeys (model provided by Dr Michael Ortiz-Rios). **B.** (left) A coronal slice illustrating the location of V1 (figure from Saleem et al., 2021) below the implanted chamber (yellow) and (right) a corresponding coronal slice from monkey Fl showing viral expression (green) in V1 confirming injection and recording sites in V1. The chamber was tilted so that it was perpendicular to the brain surface. **C.** Surface stimulation schematic showing the dual-shaft Atlas probe recording activity across the cortical layers with light coming from an optical fibre connected to an external LED system. The fibre was positioned so that light falls on the recording site. **D.** Intracortical stimulation schematic showing the Plexon probe with the embedded fibre delivering light within the layers of the cortex. Light was delivered via an optical fibre coupled to the probe from an external laser system.

2.6 Experiment management and behavioural data recording

2.6.1 MWorks

MWorks (https://mworks.github.io/) was used to manage the experiment as well as record behavioural data such as the animal performance and eye-tracking information (such as eye position and pupil diameter). Custom-built scripts in the MWorks Experiment Language (MWEL) were prepared and tested to optimise stimulus presentation and timing. The size and location of visual stimuli as well as eye position were presented as visual degrees in MWorks; therefore, it was first calibrated by entering the dimensions of the monitor and the distance between the monitor and the eye of the animal to convert pixels on the screen to visual degrees. A multifunction DAQ (USB-6212 BNC, National Instruments, Austin, TX) was controlled via MWorks to produce any needed output; one output was a digital output to control (via a relay to reduce electrical noise) a pump that provided a liquid reward for the animal upon completing a correct trial. The amount of the liquid was determined by the length of the pulse sent to the pump. The reward time/liquid amount was adjusted online to ensure the reward was big enough to keep the animal motivated while short enough to allow many trials per session.

Another output was used to modulate the light source (LED or laser) used. The light modulating signal was also fed into our recording system for precise timing information about stimulation onset. Prior to experiments, the production of the square wave was optimised to ensure consistent and precise square waves to reduce jitter between the onset times for the individual pulses in a pulse train.

2.6.2 Eye Tracking

To track the position of the animal's eye, the Eyelink 1000 (SR research) was used; Eyelink is a remote video-based eye-tracker that utilises infrared tracking. The system allowed monocular monitoring with a sampling rate of 1000Hz or binocular monitoring with a sampling rate of 500Hz. For most

of the experiments, monocular eye tracking was used for more precise temporal information about the eye position. The camera and the infrared light were placed in front of the animal below the display monitor such that there is no obstruction of the display. During electrophysiological recordings, the system was powered by a battery to reduce any potential electrical noise (such as line noise). The information from the camera was transferred via an optical fibre to a computer running software from SR

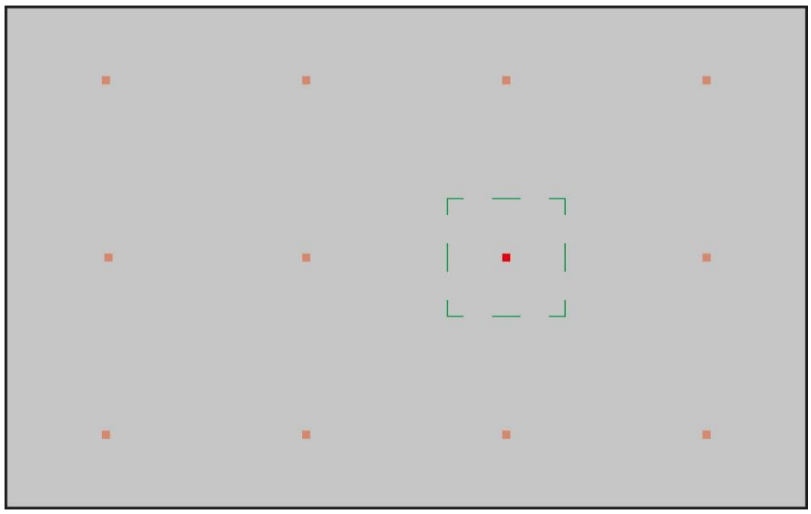

Figure 2.3 Schematic of 12-point calibration task. The calibration task was run at the beginning of each experimental session during which the animal was required to make saccades to a red square appearing randomly at one of 12 points covering the screen. The saccade window was iteratively reduced until the required accuracy was reached (usually 1-2°).

research. The eye-tracking information was then relayed, via an ethernet cable, to the experiment computer running MWorks. At the beginning of each experiment, a calibration task was performed by the animal to calibrate the eye position data from Eyelink to visual degrees which were then used throughout MWorks. In the task, a red square target (0.15^0 diameter) appeared at one of 12 locations on the display (pseudo-random locations at x = -12^0, -4^0, 4^0, 12^0 & y= -8^0, 0^0, 8^0, Figure 2.3) and the animal received a reward by making a saccade towards the target that appears. At the beginning of the calibration, the saccade window around the target was large (around 5^0 for a non-naïve animal) and got iteratively smaller (down to 1^0) until the required level of accuracy was reached.

Chapter 3: Validation and characterisation of ChR2 photostimulation

3.1 Introduction

The opsin used in the experiments described was Channelrhodopsin (ChR2) and it has been one of the earliest identified and developed opsins for use in optogenetics (Lin, 2012; Nagel et al., 2002, 2003). ChR2 has been extensively used in rodents (Aravanis et al., 2007; Grossman et al., 2011; Liske et al., 2013; Ramirez et al., 2012) as well as nonhuman primates (Andrei et al., 2019; Chernov et al., 2018; Han et al., 2009; Klein et al., 2016; Nassi et al., 2015; Tremblay et al., 2020). In addition to the genetic information to express the opsin itself, the viral vectors used in optogenetics are loaded with genetic information to express fluorescent proteins (FPs). There are many examples of FPs used in optogenetics and some of the commonly used ones are the enhanced yellow FP (eYFP) and green FP (GFP)(Tantama et al., 2012). When those proteins absorb a particular wavelength, they emit light at a different wavelength allowing visualisation of the protein expression location; for example, GFP emits green light when it absorbs ultraviolet light (Chudakov et al., 2010; Snapp, 2009). In vivo, some studies utilised 2-photon (2P) imaging to visualise the fluorescence indicating the location of viral expression (Ju et al., 2018) while other studies used the implanted optical fibre not just to deliver light into the brain, but also to collect some of the fluorescence light and measure it via a custom optical setup (Ilker et al., 2013; Mohanty & Lakshminarayananan, 2015). Since this project was not focused on fluorescence detection in vivo, the effects of optogenetic stimulation were measured via the changes in the neural activity itself. FPs make it possible, however, to examine and localise viral expression through immunostaining ex vivo which would be examined in the next chapter.

One approach to examining if neurons are optogenetically modulated is to compare neural activity when light is delivered to the neural population to

the absence of optical stimulation. With optical stimulation at the appropriate wavelength, neurons expressing the opsin should exhibit an increase or decrease, depending on the opsin, in their firing rates. Additionally, the latency of that change can be also used as confirmation since opsins have distinct latency profiles that have been extensively examined in vitro. ChR2 is characterised by a very short latency of activation that ranges between 2-10ms (Lin, 2012). That response time can be a good indication that the recorded neural activity is indeed due to optogenetic stimulation rather than an evoked visual response that does not start before 40ms (Bair et al., 2002; Raiguel et al., 1989) or heating effects that would take place hundreds of milliseconds to seconds after stimulation onset (Horváth et al., 2020; Owen et al., 2019). Furthermore, different opsins are activated by different optical stimulation wavelengths such that the opsin responds optimally to one wavelength with the response falling the further away the optical stimulation wavelength is. Therefore, a wavelength that is far enough from the optimal wavelength should not modulate, or only weakly modulate, the opsin. Most studies that utilised optogenetics in NHPs have examined the effects of optogenetic manipulation on neurons' spiking activity (reflected in 1P/2P calcium imaging and electrophysiological recordings showing single and multiunit activity) (Chernov et al., 2018; Ju et al., 2018; Nassi et al., 2015) or behaviour (Jazayeri et al., 2012).

This chapter aims to validate the optogenetic stimulation of macaque V1 neurons. To achieve this, I first examined whether blue light affects neurons and causes increases in firing rates and whether this modulation was wavelength specific. After this, I examined the latencies of such activation. Then, I examined the effects of stimulation parameters such as stimulation power and frequency on the modulated activity.

3.2 Methods

3.2.1 Multiunit activity (MUA)

Multiunit activity (MUA) was extracted to reflect the spiking activity of the recorded neural populations. Blackrock Offline Spike Sorter (BOSS, Blackrock Microsystems, UT, USA) was used for MUA extraction. MUA was extracted by applying a high pass filter (4th order Butterworth, with a cut-off at 250Hz) to the raw signal (30kS/s). A threshold (2.5-3.5 of the noise RMS for each channel) was applied to the filtered signal and a spike was detected when it crossed the threshold. For each channel, all units were

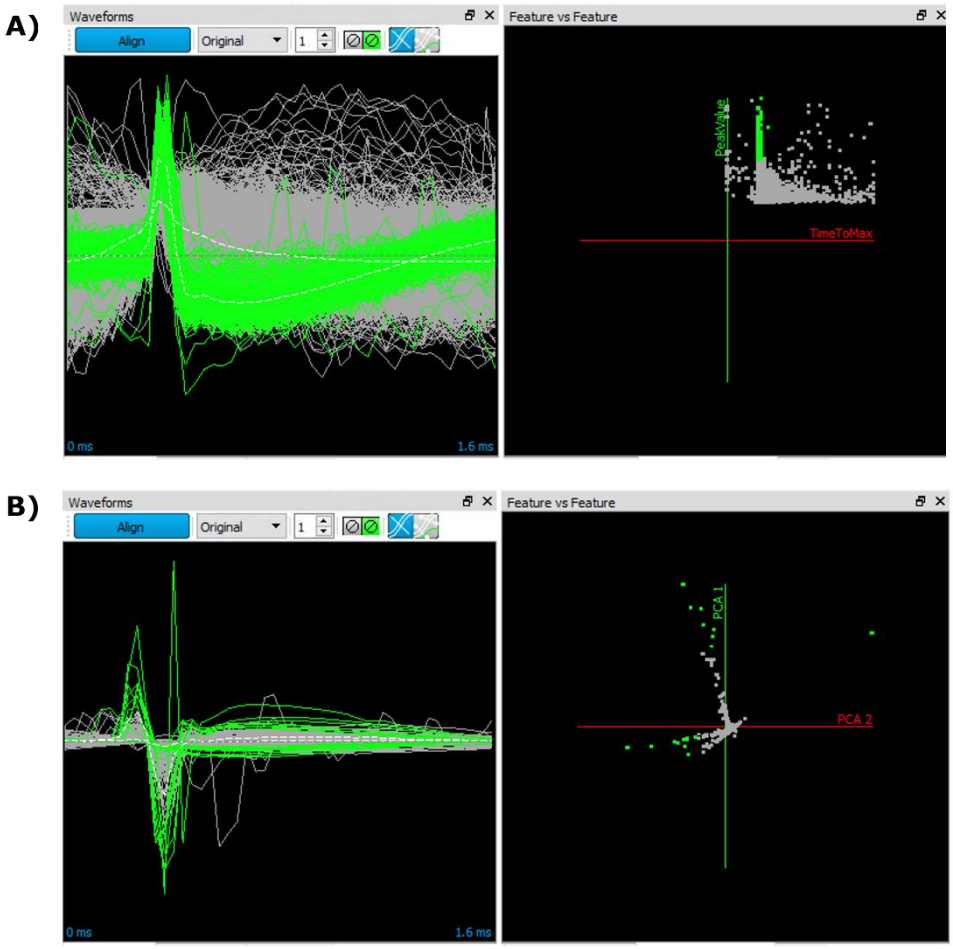

Figure 3.1 Multiunit sorting examples. **A.** An example illustrating manual sorting of the LED onset artifact. (left) The artefact had a distinct waveform (green) with a sharp peak followed by a slow return to baseline. (right) This was reflected in the 2D feature plot with the waveforms having high peak values and faster times to reach this peak value (green dots). **B.** An example illustrating the manual sorting of movement artefact before removing the waveforms. (left) The waveform of such artefacts was irregular with extreme values (green). (right) They were selected by manually selecting the outliers (green dots) in a 2D plot of the first and second components resulting from principal component analysis (PCA).

pooled together into one multiunit per channel. Some examples, such as the LED onset artefacts were manually sorted into different single units for illustration. Sorting LED onset artefacts waveforms was performed manually using a combination of visual inspection of the waveforms and the extracted waveform features such as the peak value of the signal and the time to reach that peak value (Figure 3.1A). Artefacts due to animal movement were sorted manually into units first and then removed. Sorting movement waveforms was performed by visual inspection of the waveforms and selecting irregular waveforms; in addition, the first and second components resulting from principal component analysis (PCA) were used to highlight outliers (Figure 3.1B). PCA was performed using BOSS after the detection of units. MUA extraction and analyses were performed for a limited number of data segments for the purpose of illustrating the LED onset artefacts and the noise introduced from using the red LED as described later in the results section.

In addition, the envelope of the MUA (MUAe) was also extracted and used as the primary signal to represent neural spiking activity. While single unit activity (SUA) has been typically used to investigate the function of specific neurons in the brain, it does not fully represent the activity of a neural population since it would be biased towards larger pyramidal neurons and ignoring smaller spiking activity (Supèr & Roelfsema, 2005). On the other hand, MUA provides a better estimate of the larger population since it represents the sum of multiple SUA including those of smaller neurons. MUAe has been shown to reliably reflect spiking activity and show a close resemblance to both MUA and SUA (Drebitz et al., 2019; Shapcott et al., 2016; Supèr & Roelfsema, 2005). MUAe was used instead of MUA when the signal did not include a lot of noise or movement artefacts. MUAe was extracted by applying a high pass filter (8^{th} Chebyshev, with a cut-off at 150Hz) to the raw signal; the signal is then rectified and downsampled to 500Hz.

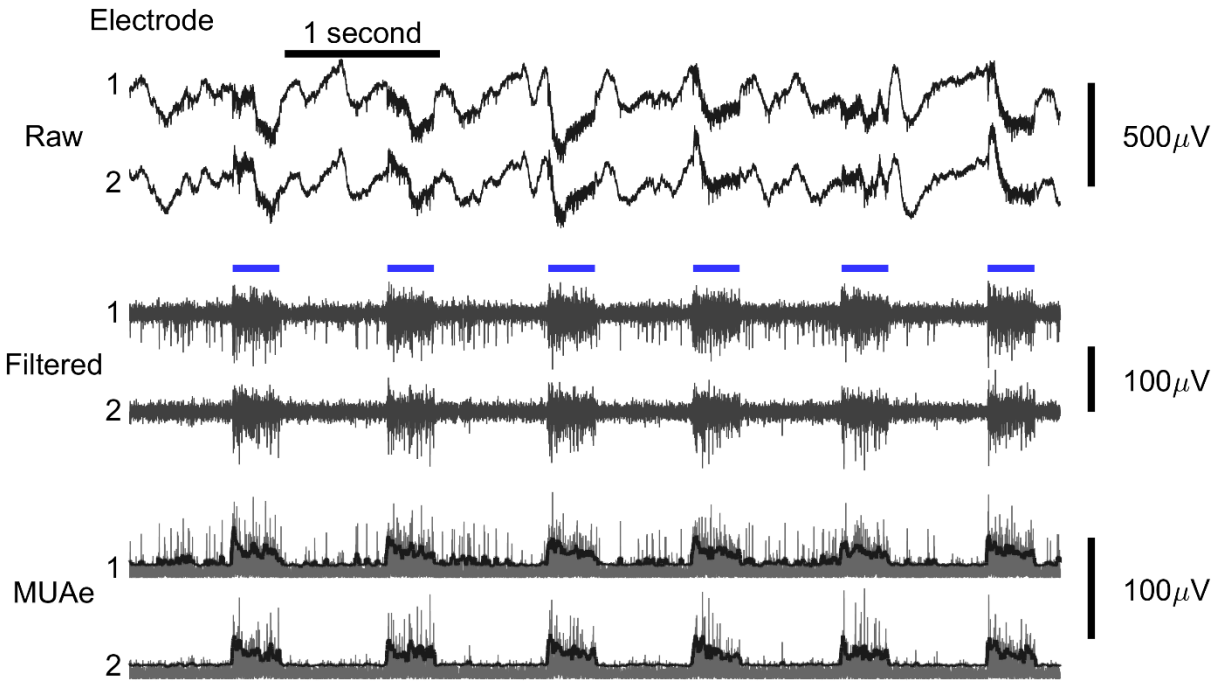

Figure 3.2 Example of MUAe extraction during optogenetic stimulation. Raw signal (top panel, examples from two channels, monkey Fl) is high-pass filtered (>150Hz) to extract the fast signal components representing neural spiking activity (middle panel) and then the signal is rectified and downsampled (grey, bottom panel) to produce MUAe signal that encompasses both the larger neural spikes as well as the smaller spiking activity (black, bottom panel). Blue lines indicate stimulation using blue light.

3.2.2 Local field potential (LFP)

Local field potentials (LFPs) were extracted to reflect the activity of the larger neural population and to capture any oscillatory activity that would be otherwise not obvious in the MUA signal. The LFP signal was processed by simply downsampling the raw signal to 500Hz. The downsampled rate (250Hz Nyquist frequency) allows the analysis of the higher frequencies of the LFP power, up to the high-gamma range (~60-200Hz), which has been found to reflect neural spiking activity (Ray et al., 2008; Ray & Maunsell, 2011). The recording booth was electrically floating and not connected to any outside electrical outlets and the electrode referencing configuration was adjusted prior to experiments to not be susceptible to line noise, validated by frequency spectrum analysis, therefore no filtering was applied to remove line noise from the LFP data.

3.2.3 LED light artefact

It is a well-recorded phenomenon that when light hits a metal surface it can result in a photo-voltaic artefact, also known as the Becquerel effect, due to the generation of currents or voltages on that surface (Kozai & Vazquez, 2015); such a phenomenon has been observed to affect electrophysiological recordings (Cardin, 2011). It would cause deflections in voltage that are more evident in the LFP that contain more low-frequency components. In my recordings, the artefact was observed in the data obtained from monkey Th at the onset of blue light stimulation and for the whole duration of red-light stimulation. Such an artefact can be distinguished as a sharp waveform at the onset of stimulation during MUA extraction; however, it can be isolated and rejected (Figure 3.6C, unit 8). Such an artefact was not observed in other animals which could be attributed to using different electrodes with different recording contacts materials (Ir/Ox in Th and Pt/Ir in Al, Dp & Fl). Therefore, the use of MUA was sometimes necessary for data from Monkey Th.

3.3 Results

3.3.1 Increase in firing rates in response to optical stimulation

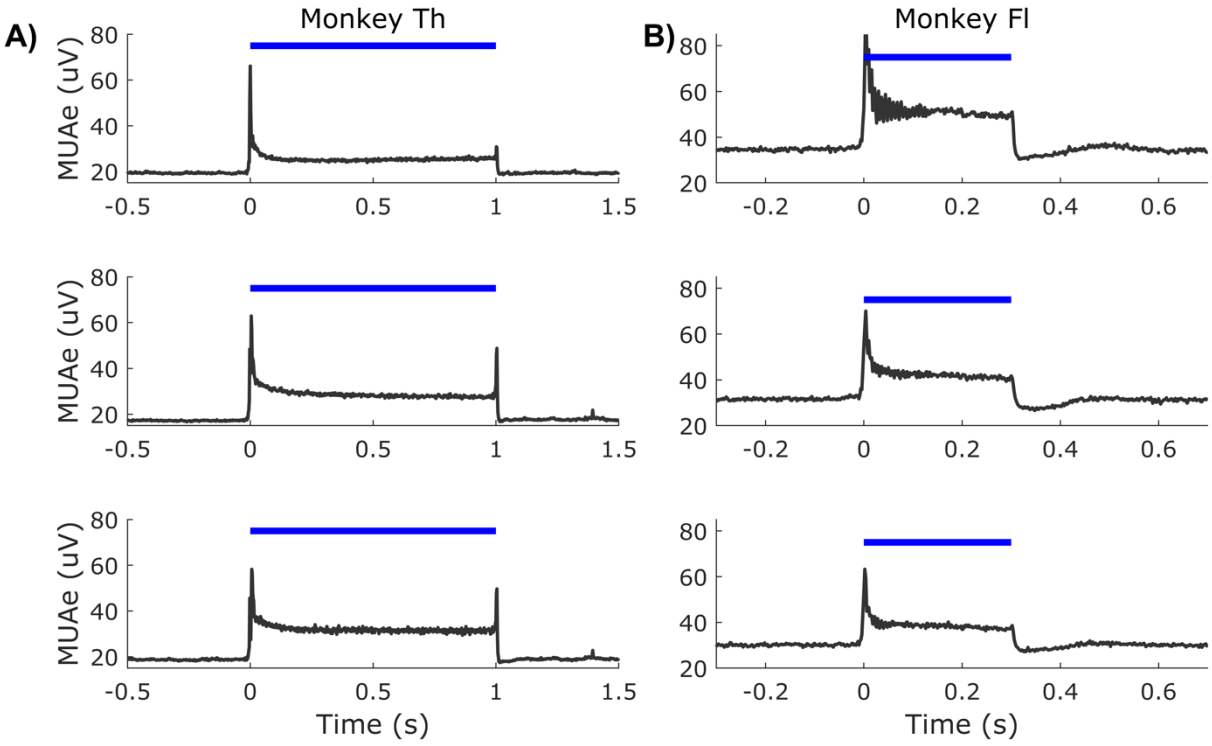

Figure 3.3 Examples of optogenetic modulation from different recording sessions. **A.** MUAe responses (mean in blue and SEM is in black) to 1s pulse of blue light (451nm) in monkey Th. **B.** MUAe responses to 300ms pulse of blue light (473nm) in monkey Fl.

Out of the four animals tested, clear optogenetic manipulation of neural activity was observed in two: Fl and Th (examples Figure 3.3).

The first set of recording sessions was done in monkey Th. For optogenetic stimulation, light was delivered to the surface of the tissue as described in chapter 2. We recorded 134 channels, across 5 sessions, that showed significant MUAe modulation ($p < 0.05$, Wilcoxon signed-rank test) by visual stimuli (full-field white flash) compared to baseline or by optogenetic stimulation (1s pulse, 451nm, 40-62mW, Figure 3.3A). 101 units (75.37%) of them were responsive to both visual and optical stimulation with 15 units (11.19%) responsive to visual stimuli only and 18 units (13.43%) responsive to optogenetic stimulation only. Training of monkey Th proved challenging due to excessive movements that introduced several artefacts

in the recordings as well as reduced the lifetime of electrodes, so we moved on to the other animals.

The second set of successful optogenetic experiments was done in monkey Fl. For optogenetic stimulation, light was delivered intracortically as described in chapter 2. We recorded 987 channels, across 43 sessions that showed significant MUAe modulation ($p < 0.05$, Wilcoxon signed-rank test) by visual stimuli (drifting gratings) or optogenetic stimulation (300ms pulse, 473nm, 38-52mW, Figure 3.3B). 799 channels (80.95%) of them were responsive to both visual and optogenetic stimulation with 49 units (4.96%) responsive to visual stimuli only and 139 units (14.08%) responsive to optogenetic stimulation only. Although not systematically measured, optical stimulation resulted in an increase in firing rates up to 3mm away from an injection location (Figure 3.4).

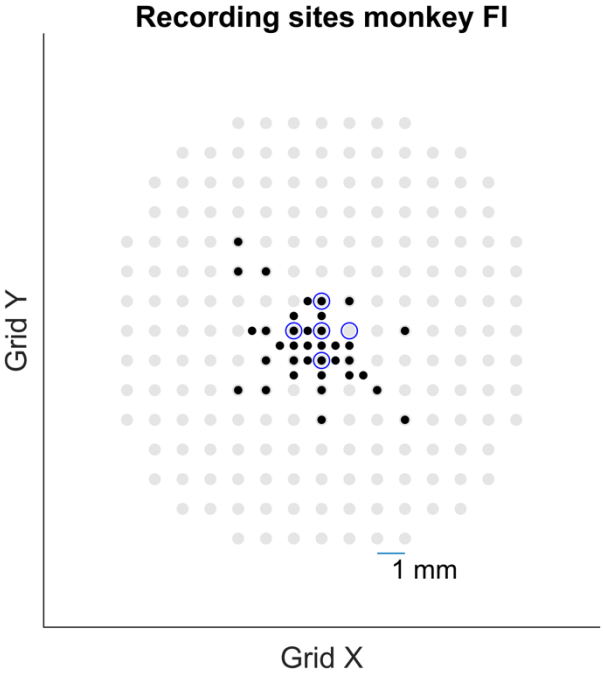

Figure 3.4 Schematic of recording and injection sites in monkey Fl. Injection sites were at the centre of the grid (blue circles) while recording sites sampled the area near the injection sites (black dots). Distance between in grid sites was 1mm.

3.3.2 Latency of modulation confirms ChR2

The latency of the optogenetically modulated MUAe was calculated on a trial-by-trial basis for the significantly modulated channels; the modulation latency (t_0) was defined as the following:

$$t_0 \; where \; x(t_0) \geq \mu_{baseline\ (t<0)} + 1\sigma_{baseline\ (t<0)}$$

Equation 3.1

where the modulation latency (t_0) is the first time point when the signal, $x(t)$, crosses a threshold defined as one standard deviation, $\sigma_{baseline}$, above the baseline, $\mu_{baseline}$ (-500ms to -100ms for monkey Th and -300ms to -100ms for monkey Fl) for that trial. The modulation latency for a channel was calculated as the mean of the latencies across trials. In monkey Th, the mean latency of modulation for the 119 optically modulated channels was 5.76±0.4596ms with the majority (n = 68, 75.13%) of the optogenetically modulated channels having shorter latencies (Figure 3.5A). In monkey Fl, the mean latency of modulation was 3.37±0.155ms with the majority (n = 598, 67.27%) of optically modulated units having shorter latencies (Figure 3.5B). Additionally, the intertrial variability of the

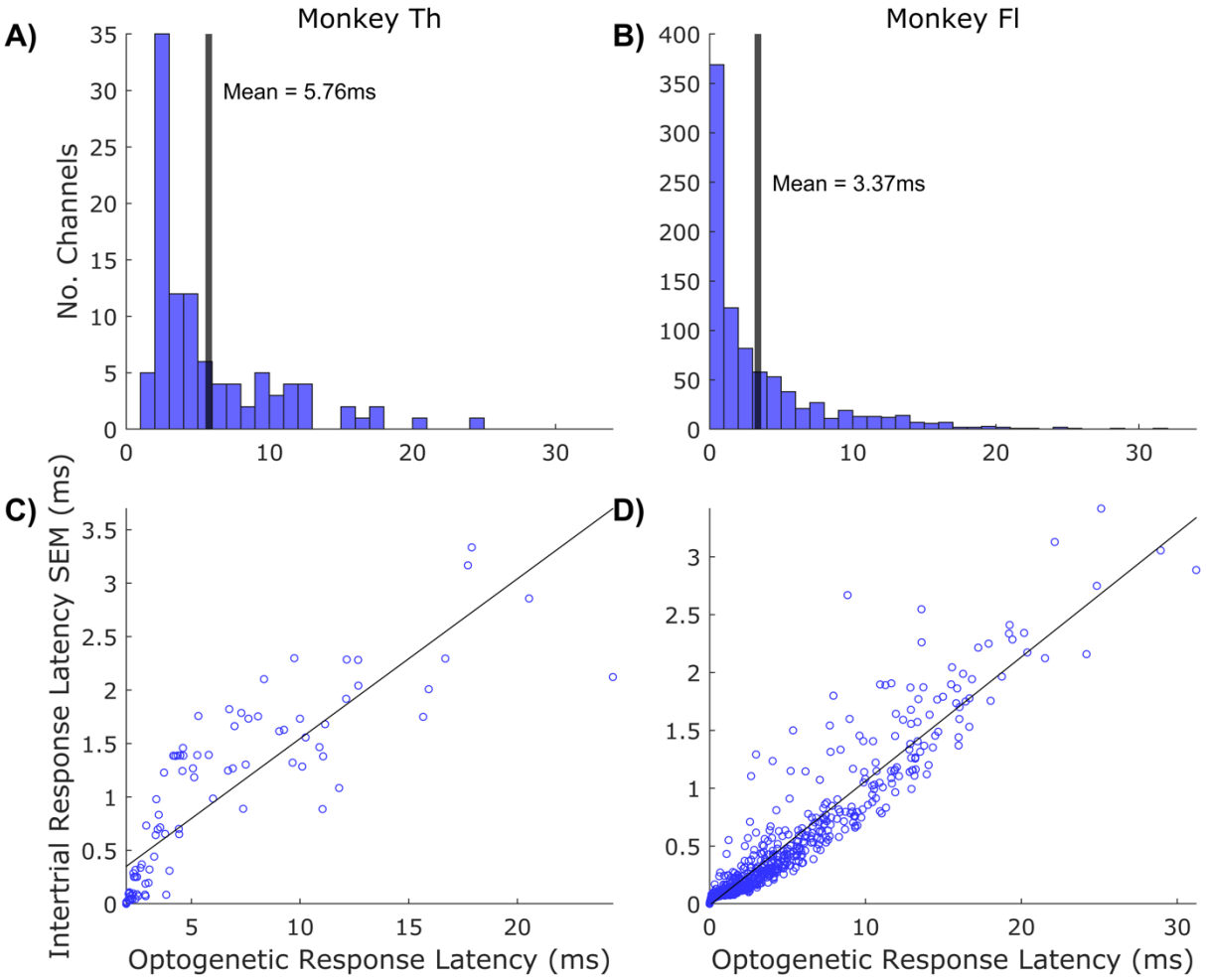

Figure 3.5 Latency of optically modulated channels. **A, B** Histograms of onset latencies for the optogenetically modulated channels in monkey Th (left) and monkey Fl (right). **C, D** Scatter plot of the mean latencies of the optogenetically modulated units and intertrial standard error of the modulation latencies in monkey Th (left) and monkey Fl (right).

modulation latency was significantly correlated with the mean latencies with the shorter latencies having a smaller standard error (Figure 3.5C, D, Spearman's ρ = 0. 0.8424, p <= 0.0001 for monkey Th & ρ = 0.9463, p <= 0.0001 for monkey Fl).

3.3.3 Wavelength specificity of optical modulation

To examine if the optically modulated neural activity was wavelength-specific, we used a red-light source (626nm LED for monkey Th, 594nm laser for monkey Fl) for control in some of the recording sessions. Stimulation duration was identical to optical stimulation using blue light (1s for monkey Th, 300ms for monkey Fl). Stimulation intensities were also comparable (40-62mW for 451nm LED vs 50mW for 626nm LED and 38-52mW for 473nm laser vs ~42mW for 594nm laser). In monkey Th, red light caused a high level of noise that contaminated the signal. MUAe signals showed a sharp increase in response to red light; to examine this further, I extracted and analysed the MUA signal for one session. The same channel was used for comparison with the same threshold (-30uV) used to extract multiunits and the units were sorted automatically (BOSS) resulting in four units. In Figure 3.6A, the peristimulus time histogram (PSTH) and the raster plot of the extracted multiunits showed an increase in response to red light in monkey Th; however, the increase can be attributed to one or two units in particular, units 1 and 2 (Figure 3.6B) which does not resemble typical single or multiunits waveforms indicating that they are likely artefacts. On the other hand, the other extracted units, units 3 and 4, are more representative of neural activity (Figure 3.6B) and did not exhibit an increase in response to red light (Figure 3.6A). In comparison, blue light did not exhibit such behaviour (Figure 3.6C); the waveforms of the extracted units reflected typical multiunit waveforms (Figure 3.6D, examples unit 5, 6 & 7) with one waveform (Figure 3.6D unit 8) which is likely due to a photoelectric artefact that occurs only at the onset of light (Figure 3.6C in green) ; the artefact waveform was not observed otherwise. It was a simple process to remove waveform 8 and thus removing the

photoelectric artefact from the blue LED. It is worth noting that unit 3 and 7 likely reflect the activity of the same unit due to their similarity in waveform (Figure 3.6B, D) and that this unit only responded to blue light. In monkey Fl, no artefacts were observed in response to either wavelength. In the control sessions (n = 8), there was no significant increase in neural activity in response to red light (examples Figure 3.6E).

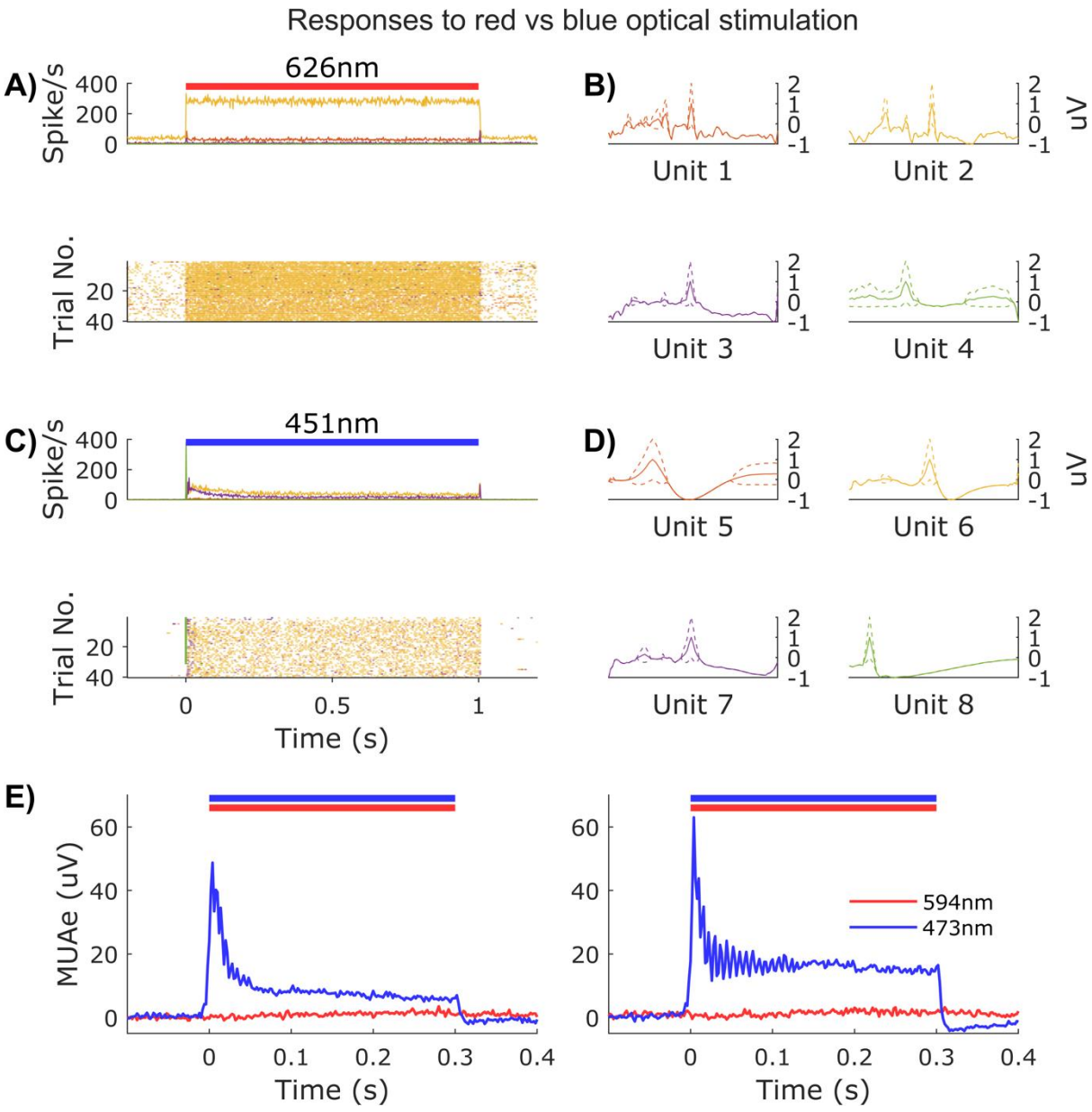

Figure 3.6 Neural response to different wavelengths. **A.** (top) Peristimulus time histogram (PSTH) of four units in response to a 1s pulse of red light (626nm) and the corresponding raster plot (bottom) in monkey Th. **B.** Waveforms of the units in **A**. **C.** PSTH (top) and a raster plot (bottom) of four units in response to a 1s pulse of blue light (451nm). **D.** Waveforms of the units in **C**; unit 8 is a typical artefact observed at the onset of blue light stimulation. **E.** Example response to red (594nm) and blue (473nm) 300ms light pulse from two sessions in monkey Fl.

3.3.4 Effect of stimulation power on neural activity and latency

In monkey Fl, the neural modulation described previously was in response to optical stimulation at one light intensity level ~50mW measured at the

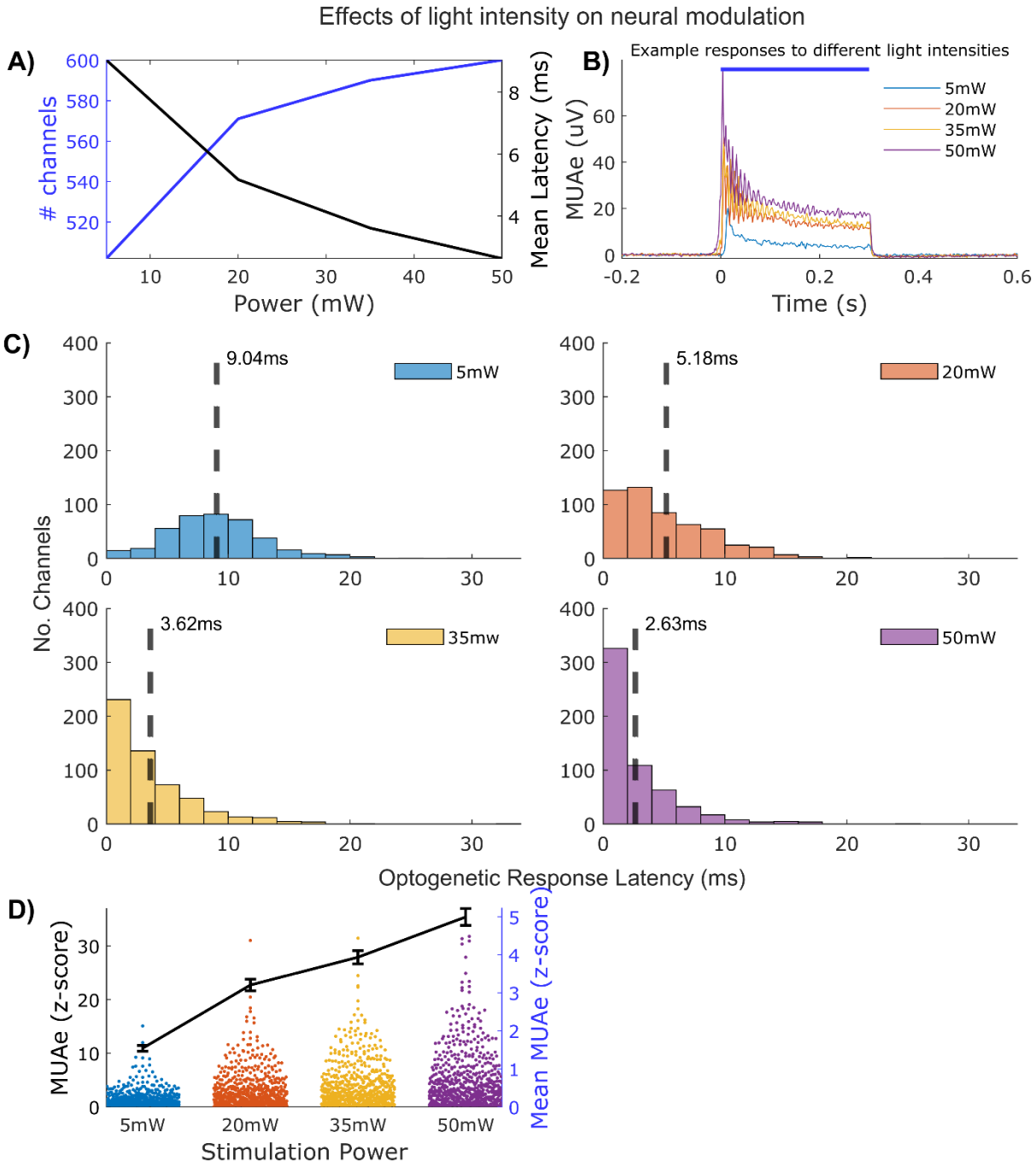

Figure 3.7 Effects of light intensity on neural modulation. **A.** Effect of light intensity on the number of modulated channels (blue) and the modulation latency (black). **B.** Example channel responses to different power levels in one session. **C.** Histograms of response latencies for each light intensity with mean latency (dashed black line). **D.** Scatter plot of normalised MUAe levels (100-300ms from stimulation onset) for modulated channels (grey) and mean normalised MUAe level for each stimulation intensity (blue).

optical fibre tip coupled to the laminar probe. In a subset of the recording sessions (n=27) in monkey Fl, the light intensity was varied (5mW, 20mW, 35mW and 50mW, example in Figure 3.7B). The number of channels significantly ($p < 0.05$, Wilcoxon signed-rank test) modulated with blue light increased with the increase in power (Figure 3.7A). Additionally, the mean onset latency decreased with the increase in power (Figure 3.7A, C) with increasing power. The onset latency variability between trials was significantly highly correlated with mean onset latency for each channel across the different power levels (Spearman's $\rho = 0.8998 \pm 0.0171$, $p <= 0.0001$).

In addition to more channels being optically modulated with decreasing latency, increasing the stimulation power also increased the optogenetically modulated spiking activity, reflected in the normalised (z-scored) and averaged MUAe signals over time (100-300ms, Figure 3.7D). The increase in power was not proportional to the increase of the MUAe across channels; for example, the increase of power by a factor of 10, 5mW to 50mW, only increased the overall MUAe by 3.2, ~1.5 to 5. Additionally, the increase in the overall MUAe seems to be driven by a smaller number of channels rather than uniformly across channels (Figure 3.7D).

3.3.5 Optically modulated activity follows the stimulation frequency

In addition to continuous stimulation, blue light was modulated by a train of pulses at different frequencies (5Hz, 10Hz, 40Hz) at a 50% duty cycle for 1 second. Similar to continuous stimulation, MUAe was modulated by the pulsed stimulation. Optically modulated MUAe followed the stimulation frequencies (examples in Figure 3.8A, B, C). For each channel that is significantly modulated compared to baseline ($p < 0.05$, Wilcoxon signed-rank test) by blue light at each frequency, I calculated the frequency spectrum for the stimulation period (1s) and plotted the frequencies with the peak power for that channel (Figure 3.8A, B, C). Across sessions and channels, the median frequency was close to the stimulation frequency (m

= 3.7Hz for 5Hz, m = 9.1Hz for 10Hz and m = 31.2Hz for 40Hz). Next, I examined whether stimulation frequency influences the strength of the modulated MUAe. MUAe signals were normalised (z-score) and averaged over time (100-300ms for continuous stimulation and pulsed stimulation, Figure 3.8D). Pulsed stimulation at 5Hz resulted in a slightly, but significantly ($p<0.01$, one-way ANOVA test), reduced modulation compared to continuous stimulation. There was not a significant difference ($p>0.5$,

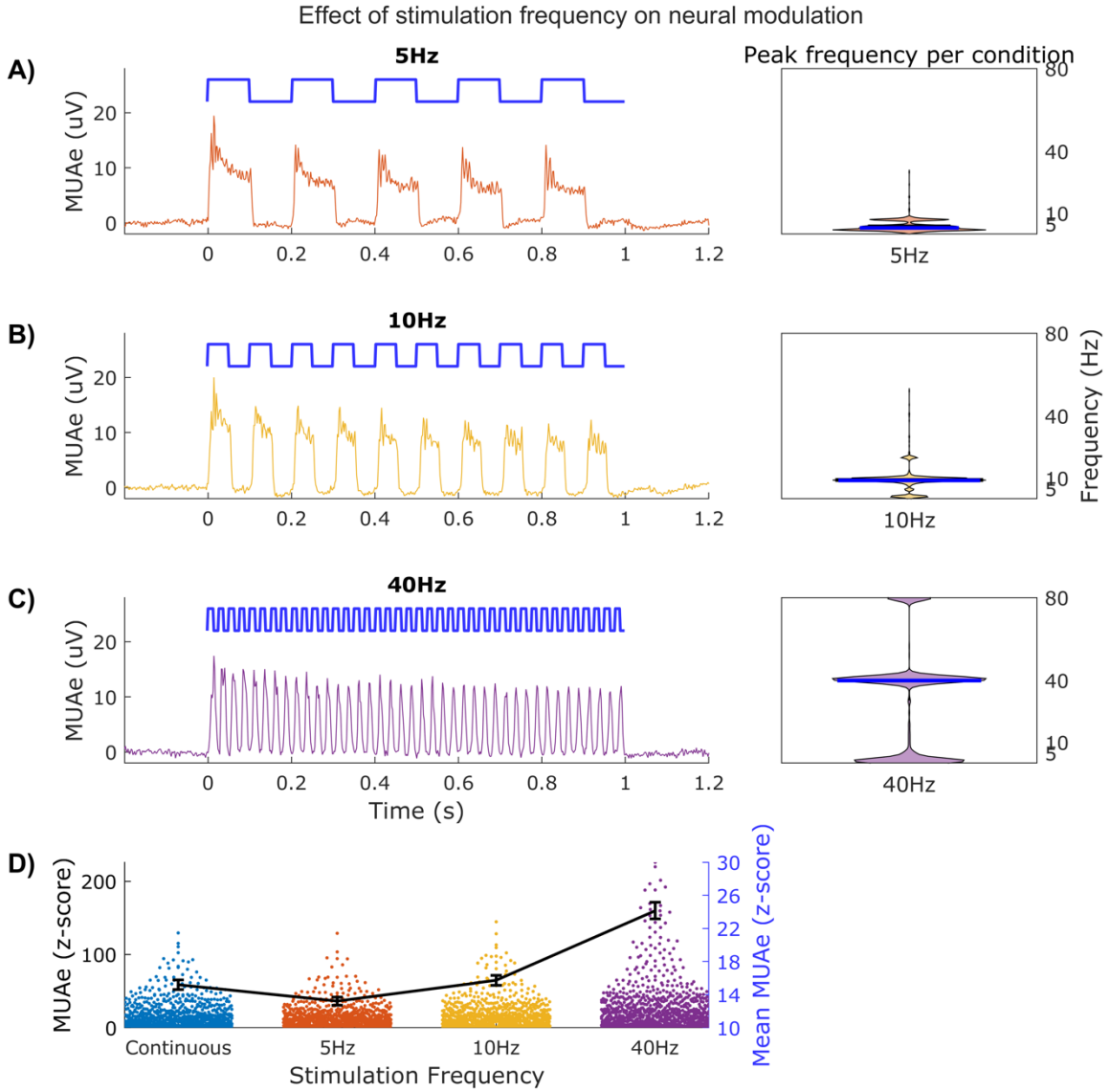

Figure 3.8 Effects of stimulation frequency on spiking activity (MUAe). **A.** (left) Example MUAe response (black) to 5Hz stimulation (1s pulse train in blue, 50% duty cycle) in monkey Fl. (right) A plot of the frequencies with the peak power for each optically modulated channel (median frequency in blue); the frequency spectrum is calculated for the stimulation period and then the frequency with the peak power is extracted. **B.** Same as **A** but for 10Hz. **C.** Same as **A** & **B** but for 40Hz. **D.** Normalised MUAe amplitudes (grey, averaged for the stimulation period 100-300ms post first pulse onset) in response to each stimulation frequency and the mean MUAe amplitudes across units (blue; bars represent standard errors).

one-way ANOVA test) between 10Hz stimulation and the continuous one. Finally, 40Hz resulted in a stronger, and highly significant, modulation ($p<0.0001$, one-way ANOVA test) compared to continuous stimulation.

3.3.6 Weak/unsuccessful modulation in Al, Dp

For monkeys Al and Dp, there was a significant increase in blood-oxygen-dependent (BOLD) fMRI activity in response to V1 optogenetic stimulation with blue light (Ortiz-Rios et al., 2021). However, there was no clear or significant modulation in response to optical stimulation when assessed by acute electrophysiological recordings. Both stimulation methods were used:

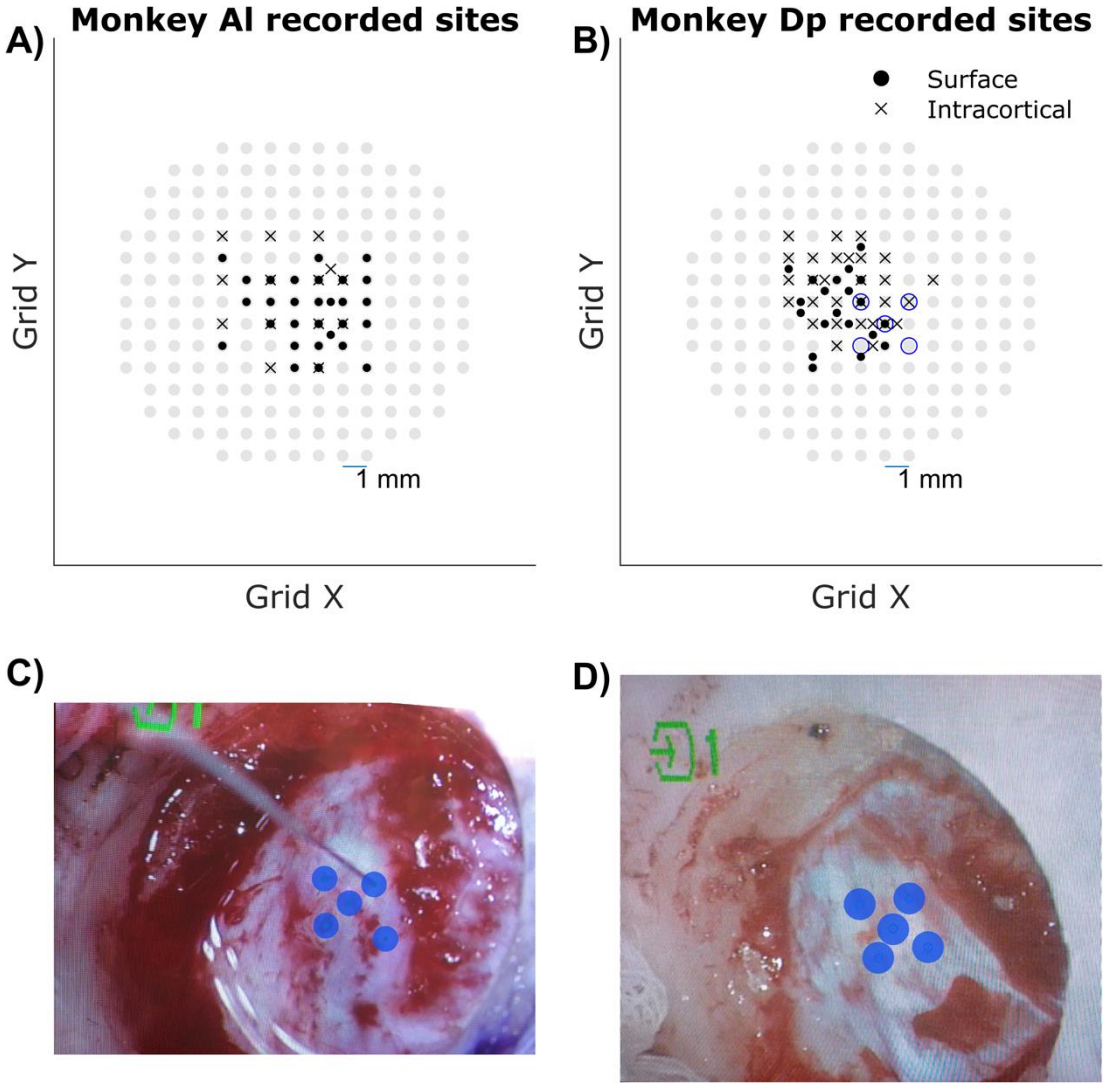

Figure 3.9 Schematic of recording and injection sites in monkeys Al and DP. **A, B** Schematic of recording sites using both surface and intracortical stimulation. In monkey Dp, the second set of injected are presented in blue. **C, D** Images taken during the surgery where the injections were first made. An estimate of injection sites is presented as blue circles.

surface and intracortical stimulation, and single and laminar probes were used as well (see Table 2.2 for details). In monkey Al, surface stimulation (PL-32 & LED) was used in 14 sites and intracortical stimulation (PL-24 & embedded fibre) was used in 37 sites (Figure 3.9A). In monkey Dp, surface stimulation was used in 35 sites and intracortical stimulation was used in 20 sites (Figure 3.9B); during initial experiments, a single electrode was used in addition to surface stimulation in 20 sites. In some stimulation blocks, there was a weak increase in MUAe in response to blue light, but its latency was >50ms which is more consistent with a visual response.

In those monkeys, as well as monkey Th, injections were made following the craniotomy and before the chamber implant; therefore, the injection sites were not marked according to the chamber grid that would be used later for recordings. From the surgeries, the injection sites appear to be localised in the more medial anterior part of the craniotomy (Figure 3.9C, D) and therefore the recording targets were concentrated there. Due to the lack of certainty about injection sites, additional injections were made in monkey Dp (Figure 3.9B). After 4 weeks following the new injections, the new sites were tested, but there were no optogenetic effects in the newly injected as well. For the remaining duration of the project, the chamber was explored for optogenetic effects, and no responsive sites could be detected throughout the chamber region.

3.4 Discussion

3.4.1 Validation of optogenetic stimulation

The first focus of this chapter is the validation of optogenetic stimulation of V1 neurons using ChR2 opsins and blue light. The results showed a significant increase in firing rates in most of the channels in response to continuous optogenetic stimulation in two monkeys Th and Fl. Most of those channels were also modulated by visual stimuli with a few channels exclusively modulated by either visual or optical stimulation. The larger number of channels modulated with blue light, compared to visual stimuli,

is not surprising either; visual stimuli were not optimised to the characteristics of the recorded neurons. For example, the sizes of the stimuli were larger than the recorded RF potentially resulting in surround suppression decreasing the overall response (Bair et al., 2003). In addition to size optimisation, the orientations of drifting gratings were not selected based on the orientation tuning of the recorded neurons which has a large effect on the macaque V1 neurons (Ringach et al., 2002, 2003). Therefore, optimisation of the different visual stimuli features for the recorded neurons would have required running a bank of paradigms at the beginning of each acute recording session. Furthermore, stimuli optimisation for maximal response across layers (or probe contacts) is complicated. While neurons in a V1 cortical column are functionally similar (Lund et al., 2003), there are laminar differences for both orientation and size tuning (Sceniak et al., 2001; Wang et al., 2020) and therefore it will be a challenge to ensure the strongest drive across all layers. Under the animal project license used, the animals can be involved in experiments outside their home cage for a limited time, 5 hours; a large portion of that time would be used to fix the head of the animal, clean the chamber as well as carefully inserting and removing the recording probe. It was decided to focus more on the optogenetic stimulation components since it would not have been affected by the preferences of the recorded neurons but rather by the opsin expression. Similarly, the time constraints of the experiment and the project did not permit the comparison to electrical microstimulation. It would be more optimal in a future project to compare the effects of visual, microstimulation as well as optogenetics on neural activity; similarly, to compare the efficacy of microstimulation and optogenetics in generating a phosphene.

Another important step in ChR2 verification is the latency of modulated response. Studies examining the onsets of neural responses in the visual system have calculated the latencies based on the signal reaching a certain percentage of the maximum response (Bair et al., 2002, 2003). However,

since we did not know the characteristics of optogenetically modulated responses, we used the baseline to calculate our threshold. The observed latencies in both animals were in the lower range of ChR2 response latency (2-10ms, Lin, 2011). On the other hand, the earliest visually evoked responses in the macaque V1 have latencies >=30ms (Bair et al., 2002; Raiguel et al., 1989). Those results confirm that the observed responses are due to direct activation of neurons expression ChR2 opsins by blue light. The modulation latencies were calculated on a trial-by-trial basis, and we observed a significant and high correlation between the latency of activation and the latency variability between trials. One possible explanation is that the responses with shorter latencies are a result of direct activation of neurons expressing ChR2 with blue light while the later (10-30ms) responses are due to an indirect network effect. Network latencies of 10-40ms can be observed in the macaque V1 after the arrival of visually evoked signals in layer 4C (Bijanzadeh et al., 2018). Most of the modulated channels, however, had a short latency expected of ChR2 indicating that a big portion of the observed modulation was due to a direct optogenetic drive accompanied by a smaller, but still significant, indirect drive propagated by the local network.

Our final verification method is to examine if the overserved modulation is wavelength specific. In monkey Th, red light introduced artefacts in the signal that could be mistaken for a neural response; however, inspecting the optically evoked MUA waveforms refuted this as illustrated earlier in Figure 3.6B (units 1 & 2). It is not clear why such an artefact was not observed in monkey Fl. The combination of the light source and the material of the electrode contacts could be a factor or the red LED system itself could have been introduced an electrical artefact that was not observed with the other light sources. The observation of artefact waveform prior to light emission supports the electrical nature of the artefact. Red light stimulation was not successful in modulating neural activity confirming the blue light specificity of modulation. Additionally, optical stimulation with a different

wavelength indicates that it is not likely the modulation was induced by heat. In monkey Fl, blue light with a much lower intensity (5mW) than red light (40mW) could still reliably modulate neural activity. If any neural activity would be modulated due temperature increase in response to light, then the higher power of 40mW would have achieved this effect. Another study by Stujenske and colleagues demonstrated increased brain tissue temperature by more than 1.5°C leading to increased spiking activity in response to as little as 10mW of yellow light (Stujenske et al., 2015); however, the authors measured the power at the fibre tip and directly inserted it in brain tissue while our measurement at the fibre tip was before coupling it to the Plexon probe with the embedded fibre. It is likely that there is a considerable power loss resulting from coupling the fibre to the probe; however, we did not possess the tools to measure the power coming out of the probe without damaging the probe itself. One limitation of the study is that non-transfected tissue was not tested using blue light; however, the wavelength specificity and the short latency of activation provided enough evidence for the effects of optogenetic stimulation.

3.4.2 Effects of stimulation parameters on neural modulation

After verification of optogenetic stimulation, we examined the effects of different stimulation parameters, such as light intensity and stimulation frequency, on neural modulation in monkey Fl. Increasing stimulation intensity resulted in an increased number of optogenetically modulated channels. Increasing the stimulation intensity also significantly ($p < 0.0001$, two-tailed Wilcoxon signed-rank test) reduced the modulation latency across the modulated channels for every step of intensity increase. Even though the modulation latency for the lowest intensity (5mW) was close (9.04ms) to the upper limits of ChR2 onset latencies, the majority (>60%) of the modulated channels are still within the expected latency (<10ms) of ChR2 (Lin, 2011) indicating direct activation with blue light. Increasing the stimulation intensity resulted in an increase in the number of channels with modulation latency of less than 10ms which could be attributed to more

blue light reaching the recorded neurons. That effect is expected since transmission of blue light in the mammalian brain tissue is limited with power halving less than 0.2mm away from the source of light (Yona et al., 2016). The findings show that even though low stimulation intensity may have not resulted in direct activation of neurons, the optogenetic drive was sufficient to modulate a large number of neurons and cause a widespread activation along the cortical column (more on that in the next chapter) which can be seen in the plateau in Figure 3.7A. Finally, the increase in stimulation intensity resulted in an increase in the modulated MUAe that is more linear than the effects on modulation latency or the number of modulated channels. This indicates that while the effects of optogenetic stimulation are widespread at lower intensities, higher intensity could increase the firing rates even further. The increase in firing rates with an increase in power has been observed previously (Cardin et al., 2009; Nassi et al., 2015). The observed increase in firing rates could be attributed to more blue light reaching opsin-expressing neurons or a stronger excitatory drive to the local network recruiting more neurons indirectly. The number of modulated channels show minimal increase with power and the overall MUAe increase is mainly driven by few channels (Figure 3.7A & D). These results suggests that the overall MUAe increase is driven by a number of neurons that benefit from receiving more blue light rather than a uniform increase in activity. Taken together, increasing stimulation power seems to have diminishing returns at the higher levels. The MUAe increase or the activation latencies do not seem proportional to the power increase at the higher power levels. Increasing the power from 5mW to 20mW seems to have a linear relationship with a doubled MUAe and a halved modulation latency; this suggests that stimulation intensities around 20mW would be ideal. On the other hand, increasing power levels beyond 20mW resulted in marginally better results. Nonetheless, further experiments are needed to examine whether the observed effects in neural signals can be replicated in behaviour and if low intensities can be sufficient to generate a phosphene.

In addition to varying the stimulation intensity, the stimulation frequency was also varied. One benefit of pulsed stimulation is the reduction of the heat generated that could harm the brain (Kole et al., 2012). In addition, it is important to characterise the effects of different optogenetic stimulation frequencies since there are no studies that systematically examined such effects in the primate brain (Gerits & Vanduffel, 2013) with studies using specific frequencies such as 24Hz (Chernov et al., 2018) 16Hz (Williams et al., 2019), 25Hz (El-Shamayleh et al., 2016) and 50Hz (Fabbrini et al., 2019) without a specific rationale. Typical electrical stimulation frequencies are high (>200Hz) (Graziano et al., 2002; Tehovnik et al., 2005; Tehovnik & Slocum, 2007) with higher frequencies being more effective to a certain limit, when higher frequency stimulation starts to have an inhibitory effect (Mattis et al., 2012; Waataja et al., 2011). ChR2 remains one of the most common opsins used in primate optogenetics (Tremblay et al., 2020) and it is important to understand how it responds to different stimulation frequencies. Our findings indicate that spiking activity can follow the stimulation frequencies at 5Hz, 10Hz and 40Hz. Those frequencies were chosen since oscillations in those ranges have been associated with affecting the performance of the cortical circuits (Deisseroth, 2014; Sohal et al., 2009). Stimulation at 5Hz resulted in reduced MUAe compared to continuous stimulation which can be attributed to a shorter stimulation period (100ms pulses for 5Hz at 50% duty cycle) compared to continuous stimulation (300ms pulse). However, stimulation at 10Hz and, especially, 40Hz resulted in a much stronger spiking activity than continuous stimulation. The observed effects can be attributed to an intrinsic adaptation in the ChR2 opsin that is accompanied by reduced depolarisation current the longer the ion channel is open (Nagel et al., 2003). Pulsed stimulation would allow the ion channel to close briefly, avoiding this adaption and maintaining the higher initial currents; however, even with pulsed stimulation, the channels cannot fully recover with a period of no stimulation (Lin, 2012). One can see this adaptation in the MUAe responses to pulsed stimulation (Figure 3.8) with the response

decreasing with each subsequent pulse; it is most evident when comparing the response between the first and last pulses. Even if subsequent light pulses would generate a lower transient current than the first one, pulsed stimulation is likely to result in higher depolarization currents overall compared to continuous illumination. Evidence suggests, however, that stimulation at 40Hz is the highest feasible stimulation for ChR2 (Grossman et al., 2011); the closing time of ChR2 is around 13.5ms (Bamann et al., 2008; Mattis et al., 2011; Nagel et al., 2003) and stimulation at 40Hz with 50% duty cycle allows 12.5ms for the opsin to close. In mice, evidence shows that higher stimulation can increase the effects of optogenetic stimulation (Yu et al., 2020). There is also evidence that high-frequency stimulation of ChR2 could inhibit evoked responses (Liske et al., 2013); however, we did not test this since our goal is significant activation of neurons to evoke behavioural effects and we focused on increasing responses.

3.4.3 Unsuccessful optogenetic stimulation

The lack of optogenetic effects in monkeys Dp and Al can be attributed to several reasons. The viral expression could have been unsuccessful in both animals or at least not as extensive as in the other two animals. Animals could have some immunity to AAV viruses before being administered with the viral vectors (Mendoza et al., 2017). Therefore, pre-existing antibodies could reduce the extent of viral expression. Indeed, we found some evidence of weaker viral expression in the histology of animals Al and Dp (Figure 3.10).

There is more evidence for weak/limited expression rather than no expression at all. This is supported by the histological analysis of the tissue which found very small traces of expression. In addition, the effects of optogenetic stimulation in V1 using surface stimulation were tested using functional magnetic resonance imaging (fMRI) in other experiments. Optogenetic stimulation reliably elicited blood-oxygen-dependent (BOLD) fMRI activity in V1 and extrastriate regions (Ortiz-Rios et al., 2021). One

explanation for the observed BOLD modulation is the sensitivity of fMRI to detect subthreshold activity, such as synaptic potentials, from weak activation that does not result in action potentials (Logothetis & Wandell, 2004). The subthreshold activity can be explained by weak or sparse viral expression and therefore easily missed if the precise injected sites are not targeted by the laminar probes. On the other hand, heat due to optical stimulation could affect the fMRI signal relaxation times, T1 and T2, producing signal changes not related to a BOLD haemodynamic response (Christie et al., 2013). This is unlikely since we did not observe the negative BOLD signal observed by Christie et al. nor did we observe similar large temperature increases (Ortiz-Rios et al., 2021).

An additional factor could be the light delivery method; surface stimulation was used initially in monkeys Dp and Al and while successful in monkey Th, it might not have been enough to elicit strong spiking activity. In monkey Fl, there was a very strong and significant modulation when the light was delivered intracortically but not with surface stimulation in the same session. The LFP signal shows a slow positive deflection when the surface LED light is on indicating that light reaches the electrode but there was no increase in spiking. A possible explanation is the growth of granulation tissue and therefore a bigger portion of the blue light is absorbed before it reaches the cortex. A potential explanation for the mismatch between our fMRI and electrophysiological results is that fMRI signals reflected a change in the subthreshold activity of neurons, rather than spiking activity. Evidence has been found of a high correlation between the BOLD, captured by fMRI, and LFP signals that reflect the subthreshold activity (Logothetis et al., 2001). Nonetheless, optogenetic stimulation of monkeys Dp and Al failed to produce similar electrophysiological results to monkeys Fl and Th.

Additional injections were made in monkey Dp using the recording grid as a reference to avoid the uncertainty about injection sites. Both intracortical and superficial optical stimulation did not affect neural activity in the newly injected areas. Injections' depths were similar to those with a fresh

craniotomy (500µm, 1000µm and 1500µm from the tissue surface); however, there was granulation tissue growth on top of the dura after a craniotomy was made.

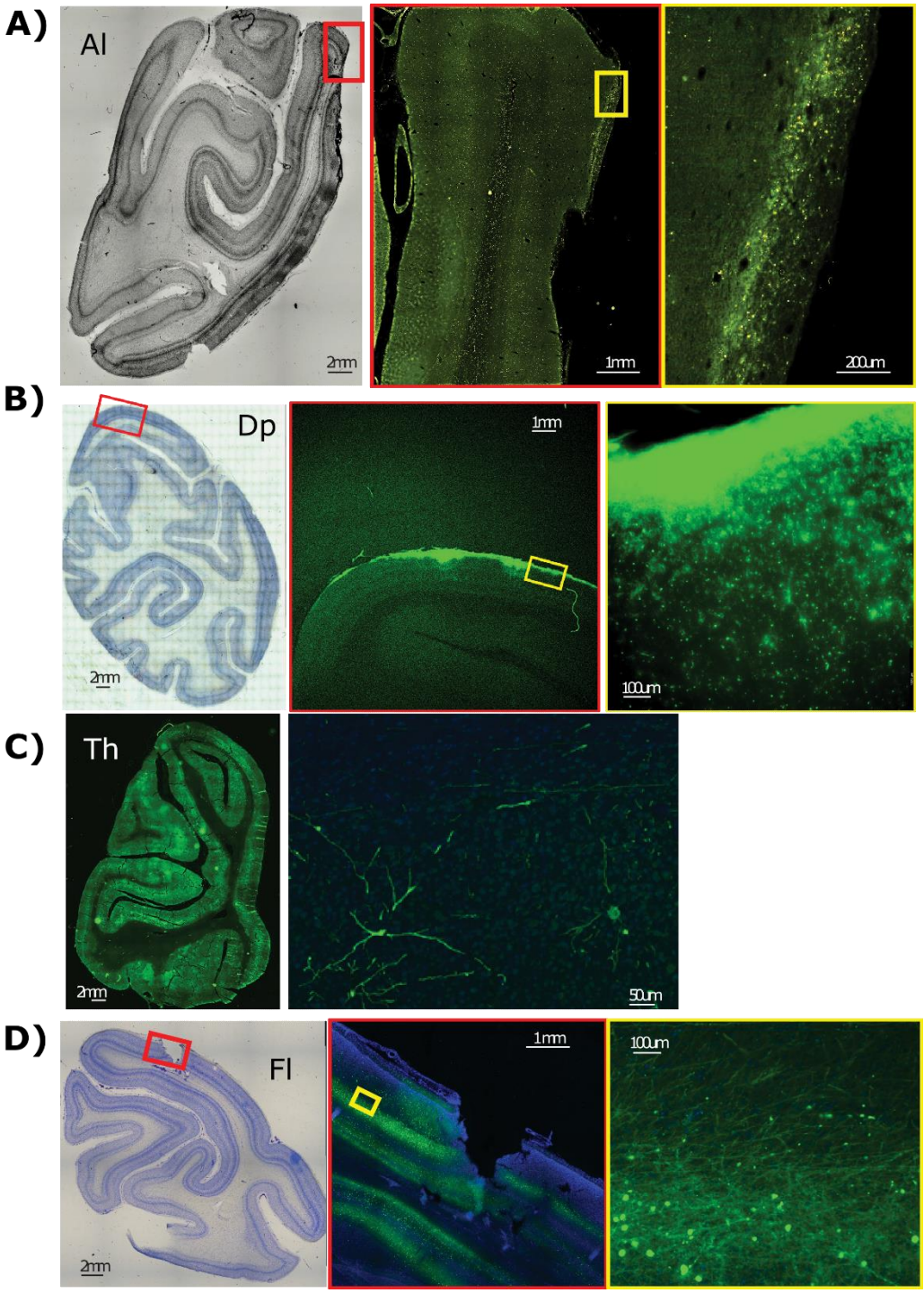

Figure 3.10 eYFP expression examples from all animals. Each row contains an image of a coronal brain slice (**A:** Al, **B:** Dp, **C:** Th, **D:** Fl) with a close-up of V1 showing eYFP expression of the optogenetic construct can in green. Figure provided by Dr Marcus Haag.

A dura scrape was performed prior to the injections, but to avoid any damage to the brain or dura, the scrape did not reach the dura and therefore there was still tissue remaining above the dura. That tissue could have been thicker than 1.5-2mm and therefore the virus might not have reached the brain, to begin with.

Chapter 4: Laminar examination of optogenetic manipulation of V1

4.1 Introduction

As described earlier, there is a fairly limited number of studies examining the physiological effects of optogenetic stimulation in NHPs and a small portion of those studies have used electrophysiology to assess the effects (Andrei et al., 2019; Jazayeri et al., 2012; Nassi et al., 2015). The rest of the studies have used either intrinsic optical imaging or calcium imaging (Chernov et al., 2018; Ju et al., 2018; Nakamichi et al., 2019; Ruiz et al., 2013). The studies that have examined electrophysical signals used single electrodes that did not provide laminar resolution therefore not providing information about the optogenetic stimulation effects on the different cortical layers (Jazayeri et al., 2012; Nassi et al., 2015).

Examining the laminar effects of optogenetic stimulation serves several purposes. To begin with, the use of different viral vectors leads to different expression patterns across the layers depending on the serotype of the virus and the promoter (Gerits et al., 2015; Lerchner et al., 2014; Watakabe et al., 2015). It is unknown how impactful those expression patterns are on the laminar activity. While it is likely that the existing microcircuitry of V1 have a very strong effect on the resulting effects (Bloch et al., 2022), it is important to consider the effects of viral expression and stimulation patterns on the resulting activation. Additionally, microstimulation current thresholds required to induce a phosphene were found to vary depending on depth (Figure 1.2); this is likely due to the stimulation of axonal projections from the deeper layers to the output superficial layers of V1 (Tehovnik & Slocum, 2009). It would be informative to examine any depth dependency of optogenetic stimulation or if expression patterns are more of a determining factor in the overall resulting effect.

Schroeder et al. pioneered the use of multicontact laminar probes to examine neural activity across the layers of the macaque V1 (Schroeder et al., 1990, 1991, 1998). Schroeder et al. examined the laminar sources of the different components of visually evoked potentials (VEPs) recorded at the surface of the brain; their work was pioneering in finding physiological signals predicted by V1 anatomy (Schroeder et al., 1991). That opened the way for further studies examining the laminar effects of spatial attention (Mehta et al., 2000b, 2000a). Since then, the laminar examination of the macaque V1 using multicontact laminar probes has been providing important insight into the function of the different layers during corticocortical processing (Maier et al., 2010), sustained activity (Maier et al., 2011), orientation selectivity (Ringach et al., 2002), attention (van Kerkoerle et al., 2017) and the origins of near vs far surround suppression (Bijanzadeh et al., 2018). In a study by Andrei et al., the combination of laminar probes (Plexon S-probes) and optogenetic stimulation has been used to study the effects of optogenetic stimulation in the macaque V1, using C1V1 opsins; however, the authors did not extract any laminar information or provide information about the cortical layers being stimulated (Andrei et al., 2019). On another hand, a study by Klein et al. have utilised laminar probes to identify koniocellular projections from the lateral geniculate nucleus (LGN) to the superficial layers of the macaque V1 (Klein et al., 2016). Using multicontact recording methods, Klein et al managed to delineate the konio-specific input to V1 supragranular layers. Laminar information can therefore be a vital tool to provide information about the local circuitry and how optogenetic stimulation affects the different layers of the cortex. For example, optogenetic stimulation was shown to affect cortical layers differently in rodents depending on whether selective optogenetic stimulation was delivered to the superficial or the deeper layers (Bitzenhofer et al., 2017). In both cases, pyramidal neurons were stimulated and exhibited increased firing rates but only stimulation in the superficial stimulation produced increased oscillatory activity and entrainment in the beta-gamma range. Such a difference can be attributed

to the inherent properties of the local circuitry such as the existence of inhibitory interneurons in the superficial layers (Fitzpatrick et al., 1987) facilitating such oscillation. In this chapter, the effects of optogenetic stimulation on the different cortical layers are examined. Similar to the previous chapter, we examine the effects of the different stimulation parameters on the spiking activity as well as the oscillatory activity in V1.

4.2 Methods

4.2.1 Current Source Density (CSD)

Current source density (CSD) analysis refers to the second spatial derivative of the LFP signals (Schroeder et al., 1991; Wójcik, 2014). For multielectrode arrays, the second spatial derivative results in a more localised signal to the recorded channel since the activity of the neighbouring channels are subtracted. The CSD signal is defined as the following:

$$CSD(t)_{ch} = \frac{LFP(t)_{ch+1} + LFP(t)_{ch-1} - 2 * LFP(t)_{ch}}{dx^2}$$

Equation 4.1

Where the CSD signal for once channel, $CSD_{ch}(t)$, is calculated by subtracting the LFP signal for that channel, $LFP_{ch}(t)$, from the neighbouring channels, above $LFP_{ch-1}(t)$ and below $LFP_{ch+1}(t)$, then dividing by the spacing between the channels, dx.

More importantly, CSD reflects the flow of transmembrane currents in neurons; a current sink, or a negative CSD value, reflects a positive current entering the neuron, causing depolarization, while a current source reflects a positive current leaving the neuron and corresponds to a positive CSD (Fallon et al., 2016; Pettersen et al., 2006; Schroeder et al., 1998; Wójcik, 2014). In the macaque V1, layer 4C receives its primary driving visual input coming via the LGN (Figure 4.1) (Fitzpatrick et al., 1985); therefore, in laminar electrophysiological recordings, the earliest visual response onset

will correspond to layer 4C input. As this visual onset CSD pattern can be observed reliably across tasks, conditions, and varying electrode penetrations, it will be used as a reference to examine the cortical lamina across sessions.

4.2.2 Extraction and alignment of laminar recordings

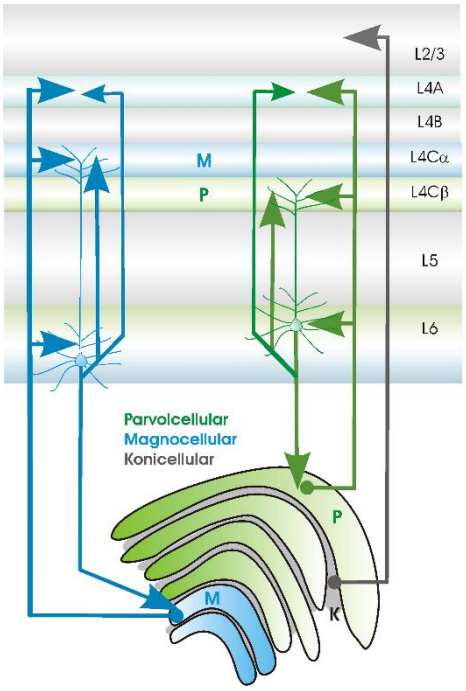

Figure 4.1 Schematic of LGN projections to V1. LGN projections from the magnocellular and parvocellular layers of the LGN arrive mainly in layers 4Cα and 4Cβ of V1 with sparse projections to layer 6 and layer 4A. Figure from Thomson, 2010

During each recording session, the probe depth was adjusted such that the whole depth of the V1 cortical sheet is recorded. To extract and align the data offline, the CSD analysis was used in addition to the latency of the visually evoked MUAe response. For each session, the latencies of visually evoked MUAe were calculated by detecting when the signal exceeds the baseline by four standard deviations. The channel with the earliest response was used as a reference as it would correspond to the input layer 4C. A number of channels are then extracted above and below the input layer to cover the cortical depth depending on the spacing between channels (13 channels covering 1.950mm for monkey Th and 20 channels covering 2mm for monkey Fl). The visual stimuli used for CSD calculation is specified in the previous chapter.

4.2.3 Histology

After the completion of data collection, the animals were euthanised with an overdose injection of an anaesthetic. Once the animals were sufficiently anaesthetized, they were perfused with saline (phosphate-buffered set at 37 °) by inserting a needle in the left ventricle with a cut in the right atrium as an output. Once the blood was rinsed with saline, paraformaldehyde (PFA, 40%, pH 7.4) was used until sufficient tissue fixation was achieved. The brains were then carefully dissected out of the skull and placed in PFA solution overnight. In the following days, the brains were transferred to containers with increasing concentrations of cryoprotection (10%, 20% and 30% solutions). Brain tissue was cut using a cooling microtome into 50um thick slices and stained with Cresyl violet with some stained using standard immunohistological protocols. To label layer 4Cβ of the V1, an antibody was used to mark cells expressing vesicular glutamate transporter (vGlut2, MAB5504, Merckmillipore); vGlut2 marks the LGN input projections to V1 (Balaram, 2011; Balaram & Kaas, 2014). Additionally, a nuclear cell body maker was used (Fluoroshield TM with DAPI, Merck). Finally, a fluorescence microscope (DM6B, Leica Navigator, Leica Biosystems, Wetzlar, Germany) was used to visualise eYFP, the fluorescence protein reporter included in the viral vectors used. eYFP was used to reflect opsin expression.

4.2.4 Frequency analysis

Frequency power spectra calculation was performed on the LFP and MUAe data using the Fieldtrip toolbox (Oostenveld et al., 2011). To obtain the frequency power spectrum, a fast Fourier transform (FFT) was performed, with a single Hanning taper, on a trial-by-trial basis then averaged across trials. The analysis window varied depending on the analysis but did not include the first stimulation onset to avoid the initial sharp transient response; for each duration of interest, a similar time length during the baseline period was analysed. For LFP spectra, the resultant power spectra of the trials were then baseline corrected, by subtraction, and divided by

the baseline for normalisation. LFP frequency analyses results are expressed as a percentage relative change from the baseline where a positive number would indicate an increase in that frequency. MUAe frequency analyses results are expressed as the absolute artificial units (a.u.).

4.2.5 Granger Causality

Granger Causality (GC) is a statistical test that measures the causal relationship between two signals and if one signal can help predict the other. For two signals that can be represented by the bivariate autoregressive models $X_1(t)$ and $X_2(t)$ (Equation 4.2), $X_2(t)$ would be said to cause signal $X_1(t)$ if the inclusion of the past values, $X_2(t-j)$, reduces the prediction error variance, $E_1(t)$, and vice versa (Kamiński et al., 2001). That means that there are parts of the signal $X_1(t)$ that cannot be explained by the past values of $X_1(t-j)$ on their own.

$$X_1(t) = \sum_{j=1}^{p} A_{11}(j)\, X_1(t-j) \; + \sum_{j=1}^{p} A_{12}(j)\, X_2(t-j) + \; E_1(t)$$

$$X_2(t) = \sum_{j=1}^{p} A_{21}(j)\, X_1(t-j) \; + \sum_{j=1}^{p} A_{22}(j)\, X_2(t-j) + \; E_2(t)$$

Equation 4.2

GC can be a useful tool to find which signals "cause" other signals as an estimation of information propagation from one brain region or cortical layer to another. GC can be also examined in the frequency domain to examine causal relationships for frequencies of interest. This is done by first Fourier transforming the signal and examining the contribution of one signal, $X_1(f)$, to another, $X_2(f)$ (for more details, see Brovelli et al., 2004; Kamiński et al., 2001). Bivariate Granger Causality analysis in the frequency domain was performed on the LFP data. Spectral Granger causality indices (GCIs) were calculated for a duration of 200ms at the end of the stimulation period (100-300ms for continuous stimulation and 800-1000ms for pulsed stimulation) and using the Fieldtrip toolbox (Oostenveld

et al., 2011). First, the amplitude and phase of the different frequencies were extracted using FFT with a single Hanning window and then Fieldtrip's connectivity function was used to calculate Granger causality from the complex output. In the time domain, conditional granger analysis was performed using the MVGC toolbox, a freely available Matlab toolbox (Barnett & Seth, 2014). Time GCIs were calculated for the same time periods used in the frequency domain. A vector autoregressive model (VAR) was estimated for each session and condition with an order selected based on the Bayesian Information Criterion (BIC); BIC model estimation is suggested for data with larger data points (Ding et al., 2006).

4.3 Results

4.3.1 Alignment of sessions and depth information

For monkey Fl, CSD responses to a patch of drifting gratings were calculated on a session-by-session basis (example in Figure 4.2A). For each session, the earliest sink was identified visually and then the lower bound of that sink was taken as the reference point and the input layer 4C. After extraction (see methods), data could be combined across sessions (n=22) robustly with early sink location consistent across sessions (Figure 4.2B). For confirmation, the onset latencies of the visually evoked MUAe responses were calculated as well. The shortest latencies coincided with the input layer 4C (based on the CSD) confirming our CSD results (Figure 4.2C). Since monkey Th was not successfully trained on central fixation, the eye-tracking information was used to detect when the animal was looking towards the screen during full-field white flashing resulting in noisier data. Trials were then extracted based on eye detection during the full-field white flash. As CSD signals were noisy, the onset latencies of the visually

modulated MUAe signals were used instead to detect the earliest response and therefore layer 4C (Figure 4.2D).

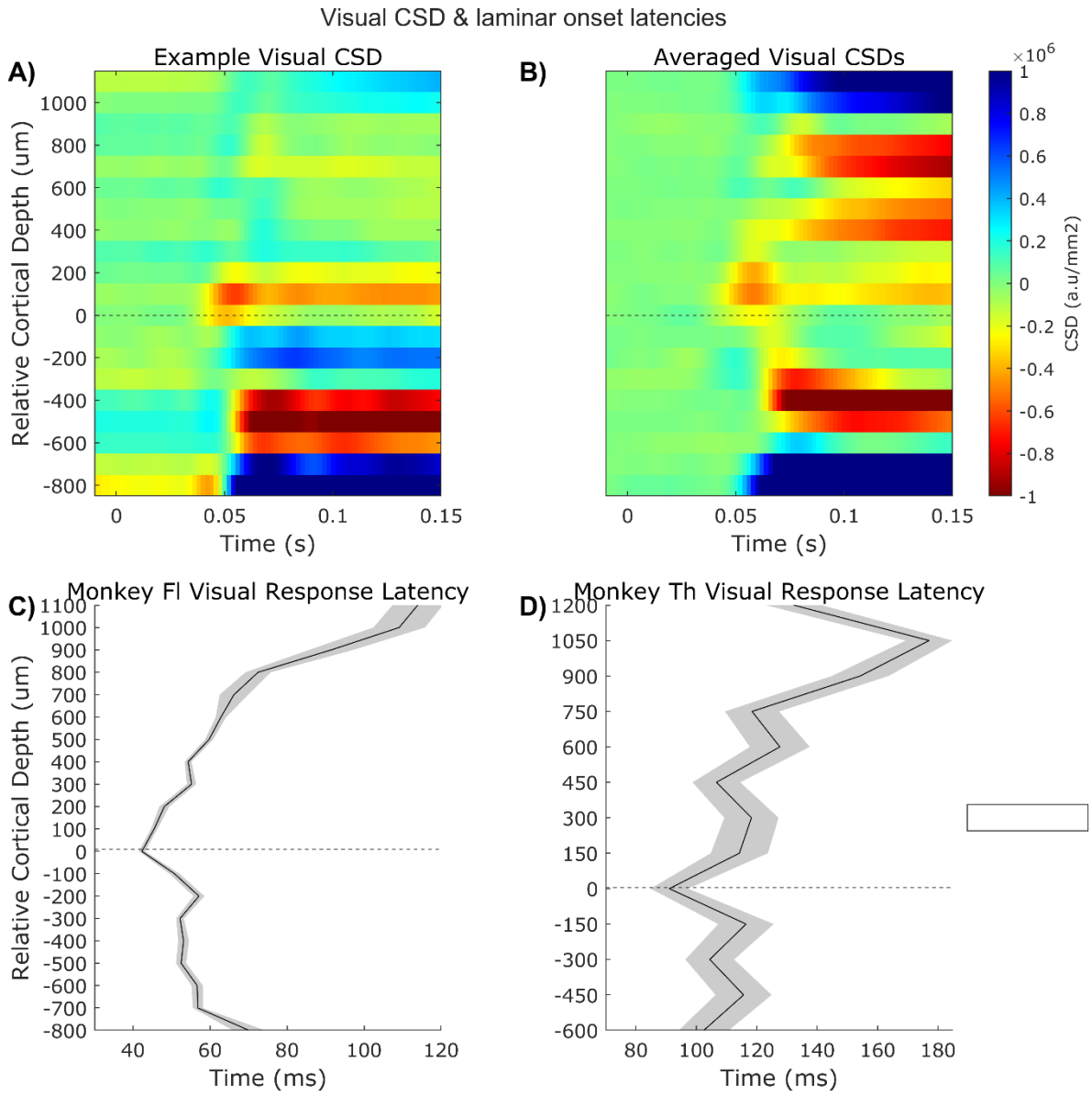

Figure 4.2 Current Source Density (CSD) and latency of visually evoked MUAe responses in V1. **A.** Example CSD response profile to a 5° patch of drifting gratings (spatial frequency 2 cycles/°, speed: 2-4 cycles/s) from one session in monkey Fl. The lower border of the first sink (in red, thalamic input to L4C) is used as a reference to align laminar data across sessions. **B.** Similar to **A** but averaged across sessions. **C.** Response onset latency for the visually evoked MUAe across cortical depth across sessions (n=22) for monkey Fl. Latency onset was extracted when the signal crosses 4*SD of the baseline. **D.** Similar to C but for monkey Th (n=10).

4.3.2 Optogenetic stimulation increased firing rates along the cortical column

In the previous chapter, blue light was shown to significantly modulate most of the channels. Here, the effects of optogenetic stimulation are shown with a laminar resolution. In both monkeys, blue light stimulation resulted in a significant increase (monkey Fl: $p<0.001$ in 20/20 channels, monkey Th: $p<0.001$ in 12/13 channels with $p<0.05$ in the remaining channel, Wilcoxon signed-rank test) in the MUAe activity recorded by every channel across the cortical sheet (Figure 4.3). In both animals, optogenetic stimulation resulted in 3 peaks of activation at similar cortical depths in the two animals. The superficial peak aligns with the middle of layers 2/3

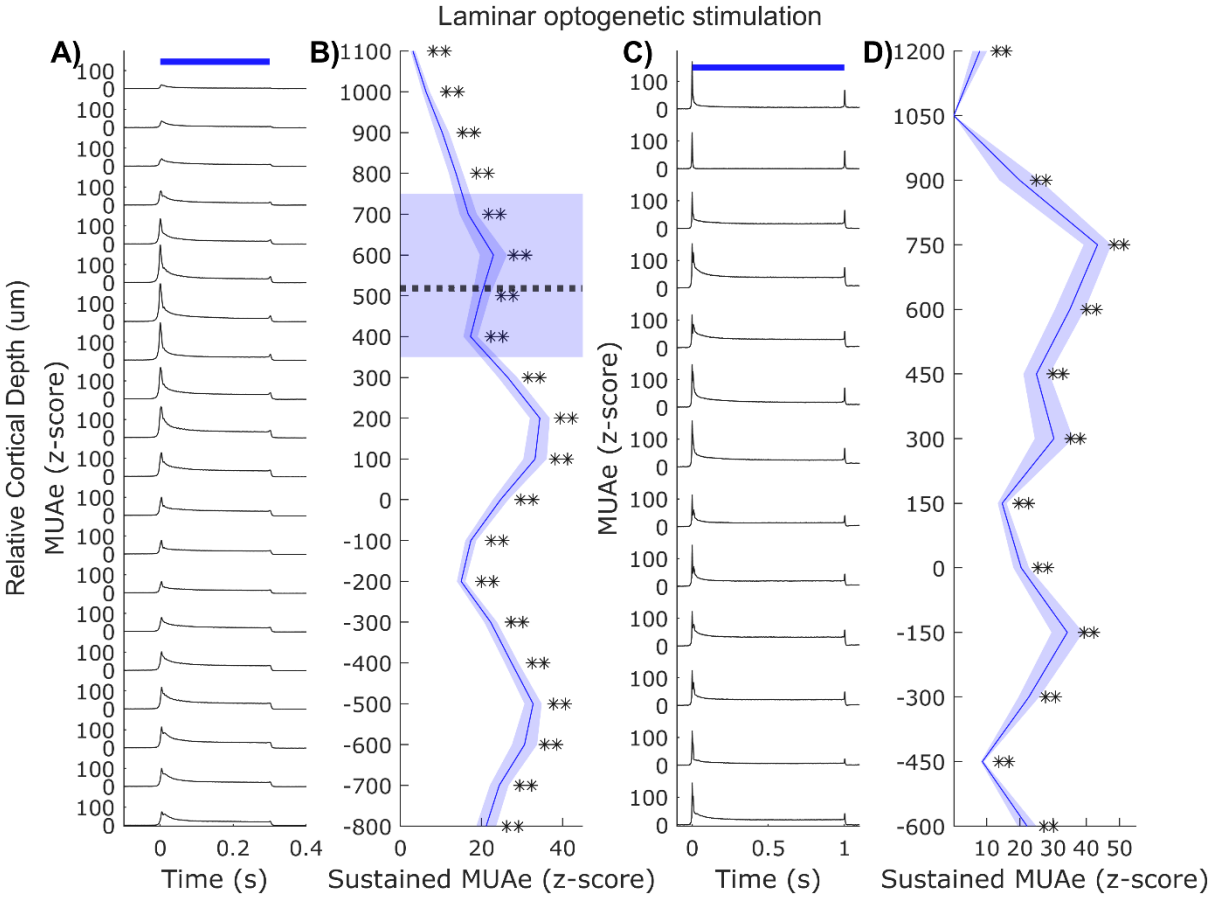

Figure 4.3 Optogenetic stimulation increases firing rates across the cortical layersA. MUAe responses (z-scored) to continuous blue light (300ms) averaged across sessions (n=22) for monkey Fl. **B.** Sustained (100-300ms) laminar activation pattern for the responses in **A**. The location of the optical fibre in the probe (relative to the cortical layer 4B) across sessions is presented in blue with a dashed line presenting the mean location. Significance is indicated by * for $p<0.01$ and ** for $p<0.001$. **C.** Similar to **A** for monkey Th with responses to 1s of continuous blue light (n=10). **D.** Similar to **B** but for monkey Th's sessions. Shaded bars are ± 1 SEM across sessions

(relative cortical depth ~400 to 1000 μm). The middle peak aligns with layer 4B (relative cortical depth ~100 to 300 μm). The deeper peak aligns with layers 5 and 6 (relative cortical depth ~-100 to -700 μm).

4.3.3 Optogenetically modulated activity aligns with opsin expression

To examine further the observed laminar activation pattern in electrophysiology, we compared it to the histological expression pattern across the layers. In monkey Fl, cells in layer 4Cβ were labelled using an antibody for vGlut2 (cell bodies in red, Figure 4.4B). This allowed precise alignment of the histological analysis results to the recorded laminar activity. Histological analyses indicated an increase in the percentage of

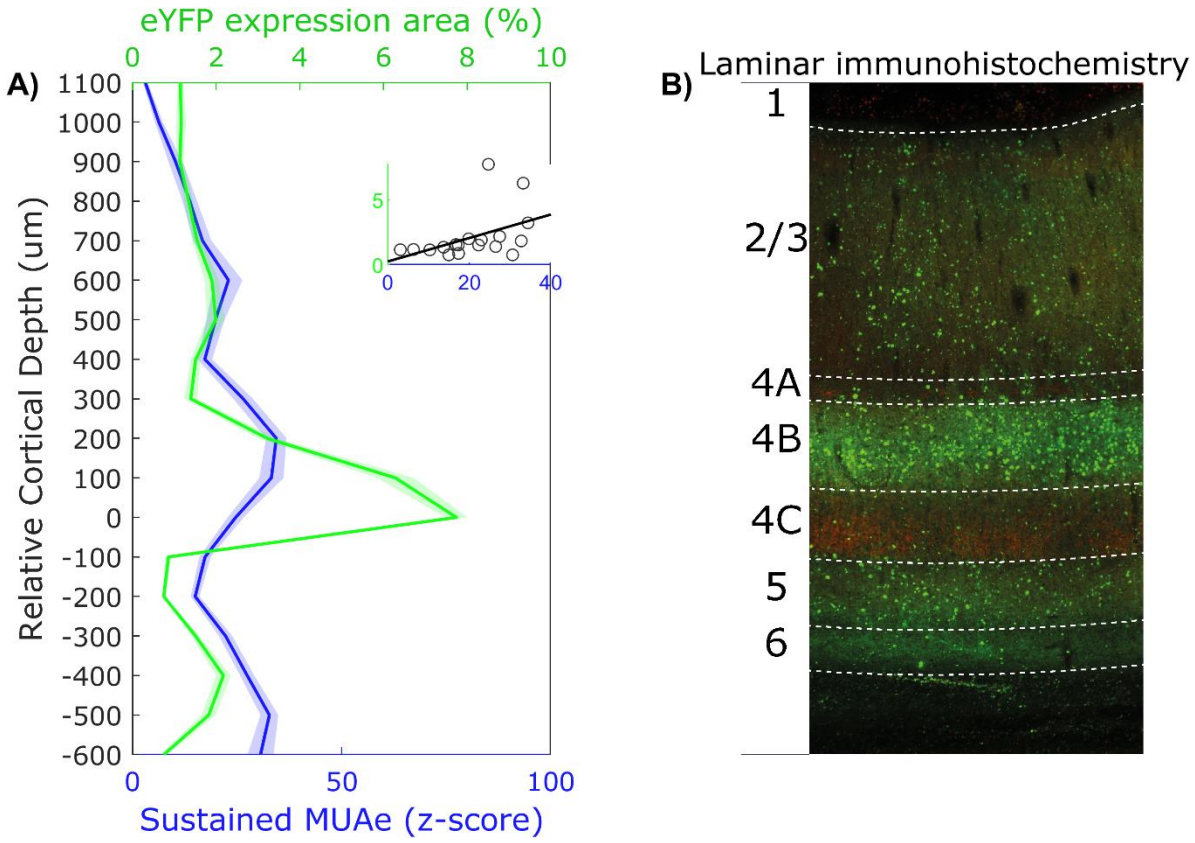

Figure 4.4 V1 neural activity closely matches immunohistochemistry expression. A. Sustained (100-300ms) laminar activation pattern (blue) for continuous (300ms) optogenetic stimulation and area percentage expressing eYFP (green) as a function of relative cortical depth (aligned to layer 4C). Alignment was calculated based on the earliest response to a visual stimulus. Shaded bars are ± 1 SEM across sessions. Inset: Scatter plot of values in A with the same colour codes with a line fitted to the data **B.** Laminar profile of V1 near the injection site. eYFP expression of the optogenetic construct can be seen in green, layer 4C (particularly 4C beta) was co-stained using an anti-vGlut2 antibody using standard immunohistochemistry (red).

eYFP positive cell expression in layers 4B, 5 and 6 with a less extensive expression in layers 2/3. To quantify the expression of the injected viral vector, the image was divided into 100umx100um regions of interest (ROIs, similar to the spacing of the electrode contacts) and the percentage of that area labelled with eYFP was calculated. Then ROIs values were averaged across multiple cortical columns (n= 10) covering a 1mmx1mm area of the injected V1. The eYFP expression was highly and significantly correlated to the laminar electrophysiological responses (Figure 4.4A inset, Spearman's $\rho = 0.5583$, $p = 0.017$). The number of cells expressing eYFP was calculated similar to the eYFP area and was not strongly correlated to neural activity and not significantly (Spearman's $\rho = 0.05$, $p > 0.05$).

4.3.4 Increasing stimulation intensity increases firing rates and reduces activation latency

Next, we examined the effects of varying the stimulation intensity on the laminar activation pattern and activation latencies across the cortical layers. All stimulation intensities (5mW, 20mW, 35mW and 50mW) caused a significant increase ($p<0.005$, Wilcoxon signed-rank test, except the most superficial channel for stimulation at 5mW, Figure 4.5A) in MUAe response to blue light. The laminar activation pattern was similar for the different intensities with two prominent peaks around cortical depths corresponding to layer 4B (200um) and layers 5 & 6 (-500um). The activation level uniformly decreased with the decrease of stimulation intensity; however, the activation pattern peaks at layers 4B, 5 & 6 decrease was much more pronounced for 5mW stimulation. In addition to the strength of the response, we examined the modulation of onset latencies across the layers (similar to chapter 3). Overall, activation latencies were low (<6ms for stimulation intensity >= 20mW and <12ms for the lowest stimulation intensity, Figure 4.5B) and within the characteristic range of ChR2 activation (Lin, 2012). The lowest activation latencies were observed closer to the light source; however, lower activation latencies were also observed at deeper channels with high MUAe responses. There was a significant and

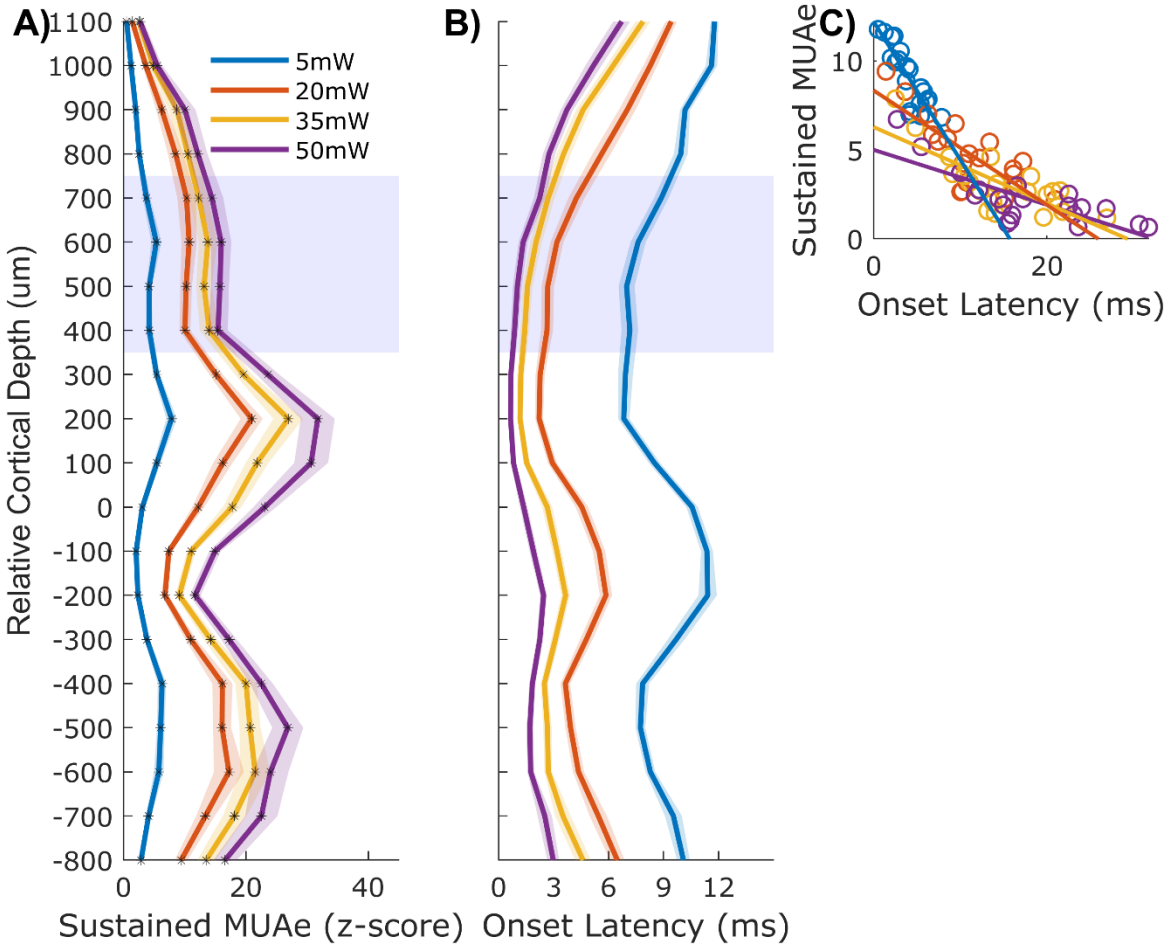

Figure 4.5 Stimulation intensity affects the laminar activation strength and latency. **A.** Sustained (100-300ms) laminar activation pattern for the different stimulation intensities. * indicates significance ($p<0.005$) of activation compared to baseline. **B.** Activation latencies across the cortical layers for the different stimulation intensities. The shaded rectangle indicates the location of the optical fibre in the probe (relative to the cortical layer 4B) across sessions. Shaded bars are ± 1 SEM across sessions. **C.** Scatter plot of Sustained MUAe vs the onset latencies for the different stimulation intensities with a least-square linear fit.

strong negative correlation between onset latencies and the strength of the evoked MUAe (Spearman's ρ = -0.87, -0.73, -0.73 -0.72 and $p<0.001$, Figure 4.5C).

4.3.5 Stimulation intensity increases LFP gamma and high gamma power

In addition to an increase in MUAe and a reduction in onset latencies, increasing stimulation power resulted in an increase in frequency power spectra in the low (35-80Hz) and high gamma (80-150Hz) ranges. For each session (n=17, one outlier session was excluded), the power spectra for the stimulation period were calculated (see methods) and the power was

averaged across the frequency bands of theta (3-8Hz), alpha (8-14Hz), beta (15-25Hz), gamma and high gamma and then the extracted powers for each band were averaged across sessions (Figure 4.6). Continuous stimulation, regardless of stimulation power, caused a significant decrease in power in the theta, alpha and beta bands along the cortical column

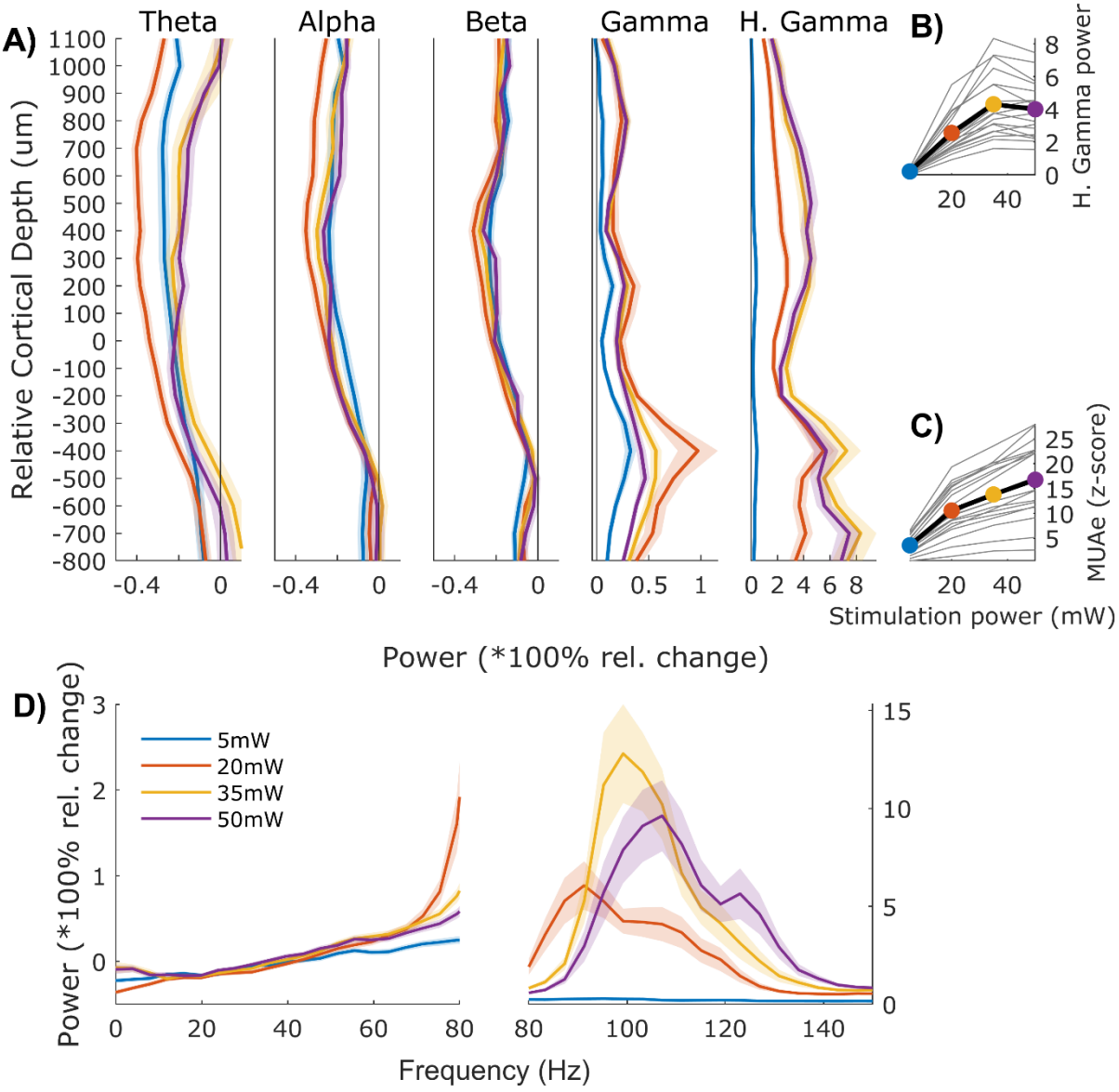

Figure 4.6 Continuous stimulation increases power in the gamma and high gamma ranges. **A.** Laminar profiles of the LFP power (relative change to baseline) in the theta (3-8Hz), alpha (8-14Hz), beta (15-25Hz), gamma (35-80Hz) and high gamma (80-150Hz) ranges. * indicates significant change from zero for the lowest stimulation power (5mW) and significance change due to stimulation power increase for the subsequent powers. **B.** High gamma power across channels for the different stimulation intensities. **C.** Sustained MUAe across channels for the different stimulation intensities similar to **B**. **D.** LFP frequency power spectra for the different stimulation intensities. Spectra were averaged across sessions and channels. There were broadband power differences but no significant peaks below 80Hz. Power levels represent relative change from the baseline where a positive value indicates an increase in power, Shaded bars represent S.E.M.

($p<0.0001$, one-way ANOVA test compared to no change in power); however, there were no significant differences between the stimulation powers in those frequency bands. Continuous stimulation caused a significant increase ($p<0.0001$, one way ANOVA test compared to no change in power) in gamma power but increasing stimulation power levels did not result in any further significant overall increase compared to lower stimulation powers (Figure 4.6B). For high gamma, the stimulation caused a significant increase in power and increasing stimulation power increased the high gamma power significantly ($p<0.005$, one way ANOVA tests) till it reached a plateau for the two highest stimulation powers (Figure 4.6C). The increase in high gamma power was highly and significantly correlated with the sustained MUAe levels (spearman's $\rho = 0.65$, $p = 0.0027$). All changes in power spectra for frequencies <80Hz were broadband with the only oscillation peaks emerging for higher frequencies (Figure 4.6D).

4.3.6 Higher rate of optical stimulation changes the laminar activation pattern

In addition to continuous stimulation, the effects of stimulation frequencies on MUAe recorded the different cortical layers were examined. Comparable to continuous stimulation, optogenetic stimulation at the different frequencies, 5Hz, 10Hz and 40Hz, increased the MUAe activity across the cortical column (Figure 4.7). However, pulsed stimulation resulted in significantly ($p<0.05$, Wilcoxon signed-rank test) higher activity compared to continuous stimulation for the same sustained duration (100-300ms post stimulation pulse train onset) in the supragranular layers of V1 for the 5Hz and 10Hz stimulation frequencies with a significantly increased activation in all channels for the 40Hz stimulation frequency (Figure 4.7). While the 5Hz and 10Hz stimulation frequencies caused a small and uniform increase in the laminar activation profile compared to continuous stimulation, 40Hz stimulation resulted in a much bigger and much more significant increase in activation in the supragranular layers ($p<0.001$, Wilcoxon signed-rank

test) with the overall activation larger than continuous or pulsed stimulation at lower frequencies ($p<0.0001$, one-way ANOVA).

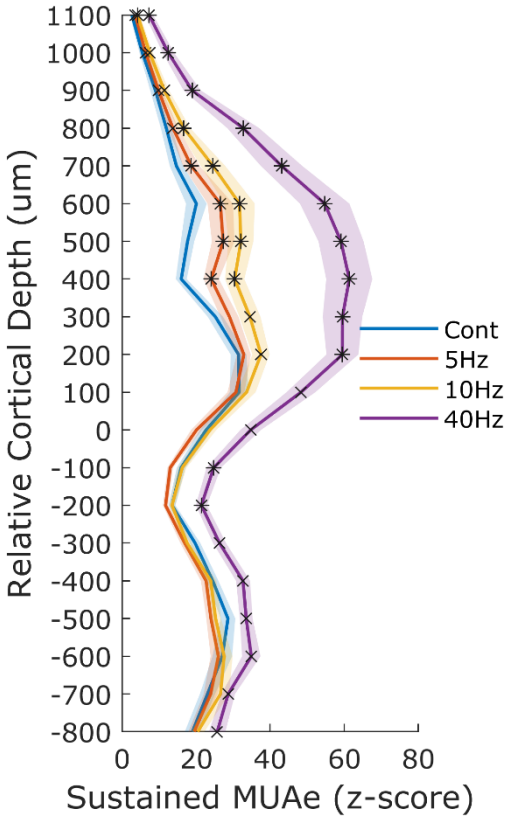

Figure 4.7 Stimulation frequency affects the laminar activation strength and pattern. Sustained (100-300ms) laminar activation pattern for the different stimulation frequencies. Significance of activation compared to continuous stimulation is indicated by x for $p<0.05$ and * for $p<0.001$. Shaded bars are ± 1 SEM across sessions.

4.3.7 Frequency entrainment

For pulsed stimulation, we examined the entrainment effects of stimulation frequency on the LFP oscillatory activity along the cortical column. For each stimulation frequency, the frequency power spectra were calculated, and the power averaged across three frequency bands centred around the stimulation frequency: theta (3-8Hz) for 5Hz stimulation, alpha (8-14Hz) for 10Hz stimulation and gamma (35-55Hz) for 40Hz stimulation (Figure 4.8A). The duration of analysis was adjusted to each frequency so that it includes two cycles (400ms for 5Hz, 200ms for 10Hz, 50ms for 40Hz) of the stimulation frequency instead of a fixed duration. This was done to avoid disproportional power increases due to including more cycles for the higher frequencies. Each stimulation frequency resulted in a significant ($p<0.001$, Wilcoxon signed-rank test) increase across all channels with a peak centred at the optical fibre locations for the 5Hz and 10Hz pulsed

stimulation (Figure 4.8A). For 40Hz stimulation, however, the peak was not centred at the stimulation sites and there was another smaller peak in the infragranular layers (-400:-200um Figure 4.8A). Additionally, an inspection of the LFP power spectra indicates peaks centred at each stimulation frequency and its harmonics (Figure 4.8C).

It is not clear, however, if the LFP oscillatory activity reflects the MUAe following the different stimulation frequencies and/or a reflection on the strength of the overall induced neural activity reflected by MUAe. To get

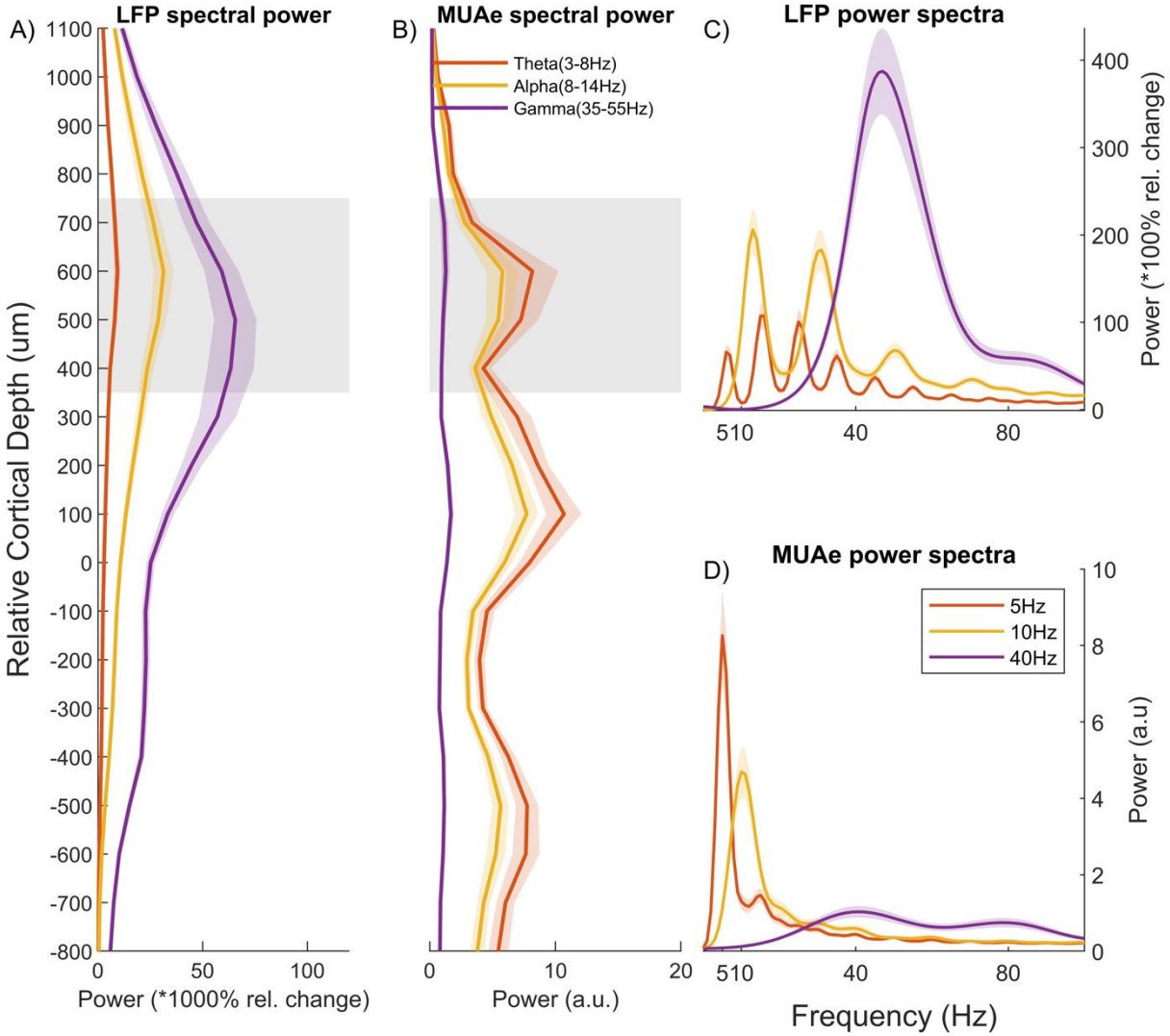

Figure 4.8. Frequency entrainment by pulsed stimulation. **A.** Laminar profiles of the LPF power (relative change to baseline) in response to each stimulation frequency infrequency bands centred around each stimulation frequency: theta (3-8Hz), alpha (8-14Hz) and gamma (35-55Hz). **B.** Laminar profiles of the MUAe power in response to each stimulation frequency similar to **A**. **C.** LFP frequency power spectra for the different stimulation frequencies. Spectra were averaged across sessions and channels. Power levels represent relative change from the baseline where a positive value indicates an increase in power. **D.** MUAe frequency power spectra similar to **C**. Power levels represent absolute power expressed in artificial units (a.u.). Shaded bars indicate S.E.M.

further insight, a simple multiple linear regression (MLR) model was built using three variables to predict the increase in the LFP spectra. The first variable was the distance from the stimulation site since the increase appears to be centred there. The second variable was the frequency power spectra of the MUAe signal as a measure of how closely neural activity follows the stimulation power. The MUAe laminar power spectra show strong oscillatory activity for the 5Hz and 10Hz stimulation frequencies with peaks at depths similar to the laminar activation patterns described earlier with a weaker and more uniform oscillatory activity for 40Hz (Figure 4.8B). Those patterns can also be seen in the MUAe power spectra (Figure 4.8D). While each stimulation frequency induced an oscillatory peak centred at this frequency, 40Hz stimulation resulted in a much smaller and broader peak than 5Hz or 10Hz stimulation. The third variable in the model was the overall evoked MUAe levels during the duration used for the LFP analysis; this variable represents the laminar activation patterns seen in the previous section. The results of each model are shown in Table 4.1. The models indicate a negative relationship between MUAe and LFP power spectra, especially for 40Hz stimulation, but a positive one between the LFP power spectra and the overall modulated MUAe strength. That suggests that the induced LFP gamma oscillatory activity is not exclusively generated by driving neurons at 40Hz, but rather due to overall increased activity.

Stim. Frequency	β	Error
5Hz	*Distance: -5.64 MUAe power: -1.59 *Mean MUAe: 2.67	0.62 0.54 0.2668
10Hz	*Distance: -18.95 *MUAe power: -6.89 *Mean MUAe: 6.87	2.00 2.29 0.64
40Hz	*Distance: -12.76 *MUAe power: -83.55 *Mean MUAe: 8.55	4.26 13.75 0.43

Table 4.1 Multiple regression models predicting the LFP change in power. For each stimulation frequency, one model is calculated with three variables: distance from the stimulation site, MUAe frequency power in the LFP band of interest and the overall MUAe level during stimulation. * indicates significance with $p<0.0001$. Only one variable was not significant with $p>0.05$.

4.3.8 Granger Causality reveals a frequency-specific directional flow

To get further insight into the flow of signals along the cortical depth, we performed bivariate spectral Granger Causality analyses. The resulting granger causality indices (GCIs) were integrated across 3 frequency bands centred around the pulsed stimulation frequencies: theta (3-8Hz), alpha (8-14Hz) and gamma (35-55Hz) (Figure 4.9A). To reduce the effects of linear mixed noise, we only included GCIs that passed a reverse granger

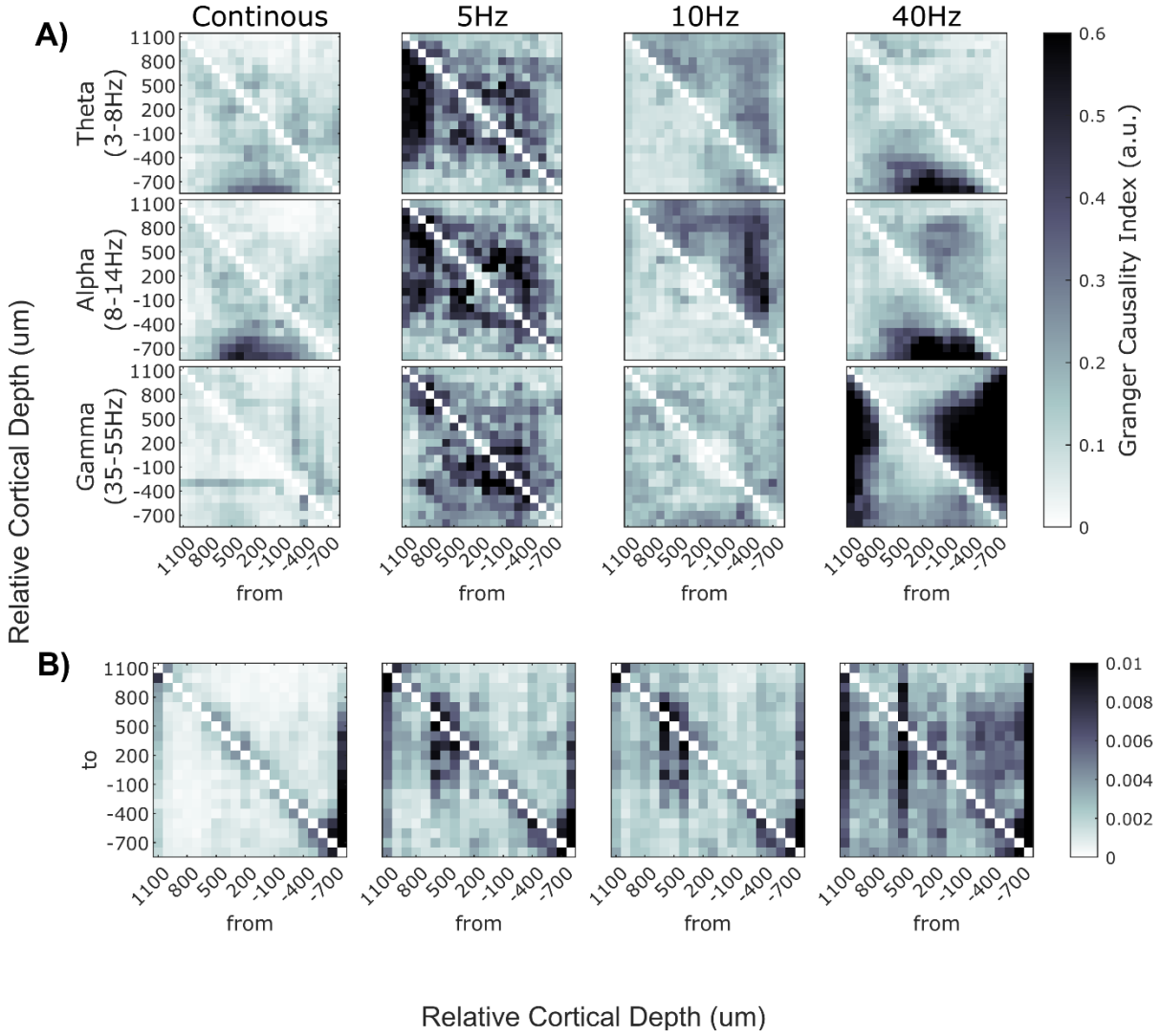

Figure 4.9. Frequency and time Granger causality metrics form continuous and pulsed stimulation for monkey Fl. **A.** Bivariate unconditional spectral GCIs for three frequency bands (Theta 3-8Hz, Alpha 8-14Hz and Gamma 35-55Hz) along the V1 cortical column. Sources of the flow are on the bottom with destination on top. GCI values are indicated by the colour bar on the right with a darker colour indicating a stronger effect. Analyses was performed on the last 200ms of stimulation and averaged across sessions with the RGT done on a session-by-session basis. **B.** Conditional time granger causality for the different stimulation frequencies. Duration of analyses and RGT are performed similar to **A**.

test (RGT) (Vinck et al., 2015). To pass RGT, the causality between two channels should reverse when the analysed LFP time course is reversed. Spectral GC revealed a downwards flow, to deeper layers, of the lower frequencies (3-14Hz) for both continuous and 40Hz stimulation (Figure 4.9A top two rows). Additionally, 40Hz stimulation showed a much stronger upwards flow, to granular/superficial layers, and downwards flow from the superficial layers to the rest of the column, in the gamma range (Figure 4.9A bottom row). 5Hz stimulation resulted in minor downwards flow from the supragranular and infragranular layers in the lower frequencies (theta and alpha, Figure 4.9A top two rows). Furthermore, 10Hz stimulation indicated a deeper origin of the lower frequencies that propagate upwards through the cortical column (Figure 4.9A, top two rows). In the time domain, GCIs indicate an outwards directionality emanating from the location of the stimulation fibre that is weakest for continuous stimulation and highest for 40Hz stimulation (Figure 4.9B). 40Hz, however, resulted in a slightly stronger upwards flow in addition to the fibre-centred flow.

4.4 Discussion

4.4.1 Optogenetic stimulation effects on the V1 microcircuit

In the previous chapter, optogenetic stimulation, using ChR2 as an opsin and hSyn as a promotor, was shown to modulate most of the recorded channels; however, it was not clear how those modulated channels are distributed across the different cortical layers. Identifying the geniculate input to V1, layer 4C, was a crucial step to identify the location of a recording channel relative to the cortical sheet. CSD analysis of visually evoked responses is often used to identify layer 4C (Bijanzadeh et al., 2018; Gieselmann & Thiele, 2020; van Kerkoerle et al., 2014) which was achieved by identifying the initial sink during the recording sessions. In addition, the onset of the earliest visually evoked MUAe response was used to identify layer 4C and produced similar results to the use of CSD in monkey Fl confirming the CSD initial sinks. For monkey Th, acquiring a

good visually evoked CSD proved challenging. As mentioned earlier, fixation training for monkey Th was not successful which limited the extent and number of experiments. Tasks requiring central fixation were not feasible with the animal; instead, we used a larger number of trials and a gaze-based selection of trials where the animal was looking at the screen. The resulting responses were aligned to the gaze of the animal rather than stimulus onset which explains the delayed response onsets based on post-saccadic responses in V1 (McFarland et al., 2015).

An attractive feature of optogenetics is the ability to selectively manipulate different compartments of the cortical microcircuit; a feature that is not possible with the traditional electrical microstimulation (Gilja et al., 2011; Histed et al., 2009) that can affect bypassing axonal projections and modulate the different cell types indiscriminately. Several optogenetic tools, such as opsins, promoters, viral vectors, and light delivery systems, have been developed enabling sophisticated and specific targeting. Animal models that enable transgenic lines have had great success in specific optogenetic targeting. However, in nonhuman primates, specific targeting remains a challenge. In our experiments, the promoter used, hSyn, targets both parvalbumin-positive and negative neurons (Diester et al., 2011; Watakabe et al., 2017) and should not be specific to either excitatory or inhibitory neurons. Despite that, most studies using optogenetics in vivo have found mostly excitatory responses, with an excitatory opsin, when hSyn was used as a promoter with a smaller inhibitory effect attributable to an indirect inhibition mediated by stimulation of inhibitory interneurons (Jazayeri et al., 2012; Ju et al., 2018). We have found similar results with an increase in neural activity in the majority of the recorded channels in response to blue light (see chapter 3). Similar patterns of mostly excitatory drive and indirect inhibition have also been observed when using CaMKII (Nassi et al., 2015); a promoter with higher specificity for excitatory pyramidal neurons.

The comparison of opsin expression patterns between studies is not a straightforward process. The limited number of optogenetic studies examining the laminar expression patterns, have revealed that expression depends not only on the promoter, but also on the viral serotype. For example, Gerits et al. (2015) found that even for the same promoter, CaMKII, different AAV serotypes resulted in different expression patterns. In that study, the authors have examined the expression of the hSyn promoter, but using an AAV7 virus which yielded more homogenous than that found in our study, using AAV9; however, since they found serotype dependence in expression, it is not surprising that their version of AAV-hSyn would result in a different expression pattern. A more similar expression pattern was found in the marmoset V1 resulting from using AAV9 and hSyn (Watakabe et al., 2015); however, the expression pattern found by Watakabe et al. was more extensive in the superficial layers compared to us. It is worth noting that the cortical nomenclature is slightly different between our study and Watakabe's study; however, considering the relative cortical depths, our expression patterns are similar. In our findings, we observed very strong expression in layer 4B followed by layer 5 and sparse expression throughout the cortical depth with an absence of expression in layer 4C. Jazayeri et al. (2012) used a similar viral vector (rAAV1-SYN1-ChR2(H134R)-mCherry) to the one used in this study and found a similarly concentrated expression in layer 4B, but with less pronounced expression in layers 5 and 6. Comparable histological findings to ours were found when an identical viral vector was injected into the marmoset somatosensory cortex (Macdougall et al., 2016). Taken together, existing literature and our findings indicate that even with a less specific promoter targeting, opsin expression and overall activation has a high degree of layer specificity.

Those studies examining the viral expression patterns in NHPs have been either mainly focused on the histology and testing the specificity of different viral vectors or have not reported the laminar electrophysiological

activation profile in response to optogenetic manipulation. In this study, we were able to clearly visualise layer 4Cβ using vGlut2 antibodies since vGlut2 is found in the projections from the thalamus to the cortical layer 4C in general, with a much higher density in layer 4Cβ (Garcia-Marin et al., 2019). This acted as a clear reference point in order to compare our histological findings to the laminar activation pattern. We found that the optogenetically modulated effects are spread along the cortical depth with two peaks that correspond proportionally to the expression of our viral vector in layer 4Cβ followed by layers 5 and 6. The strong correlation between viral expression and sustained activity suggests that the expression plays a more important role in the activation on the laminar scale than the distance from the light source which is useful for a potential optogenetic prosthesis. Another interesting finding in our study is the widespread activation as such activation was not observed in another study that utilised a similar approach; Andrie et al used a laminar probe attached to a tapered optical fibre to deliver light intracortically (Andrei et al., 2019). The authors have found the optogenetically modulated neural activity was confined to ±200um from the tip of the fibre and fell quickly outside that range. The spread of modulation was estimated based on the number of channels where increased activity could be observed. The authors, however, used a different promoter, CaMKII, and viral carrier, lentivirus, that could have resulted in a non-specific and perhaps less extensive expression and therefore no extensive or specific laminar activation pattern as a result. No histological data was presented in the study by Andrei et al. (2019), but the viral vector used was based on the study by Han et al. (2009) who found homogenous expression around the injection site in the deeper layers. However, both studies used different injection strategies with injections at single compared to multiple depths. Similar expression patterns were found in another study because of injections at single depths (Lerchner et al., 2014). We also found that the area of the cortex with eYFP fluorescence is better correlated with the laminar activation pattern than just the number of cells marked with eYFP. Those results would suggest

that a higher amount of viral expression per cell, resulting in higher opsin density, would result in stronger depolarisation currents and, as a result, optogenetic modulation. Schoenenberger et al. has found a positive correlation between opsin expression and the resulting current in vitro (Schoenenberger et al., 2008); the authors found that the increase in opsin density allows for a stronger response, to a limit, to increasing the stimulation power.

It is not clear, however, if the specific expression pattern observed in monkey Fl is the key to a strong optogenetic modulation along the cortical column or to further activation along the visual pathway. Indeed, with the viral vector used, we have observed activation in areas V2 and MT using fMRI and surface stimulation (Ortiz-Rios et al., 2021). This finding matches well with the known projections from layer 4B, where we observed the highest opsin expression, to V2 and MT (Nassi & Callaway, 2007). Therefore, with the goal of driving the overall across V1 layers and along the dorsal visual pathway to V2 and MT, then a similar expression pattern would be effective. That being said, it is uncertain which viral vectors can result in that expression pattern. Two previous studies have found similar opsin expression patterns, especially in layer 4B, when using an AAV virus with the hSyn promoter (Gerits, et al., 2015; Jazayeri et al., 2012); however, those studies have used different serotypes: AAV1 and AAV7. On the other hand, there is evidence that viral expression is dependent on the viral serotype used (Watakabe et al., 2015). Therefore, it is challenging to draw generalisable conclusions at this stage and more studies are required to increase our knowledge of the viral expression patterns in NHPs.

One possibility of the spread of optogenetic activation is a strong light intensity that utilises the higher opsin expression density. To examine this further, we examined the laminar activation profiles resulting from using lower light intensities and found that even using only 10% of the light intensity (5mW vs 50mW), there was a significant increase in MUAe along the cortical column. The laminar activation profile peaks around layers 4B

and 5/6 were considerably reduced for the lowest light intensity indicating a considerable decrease in opsin activity. The difference in activity in those layers could be explained by the higher opsin density in layers 4B, 5 and 6; higher opsin density would result in higher depolarisation currents in response to high-intensity optical stimulation (Schoenenberger et al., 2008).

A similar effect could be observed in the laminar onset latencies where an inverse correlation with the laminar activation pattern is observed. For the higher light intensities, the modulation onsets were very short <6ms confirming ChR2 activity and they were considerably increased for the lowest light intensity. Despite that increase in latency, it was still within the range of ChR2 activation (2-10ms: Lin, 2012) but indirect network effects cannot be excluded. For the initial response, the patterns of activation and onset latencies point to the effect of the expression pattern described earlier with peaks/troughs aligning with the expression peaks. Our fMRI findings show increased activation in extrastriate as well as subcortical regions in response to V1 optogenetic stimulation. While there are reciprocal projections between V1 and those regions (Klink et al., 2017; Lund, 1988; Marion et al., 2013), it is not likely that V1 activation is solely due to optogenetically stimulating V1 projections to other areas due to the low optogenetic activation latency. It is, however, possible that the interconnectivity could have contributed to the later stages of the activation and further experiments are needed to examine this further.

It is worth noting that the patterns of activation were similar between the two stimulation methods: surface stimulation (monkey Th) and intracortical stimulation (monkey Fl). In both animals, widespread activation was observed across the layers with similar locations of activation peaks; however, it remains unclear whether there is a difference between the methods regarding signal transmission to extrastriate or subcortical areas. As described earlier in the parallel study by Ortiz-Rios et al. (2021), surface stimulation was found, using fMRI, to activate extrastriate regions as well

as some subcortical regions. Intracortical stimulation was not used, however, in the fMRI study so it remains unclear if there is a difference and if intracortical stimulation is more effective in driving the connected subcortical areas such as LGN and the pulvinar (Fitzpatrick et al., 1994; Marion et al., 2013).

4.4.2 Optogenetic stimulation effects on V1 oscillatory activity

In our study, continuous optogenetic stimulation did not induce oscillatory activity in the LFP and we did not find any consistent peaks in the frequency power spectra <80Hz. This is different from Lu et al. who found that optogenetic stimulation in the macaque motor cortex consistently induced gamma oscillations that spread outwards from the stimulated site to nearby contacts (Lu et al., 2015). The authors used a different promoter, CamKII, and opsin, C1V1, but mainly targeted pyramidal neurons; however, while both targeted neurons and opsins are similar to our study, the stimulation used in that study was ramped up slowly compared to ours. Heitmann et al. suggested that such findings can be explained by the mixed targeting of excitatory and inhibitory neurons creating a bistable system where a ramping, up or down, the external drive would produce such oscillatory activity while a constant drive would not (Heitmann et al., 2017). In addition to the ramping stimulus, our excitatory effects could be much stronger than the indirect inhibitory effects and therefore not create a bistable system in the first place.

We found, however, that optogenetic stimulation resulted in significant changes in the overall power in all the traditionally examined frequency bands. Optogenetic stimulation resulted in a decrease in power with a similar laminar pattern across the lower frequency bands of theta, alpha and beta without significant differences between stimulation powers. Previous studies found that visual stimulation was associated with a decrease in alpha power along the cortical column in the macaque V1 with a pattern like what is found here with optogenetic stimulation (Scheeringa & Fries, 2019; van Kerkoerle et al., 2014); the decrease was the most

predominant in the supragranular and granular layers with a small increase in the infragranular layers. While our results do not show an increase compared to baseline, the alpha power is highest in the infragranular layers similar to what van Kerkoerle et al found. Slower oscillations (0-15Hz) in the sensory cortical areas have been found to be associated with the absence of stimuli and to be suppressed by visual stimuli (Buzsáki & Watson, 2012; Yu & Ferster, 2010). Current evidence suggests that those slower oscillations are generated in the infragranular layers and that they modulate firing rates across the cortical column, especially in the supragranular layers explaining the laminar pattern (Dougherty et al., 2017; Scheeringa & Fries, 2019; Spaak et al., 2012). Our spectral Granger causality analysis suggests a similar finding with alpha oscillations going in an upwards direction when stimulation was pulsed at 10Hz.

Additionally, our stimulation also resulted in an increased gamma across the cortical layers with a pattern that is very similar to the increase in gamma observed with visual stimulation in V1 (Self et al., 2013; van Kerkoerle et al., 2014). Gamma oscillations are often found in V1 to increase with visual stimulation with either a narrowband (Frien et al., 2000; Ray & Maunsell, 2011) or broadband (Friedman-Hill et al., 2000; Gieselmann & Thiele, 2020; Henrie & Shapley, 2005) patterns. The broadband increase observed with visual stimulation is a result of static stimuli which is similar to what we observe with continuous stimulation. Interestingly, the increase in the visual stimulation strength, such as an increase in contrast, was found to increase the induced gamma; a finding that we observed with our stimulation power increase as well. These findings suggest that our optogenetic stimulation of V1 drives the local circuitry in a manner that is very similar to static visual stimulation despite being an artificial drive. The increased gamma could be explained by an increase in coherence in the gamma frequency band; Henrie and Shapely suggest that if a stimulus is already driving a strong neural activity in V1, a stronger stimulus would instead increase the coherence between neurons

and neuronal oscillatory activity in the gamma band (2005). To our knowledge, there are no studies that examined neural oscillatory activity resulting from other artificial excitatory drives such as electrical microstimulation whether this activity reflects narrow or broad band increases.

Unlike the other slower frequency bands, increasing stimulation power significantly increased the oscillatory activity in the higher gamma band (>80Hz). High gamma has been found to be highly correlated with spiking activity (Jia et al., 2011; Ray et al., 2008; Ray & Maunsell, 2011) and that high gamma power can be used to predict the ongoing spiking activity (Rasch et al., 2008). Our results provide further evidence to those findings; there was a very high degree of correlation between high gamma power and the induced MUAe at each stimulation power. Furthermore, the increase in the induced MUAe with stimulation power was accompanied by a similar increase in high gamma power. This is not a surprising finding based on the literature, but it may be one of the first to show a causal relationship between high gamma and spiking activity. Additionally, the results might provide further evidence that high gamma might be a reflection of nearby spiking activity in addition to the directly recorded spiking; high gamma power increase was very minute for the lowest stimulation power where the light is less likely to spread far and modulate neurons further away. It also plateaued at the highest stimulation powers while the recorded spiking activity continued to increase.

4.4.3 Oscillatory entrainment by pulsed stimulation

In the previous chapter, we have shown that optogenetically modulated MUAe followed pulsed stimulation up to 40Hz with overall increased firing rates for 40Hz stimulation. The laminar activation pattern for the different stimulation frequencies showed very similar results for the 5Hz and 10Hz stimulation frequencies when compared to continuous stimulation; however, 40Hz stimulation was accompanied by much higher activity in the superficial layers of the cortex resulting in a very different LFP laminar

pattern. Electrical microstimulation delivered at ~40Hz has been shown to be much more effective in driving activity in connected cortical areas (Kampe et al., 2000; Murris et al., 2020). In fact, we found similar effects in the BOLD fMRI signal from remote activation of medial temporal (MT) and medial superior temporal (MST) areas resulting from 40Hz stimulation of V1 in a connected study (Ortiz-Rios et al., 2021). A potential explanation for the effectiveness of such frequency is the increased activity in the superficial layers that project to higher cortical areas (Salin & Bullier, 1995) possibly recruiting monosynaptic connections to the remote activated areas (Perkel et al., 1986).

Additionally, we found that while each stimulation frequency induces an oscillation at the used frequency, entrainment to 40Hz is a lot more potent especially in the superficial and deeper layers of V1. For the 5Hz and 10Hz, the strongest oscillations are induced near the optical fibre and fall off further away. A potential explanation is a stronger transient response in sites close to the embedded optical fibre contributing to the oscillatory power; this is supported by a stronger effect of distance to fibre in our MLR model. The MLR models suggest that the increased overall activity in response to 40Hz stimulation has the biggest effect on inducing the entrainment in the gamma band. It is less likely that LFP 40Hz entrainment is solely driven by the spiking activity drive at 40Hz; 40Hz approaches the frequency limits of the ChR2 opsin (Ramcharan et al., 2005; Yu et al., 2020) and the induced MUAe, while high, does not follow 40Hz closely as seen from the MUAe frequency power spectra.

A contributing factor to that gamma entrainment could be the nature of the V1 circuitry in those superficial layers. The MLR model suggests that the generally higher MUAe resulting from 40Hz is more correlated with the higher gamma oscillatory activity. Anatomical studies have long established that there are strong recurring connections between layers 2/3 and layer 4B with projections to the rest of V1 and extrastriate cortex (Blasdel et al., 1985; Lund, 1973, 1988). Indeed, those layers are usually grouped

together compromising a V1 feedforward compartment to higher cortical areas (Callaway, 1998). It is possible that 40Hz stimulation created a strong drive to this local network increasing the overall activity and inducing gamma oscillations. Those superficial layers have a higher percentage of GABAergic inhibitory interneurons (De et al., 2020; Fitzpatrick et al., 1987). GABAergic interneurons are thought to play an important role in the synchronisation of neurons and the generation of gamma oscillations (Kujala et al., 2015; Lozano-Soldevilla et al., 2014; Muthukumaraswamy et al., 2009; van Lier et al., 2018; Volman et al., 2011). The combination of GABAergic neurons and the interconnectivity of the superficial layers can shed some light on the bigger effect on gamma entrainment. Increasing evidence highlights gamma oscillation as a feedforward signature between brain regions (Bastos et al., 2014; Buffalo et al., 2011; Michalareas et al., 2016; Spaak et al., 2012; van Kerkoerle et al., 2014). In response to 40Hz stimulation, both time and spectral granger show the directionality towards layers 2-4B, the output compartment of V1, indicating a built-in quality of the network that responds more to gamma oscillations in a feed-forward manner. On a smaller local scale, Sohal et al. have shown that artificially driving neurons in the gamma frequency range improved information transmission between neurons in vitro (Sohal et al., 2009). We can see a similar pattern in the difference between continuous and 40Hz stimulation in the time granger causality with 40Hz resulting in overall increased connectivity in the V1 lamina. To our knowledge, no studies have examined the effects of gamma stimulation on the laminar scale and our study provides evidence of its effectiveness and unique effects.

It is not clear if 40Hz stimulation has unique effects on inducing gamma oscillatory activity or if it is a response to the increased overall activation. Our data suggest that the increased excitatory drive results in network resonance in the gamma range. A recent study found similar results of optogenetic stimulation of the cat V1 (Lewis et al., 2021); white-noise stimulation was used in addition to regular pulsed stimulation, and both

resulted in an increased gamma activity. This opens the way for future experiments examining if higher excitatory drives increase gamma oscillatory activity or if it is confined to stimulation delivered at gamma frequencies.

Chapter 5: Phosphene generation by optogenetic stimulation

5.1 Introduction

The ability to generate visual percepts or phosphenes by electrical microstimulation of V1 in humans has been established and refined since its inception over 50 years ago (Bradley et al., 2004; Brindley & Lewin, 1968; Schmidt et al., 1996). Tehovnik and Solcum first found that microstimulation of the macaque V1 affected visual perception (Tehovnik & Slocum, 2005) and later studies established that macaques could detect when microstimulation is delivered to V1 (Bartlett et al., 2005; Murphey & Maunsell, 2007). Shortly after, Tehovnik and Solcum established that the macaques indeed reported a visual percept in an area confined to the locations of the visual field corresponding to the stimulated neurons (Tehovnik & Slocum, 2007). Following this, Schiller et. al. (2011) used a new paradigm to specify the size and colour of the generated phosphenes; a two-alternative forced-choice (2AFC) task was used to compare the generated phosphene to visual stimuli and based on the animal's choices, the properties of the phosphenes could be inferred. In the study, the animals were initially trained to compare two visual targets and make a saccade to the target with either higher contrast or larger size; when the choice probability was at the level of chance, that indicated that both targets were perceptually similar to the animal. Schiller and colleagues then replaced one of the visual targets with microstimulation and identified the size or contrast of the phosphene as the size or contrast of the target with equal choice probability. While microstimulation of the macaque V1 has been since firmly established as a method to induce visual phosphenes (Foroushani et al., 2018) and generate distinct shapes (Chen et al., 2020), optogenetics has not.

Compared to the rich knowledge acquired about phosphene generation from electrical microstimulation, still very little is known about the

perceptual consequences of optogenetic stimulation. Optogenetic manipulation of the macaque V1 has been successful in modulating responses to visual stimulation by masking (Chen et al., 2022), indirect suppression (De et al., 2020) and augmentation of the visually evoked neural response as well as behavioural performance (Andrei et al., 2019). Jazayeri and colleagues were the first to elicit behavioural responses by optogenetic stimulation of V1 in the absence of visual stimuli (Jazayeri et al., 2012). They found that optogenetic stimulation elicited saccadic eye movements to the receptive field of the stimulated neurons, but did not confirm phosphene generation. Ju et al. (2018) later confirmed phosphene generation by using a Go/No Go task, but did not examine the nature of the phosphene. In this chapter we describe the results of a saccade to target task and a 2AFC task adapted from Schiller et al. (2011); our 2AFC task did not compare the generated phosphene to visual stimuli directly but instead compared the detection of different visual stimuli to the detection of the generated phosphene.

5.2 Methods

5.2.1 Saccade to target task

To examine if the animals can detect optogenetic stimulation, monkey Dp was trained on a saccade to target task. In the task, the animal maintained central fixation (within a <1° window) and after a random interval (500-1000ms), a white Gabor patch (1° in diameter, with luminance increase of 1-14% above the background) appeared at random locations equally distributed throughout the monitor (Figure 5.1) with different levels of luminance increase over the background. The animal received a reward upon making a saccade to the disk's location. In a subset of the trials (25%), instead of visual stimulation, continuous optogenetic stimulation was delivered epidurally via an optical fibre placed on the surface of the tissue. The optical fibre was connected to a blue LED (450nm, 50mW). The fibre was placed through a chamber cap and then the cap is closed to

ensure no light leakage. The animal received a reward upon making a saccade to the lower left quadrant visual field following optogenetic stimulation. Another subset of the trials (25%) consisted of catch trials; there was no visual or optogenetic stimulation and a reward was received if the animal maintained its fixation.

5.2.2 Receptive field mapping

To identify the receptive field (RF) of the recorded neurons, automatic RF mapping was performed. Animals were required to fixate and maintain fixation centrally at a red dot (0.2° in diameter); during fixation, black squares were presented at pseudorandom locations in the lower left quadrant of the visual field on a 5x5 grid for 100ms at each location with at least a gap of 100ms since stimuli were not allowed to appear on the same site twice in a row. The resolution of the mapping was progressively increased by decreasing the size of the presented squares (down to 0.5/1° in width). The mean MUAe response for each grid location was calculated for 30-100ms after stimulus onset and then used to estimate the centre of the minimum response RF (mRF) (Angelucci & Sainsburry, 2006; Barlow et al., 1967). Mapping stopped after obtaining a minimum of 10 trials per site.

5.2.3 Two-alternative forced-choice (2AFC) task

After RF centre identification, monkey Fl was required to perform a two-alternative forced-choice (2AFC) task with three alternatives with the same probability. The animal was required to maintain fixation centrally (within a window <1°) for a random duration between 500ms and 1250ms. After fixation, two targets (disks, 0.3° in diameter) appeared in the upper visual field ~4° away from the fixation point accompanied by one of the following: 1) a 1° white disk with varying luminance levels (2.5%, 5%, 10%, 15% and 20% increase above the background) is presented in the calculated RF, 2) optogenetic stimulation (continuous at 50mW) or 3) no visual or optogenetic stimulation representing a catch trial (Figure 5.3); all trial types were interleaved in the same session. A correct response was

detected when the animal made a saccade to the left target in response to visual or optogenetic stimulation regardless of the location of the stimulus and to the right target in the absence of any. If the animal did not respond quickly (within 600-800ms), the trial is aborted and once the animal responds to either target, the stimulation is extinguished. Initially, the animal was trained on a version of the task with only visual stimuli and catch trials and once that task was done successfully with an above-chance accuracy, we added the optogenetic component. The animal was rewarded when making a saccade to the left upon detection of a target, visual or optogenetic, or to the right in catch trials. The trials were divided equally between the three trial types. Additionally, the coupling between the optical fibre and the probe was covered to ensure that the animal cannot see the light and avoid any biases.

5.2.4 Eye movement analyses

The response of the animals was reported with eye movement and performing saccades to specific targets. The eye position was recorded after calibration to visual degrees by MWorks as described in chapter 2. Saccades were detected by first calculating the horizontal and vertical velocities of the eye movement (Engbert & Kliegl, 2003) with a 5ms moving window; velocity amplitude was then calculated from the horizontal and vertical components. Saccades were detected when the velocity amplitude crossed a threshold defined as 6 times the median estimator of the velocity amplitude for the horizontal and vertical components. Engbert and Kliegl suggest using the median estimator instead of the standard deviation as it provides more robustness to noise (Engbert & Kliegl, 2003). The peaks of the resultant eye velocity during a trial were used to calculate the number of saccades.

5.2.5 Pupil size changes

In addition to the eye position, the eye-tracking system allowed the recording of pupil diameter expressed in artificial units. We examined the

pupil size changes as an additional implicit measure that could shine some light on the nature of the elicited phosphene; a recent study found that pupillary constriction can reflect the saliency of a stimulus (Pandey & Ray, 2021; Yamagishi & Furukawa, 2020). Pupil size changes (dilatation/constriction) were estimated by calculating the relative change from the baseline by subtracting and then dividing by the average baseline (before target/stimulus onset) diameter (Peinkhofer et al., 2019).

5.3 Results

5.3.1 Saccade to target task

Across sessions (n=5), monkey Dp detected visual stimuli with a high success rate for all locations and luminance levels (~99%) and the performance of the visual trials was pooled together for all locations (Figure 5.1A & B). The saccade window for the trials with optogenetic stimulation was located in the lower-left quadrant and the animal received a reward when a saccade was made within this window. Monkey Dp had a high success rate in opto trials as well (~95%). However, for catch trials, the animal performed at the level of chance (Figure 5.1B). During failed catch trials, the animal made saccades to the lower-left quadrant similar to opto trials (Figure 5.1A, catch trials' eye traces in blue). The animal's responses during opto trials were slower (mean ~= 560ms) compared to visual trials (mean ~= 180ms). The successful catch trials' eye traces and response time reflected the additional fixation time required by the task (Figure 5.1A & C). When we examined the performance for opto trials with lower RTs

that can be compared to visual RTs (<350ms), we found that the animal's performance fell to 21.41±4.7%.

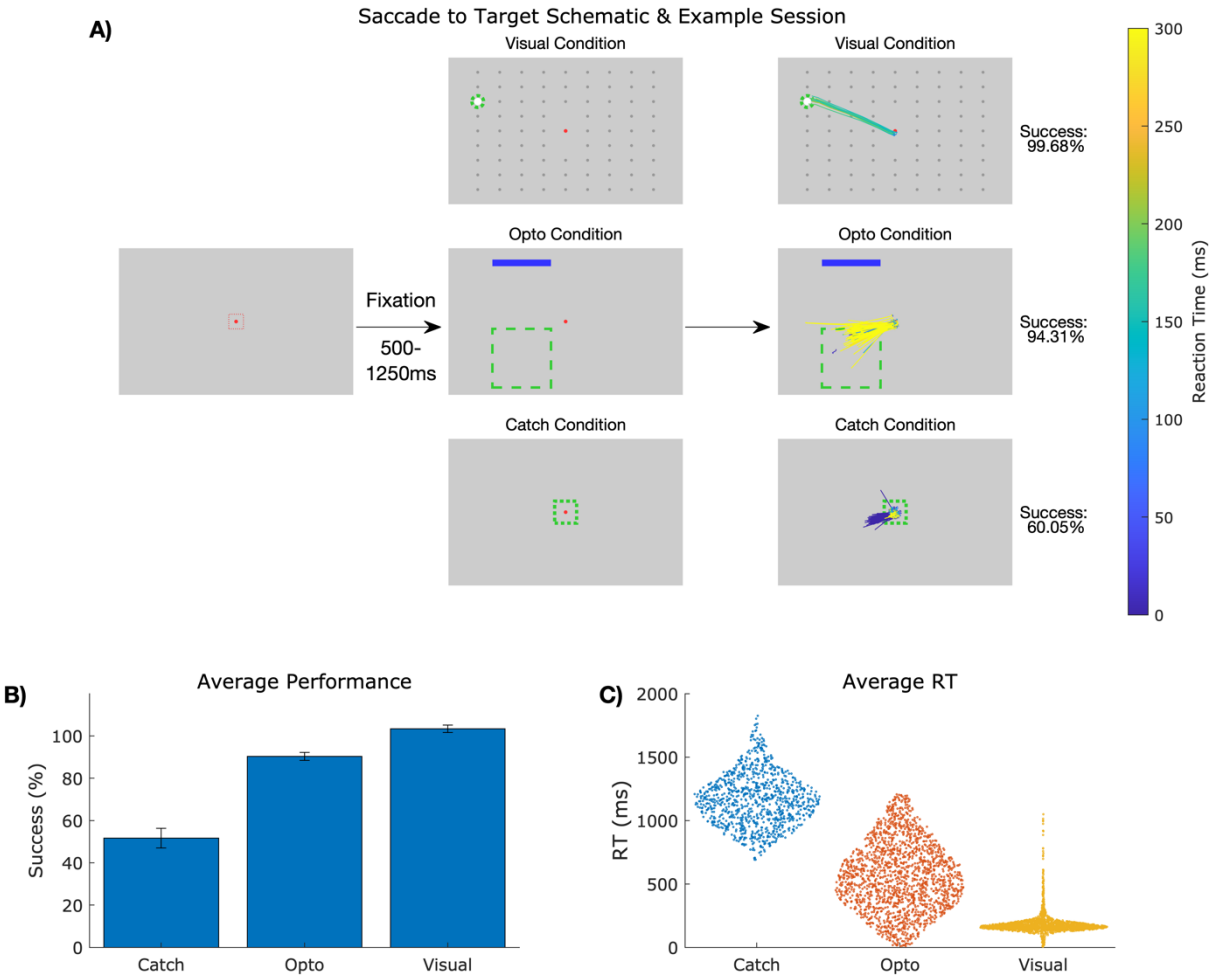

Figure 5.1 Saccade to target task schematic and performance. **A.** Task schematic and example session performance and eye traces for successful trials. The animal was required to maintain central fixation for 500-1000ms. Visual trials included a white Gabor patch (1deg) appearing at randomly selected locations across the screen (grey circles, top middle panel) and the animal was required to make a saccade to this location (top left panel). Opto trials, continuous blue light was delivered epidurally and the animal received a reward for making a saccade to the lower right quadrant (middle panels).In catch trials, the animal was required to maintain additional fixation time to receive a reward (bottom panels). Colour bar indicates reaction time for the eye traces and for catch trials, failed trials are also plotted in blue. **B.** Performance across sessions (n=5) for the three conditions. Error bars indicate S.E.M. **C.** Swarm plot of the reaction times across the three conditions.

5.3.2 Receptive fields (RF)

For monkey Fl, RFs were mapped using the MUAe responses (Figure 5.2A). For each session, RFs were compared along the laminar probe channels. Even though the RF properties change across the lamina (Gilbert, 1977), the location of the RF should be similar along the same cortical column

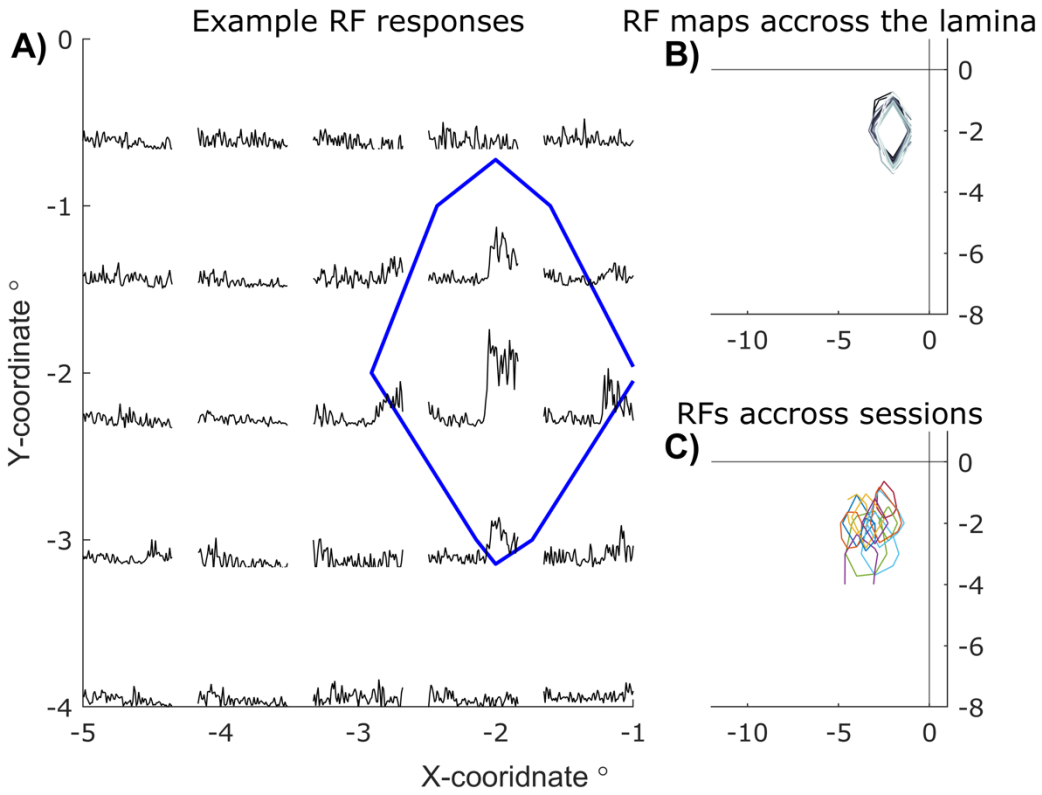

Figure 5.2 Automatic RF mapping in monkey Fl. **A.** Example MUA responses (black) to each grid location from -50ms to 100ms post stimulus onset. Blue line represents the contour of the mean MUAe responses with the boundary down to 30% of the peak response in the centre. **B.** RF contours similar to **A** for channels along the laminar probe. Data are from the same session as in **A**. **C.** RF contours across sessions (n=13). For each session, the RF maps were averaged across channels.

(Bijanzadeh et al., 2018; Callaway, 1998; Hubel & Wiesel, 1962). In our experiments, the RF mapping results were consistent indicating that the probe is perpendicular to the V1 surface and that we are recording from the same cortical column (Figure 5.2B). Across sessions (n=13), automatic RF mapping was done with a 0.5°-1° resolution (Figure 5.2C) and the location of the RF was confirmed online by placing a visual stimulus (1° drifting gratings disk) in the RF centre and listening to the spiking activity. The RFs of the cortical sites used in the 2AFC experiments are between 2°-5° from the fovea (Figure 5.2C).

5.3.3 2AFC performance

Monkey Fl was successfully trained on the visual version of the 2AFC task before adding optogenetic stimulation to the experiment (Figure 5.3A). The detection performance of the visual stimuli increased with the increase in

luminance with the lowest luminance level detection at the level of chance (Figure 5.3B). When optogenetic stimulation was added to the task, the animal successfully reported the detection of stimulation by making a saccade to the left target with a success rate >80% (Figure 5.3B). In addition to successful detection of both visual and optogenetic stimuli, the success rate with catch trials was high, >85%, indicating a correct rejection and reporting of stimuli absence. Across sessions (n=13), the animal detected optogenetic stimulation with a high success rate, >75%, and performance corresponding to a visual stimulus with a 5-10% luminance

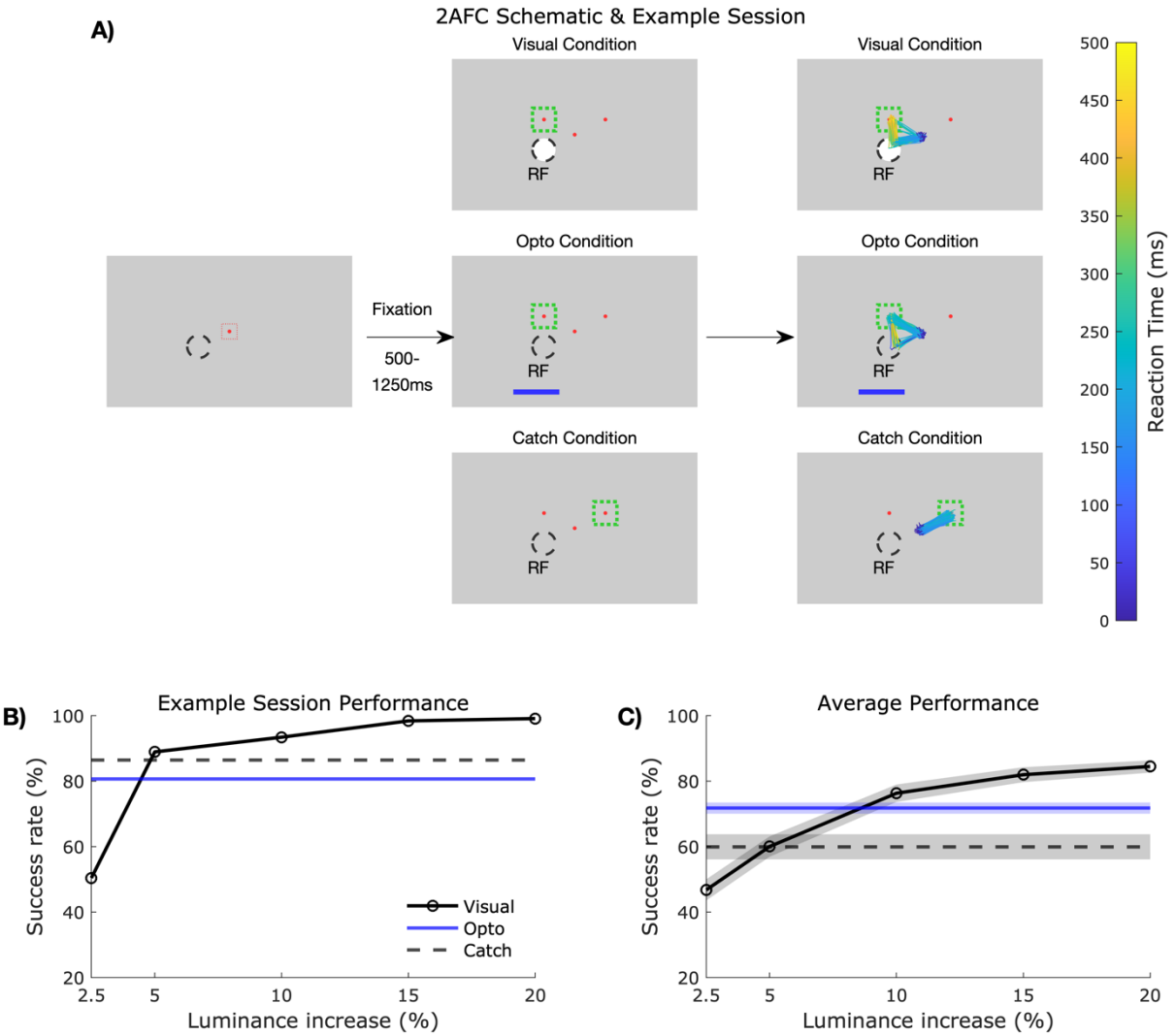

Figure 5.3 Two-alternative forced choice (2AFC) task reveals visual percept generation by optogenetic stimulation of V1. **A.** Schematic representation of the different conditions in the task. Dashed green squares indicated the correct target choice for each condition. Left panel includes example eye trajectories for successful trials in each condition with the time course indicated by the colour bar on the right. **B.** The performance of the animal for the example session in **A** with visual trials performance (solid black), opto (blue) and catch (dashed black) trials. **C.** The performance of the animal across sessions (n=13) similar to B.

increase. The performance of the catch trials decreased slightly in later sessions but was still above chance.

5.3.4 Saccadic patterns and reaction times

In addition to the detection success rate, I examined the saccadic patterns and reaction times (RTs) to get more insight into the generated percept and how fast the animal responds during the different conditions. RTs were calculated based on saccade detection, as described earlier in the methods. For visual trials, RTs decreased with the increased luminance (Example session, Figure 5.4A) which is to be expected with increased stimulus saliency (Chen et al., 2013). For opto trials, RTs were between those corresponding to a 5% and 10% increase in luminance but closer to 5% (Figure 5.4A). RTs were consistent across sessions with opto RTs being between the RTs for a 5% and 10% luminance increase. RTs were based on the detection of the first saccade because the designed 2AFC paradigm

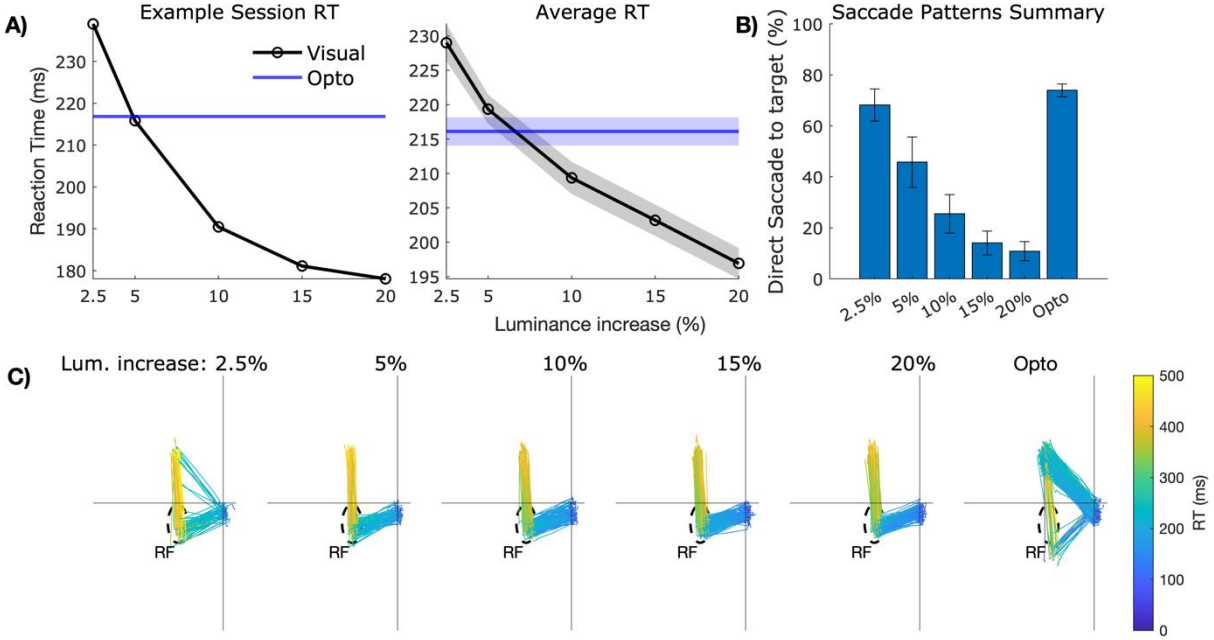

Figure 5.4 Saccadic reaction times (RT) and patterns for the opto condition are comparable to visual conditions. **A.** (left) Example session RTs for the visual conditions at the different luminance increase levels (black) and the opto condition (blue). RTs are calculated from the onset of stimulation. (right) RTs across sessions with shaded lines representing ± S.E.M. **B.** Summary of direct to indirect saccade ratios across sessions. Opto trials responses are similar to responses to visual stimuli with low luminance. Error bars represent S.E.M. **C.** Eye traces of direct and indirect saccade patterns in response to the different visual stimuli as well as optogenetic stimulation. Visual stimuli with higher luminance results in higher ration of indirect saccadic responses. Colour indicates the latency of the plotted eye traces with colour bar on the right.

did not restrict the saccade trajectory of the animal and we observed that the animal either makes a saccade first to the stimulus in the RF before the target or directly to the target (example session in Figure 5.4C). In the visual conditions, the trajectories of saccades changes based on the luminance of the stimulus. Lower contrast stimuli were often accompanied by direct saccades to the target (Figure 5.4B) while higher contrast stimuli were more likely accompanied by a saccade to the stimulus first before the target. Some of the opto trials were also accompanied by a saccade to the RF first before the target (example in Figure 5.4C) not different to the pattern observed with lower contrast stimuli (Figure 5.4B).

5.3.5 Presaccadic pupil size changes

For the 2AFC task, we also examined the pupil diameter changes before the execution of saccades to either target in correct trials, left target for visual and opto trials and right target for the catch trials (Figure 5.5A). For each trial condition, we extracted pupil diameter changes for the 100ms before the execution of the first saccade (direct or indirect) incorrect trials. In all

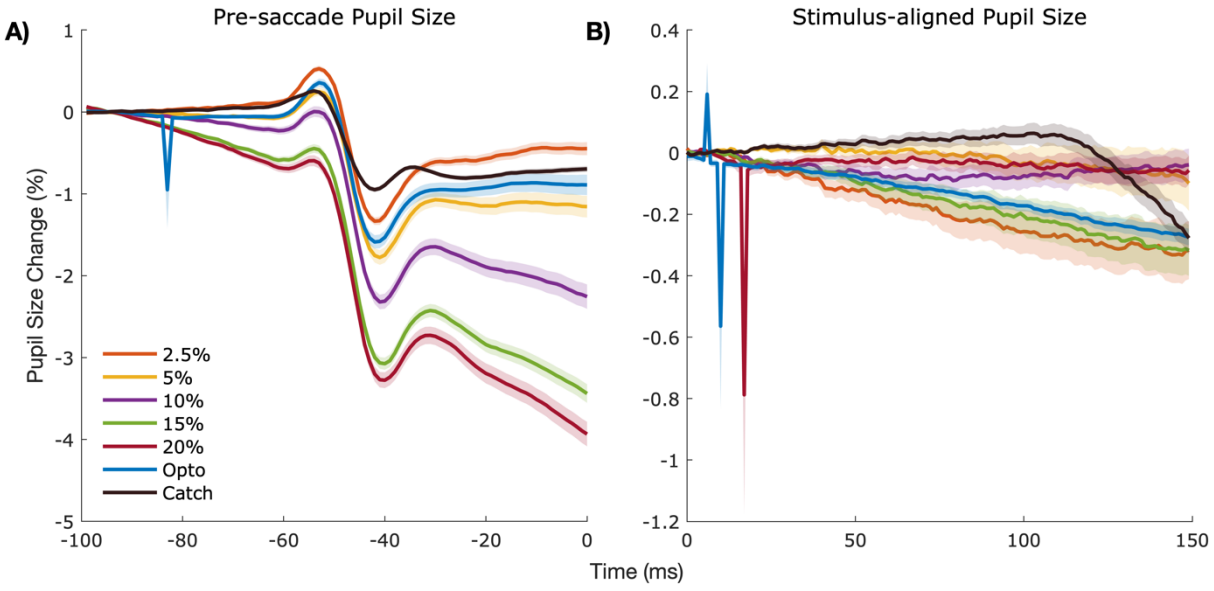

Figure 5.5 Pupil size changes in response to visual and optogenetic stimulation. **A.** Pupil size changes before (-100ms to 0ms) the first saccadic response for correct trials across conditions. Increasing visual luminance increased pupil constriction and pupil restriction to optogenetic stimulation was similar to that of visual stimuli with lower luminance. **B.** Pupil size changes aligned to stimulus onset (0ms to 150ms independent of RT) for correct trials. For catch trials, pupil size changes are aligned to the end of the fixation period.

trial types, saccadic responses were preceded by pupil constriction (Figure 5.5A). For visual trials, pupil constriction increased with the increase in luminance. For opto trials, pupil constriction was similar to the lower luminance visual stimuli. Pupil constriction was the least for correct catch trials. To examine if the observed constrictions can be attributed to a pupillary reflex to the increased luminance, we also examined the pupil diameters changes aligned to targets onsets. This resulted in alignment to the visual and optogenetic stimuli onsets and to the end of the fixation period for catch trials. There were no discernible effects of increased luminance on pupillary constriction or differences between the trial types (Figure 5.5B).

5.3.6 Stimulation power effect on phosphene induction

In a small subset of sessions (n=3), a lower stimulation power (35mW) was tested in addition to the typical stimulation power (50mW) used in the 2AFC paradigm described earlier. On average, decreasing the stimulation power resulted in a small decrease in performance (<2%) and a small increase in reaction time (<2ms). However, the differences were within the standard error of means range across the sessions (Figure 5.6).

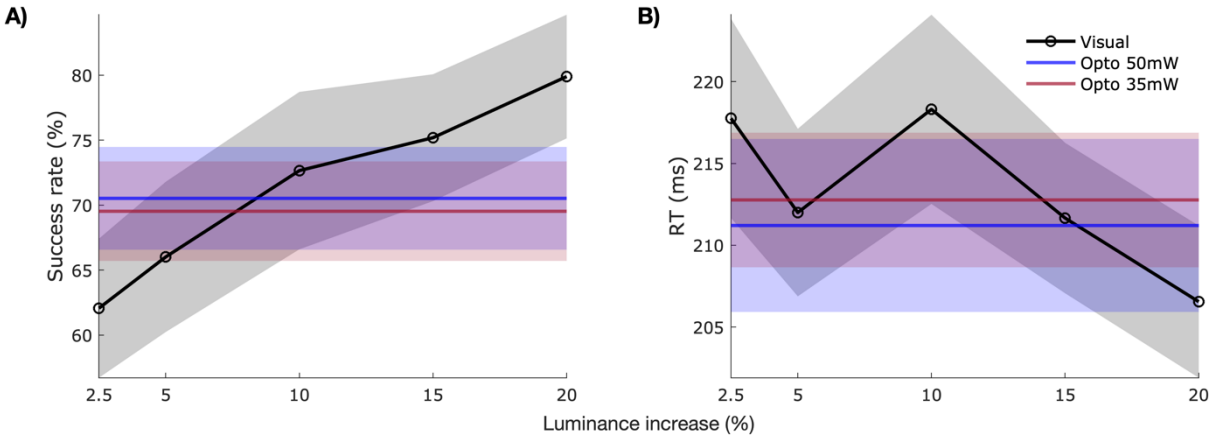

Figure 5.6 Stimulation power effect on optogenetic stimulation detection. **A.** 2AFC performance across the visual trials (black) and optogenetic stimulation at 50mW (blue) and at 35mW (red). **B.** Saccadic RTs for the different conditions similar to **A**.

5.3.7 Neural activity reflects 2AFC task performance

We examined the evoked MUAe by the different task conditions across sessions (n=12). For analysis, we selected trials with a minimum duration of 150ms (based on RT) and compared the sustained evoked responses (50-150ms post-stimulation onset for visual and optogenetic stimulation and post target onset for catch trials). We found that the evoked MUAe activity was higher for correct compared to failed trials (example Figure 5.7A) with the difference being significant across sessions (p<0.001, one-

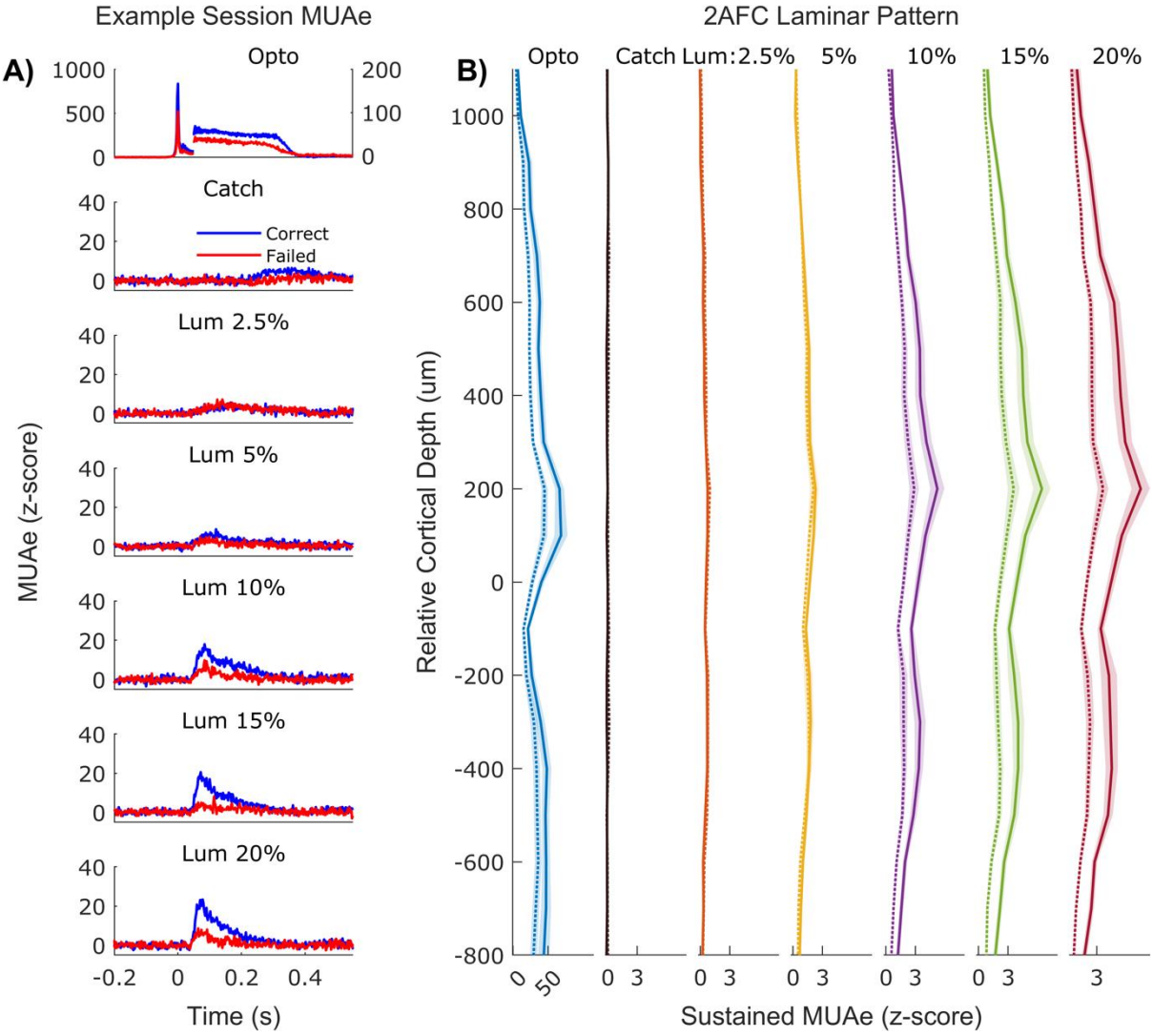

Figure 5.7. Neural activity across the 2AFC conditions reflects performance. **A.** Example MUAe responses from one channel for the different conditions for both correct (blue) and failed (red) trials. Time indicates time from the stimulation onset for visual and opto trials and from the target onset for catch trials. **B.** Laminar activation pattern for the sustained (50-150ms) MUAe across sessions and conditions for correct (solid) and failed (dotted) trials. Note: for catch trials, both failed and correct trials were not accompanied by an evoked MUAe. Shaded bars represent S.E.M.

way ANOVA) for the opto trials and visual trials with higher luminance (10-20%, Figure 5.7B) similar to findings in figure-ground segregation(Lamme et al., 2001). In visual trials, we also observed an increase in the evoked MUAe corresponding to an increase in luminance (Figure 5.7A & B) which is to be expected from responses to increasing contrast in V1 (Henrie & Shapley, 2005). The optogenetically evoked MUAe was much higher than that of the visual stimuli even at the highest luminance values; however, there was still a difference between correct and failed trials (Figure 5.7B). Catch trials did not result in an increase in MUAe (example in Figure 5.7A & summary in Figure 5.7B). Attention has been found to modulate the cortical baseline activity possibly contributing to the inter-trial variability (Ress et al., 2000). The baseline values were pooled across channels and sessions and compared for the correct and failed trials; no significant differences were found between baseline values based on performance ($p>0.8$, one-way ANOVA).

5.4 Discussion

In the pioneering study by Schiller et al. (2011), electrically generated phosphenes were directly compared with visual stimuli with varying properties. Based on those comparisons, the phosphene properties can be inferred at the point of equal choice probability. Additionally, the microstimulation currents were varied illustrating their effects on phosphene contrast, size and colour. While it has already been established that microstimulation of the macaque V1 reliably generates phosphenes (Tehovnik et al., 2005; Tehovnik & Slocum, 2007), optogenetic stimulation has not yet been established as a method to induce behavioural changes on its own, especially in V1. Jazayeri et al. were able to show direct effects of stimulating V1 using ChR2 when the authors found that spontaneous post-fixation saccades were directed towards the RF of the stimulated neurons (Jazayeri et al., 2012). The study did not establish, however, that an optogenetically induced visual percept lead to the described saccades.

Direct saccade induction by stimulating projections to the superior colliculus is a possibility; however, the saccade latencies were too long (Tehovnik, Slocum, & Schiller, 2003) making this explanation more unlikely. Therefore, it was imperative to include the appropriate controls in our task to confirm phosphene generation.

5.4.1 Saccade to target task and potential bias

Our first attempt in examining phosphene generation via optogenetic stimulation was using a saccade to target paradigm similar to a paradigm used by Tehovnik and Solcum (2005). One major shortcoming of our implementation of the task is a lack of electrophysiological recordings during the experiments; there were technical issues that prevented recordings at the time. As described earlier, however, another ongoing fMRI study found optogenetic modulation of the BOLD signal (Ortiz-Rios et al., 2021) providing evidence of successful optogenetic modulation if weak. The lack of electrophysiology prevented us from mapping the RF of the stimulated neurons and placing a smaller and more localised saccade response window for opto trials. Consequently, we can see that bias was induced in the animal's behaviour. That bias is clear in the animal's performance in catch trials; to maximise reward probability, the animal made more frequent saccades to the lower right quadrant if uncertain. Qualitatively, we observed saccades towards the lower left quadrant with optogenetic stimulation at the first session, likely before bias was induced, and quantitively there is a percentage of successful opto trials with faster RTs; however, it is difficult to conclude if there was an optogenetically induced visual percept. From the following experiments, we also found that the generated phosphenes have low contrasts possibly contributing to the animal's uncertainty and bias. This uncertainty is aggravated by the lack of electrophysiology data confirming optogenetic modulation in monkey Dp. In a separate series of fMRI experiments, we observed optogenetically induced effects in monkey Dp suggesting that there was indeed some

optogenetic effects even if not found in electrophysiology (Ortiz-Rios et al., 2021).

5.4.2 Generation and nature of the induced visual phosphene

With very helpful suggestions by Schiller, we designed a 2AFC task to first establish if optogenetic stimulation can induce a visual percept or a phosphene that is detectable by the animal. A key component was avoiding false detection or reporting of optogenetic stimulation; for that reason, we added catch trials in which the animal reports the absence of stimulation for a true rejection. Additionally, we included visual stimuli with different luminance values for two main reasons; the first reason is to train the animal to detect weak as well as strong visual stimuli since the nature of the phosphene, if any, is yet to be known. The second reason is to compare the explicit and implicit performance parameters of the visual and optogenetic stimuli. RF mapping was performed to place the visual stimuli in the same RF as the stimulated neurons and therefore create comparable conditions between opto and visual trials. As well, placing the visual stimuli in the RF would allow us to compare the neural responses across the different conditions.

The 2AFC results indicate that optogenetic stimulation elicited an artificial visual percept or a phosphene. Across sessions, the animal had a high success rate in detecting optogenetic stimulation (~80%); the performance was consistently similar to that of a low contrast visual stimulus with close to a 10% increase in luminance over the background. That finding was also reflected in the animal's saccadic reaction times (RTs); RTs for optogenetic stimulation was again similar to visual stimuli with a 5-10% increase in luminance.

RTs were calculated based on the initial saccade instead of the timing of the animal's report at the target because, although not required by the paradigm, the animal made saccades to the visual stimuli before the target. This behaviour likely reflects the increased salience of the stimuli with

increasing luminance (Schütz et al., 2012; Tatler et al., 2011). Similar behaviour was also observed for optogenetic trials; the animal made saccades towards the RF of the stimulated neurons before the target. The saccades to RF were not as precise as the visual stimuli but that is not surprising since an elicited phosphene would move with the shift in gaze (Lewis et al., 2015). The proportion of the direct vs indirect saccade provides further evidence of the nature of the elicited phosphene since it was similar to the visual stimuli with lower contrast. Finally, pre-saccadic pupil constriction in opto trials shows a similarity to the visual stimuli with lower contrasts.

Furthermore, for visual trials, pupil constriction increased with the increased luminance which could be attributed to the pupillary light reflex (PLR) (Clarke et al., 2003); however, we do not believe that the change in luminance is directly activating the PLR circuitry. PLR responses are locked to the onset of the luminance increase (May & Warren, 2020; Pong & Fuchs, 2000) while we found the change in pupil diameter is locked to the saccade. Indeed, when we aligned our pupillary changes to the stimulus onset, there was no clear effect of luminance on constriction. Instead, we interpret the change as a reflection of saliency as pupil constriction increases with stimuli saliency even for auditory stimuli (Corneil & Munoz, 2014; Wilschut & Mathôt, 2022). A recent study found similar patterns of increasing pupil constriction accompanied by decreasing RTs (Pandey & Ray, 2021) suggesting that those two metrics are related and reflect the saliency of a stimulus.

Both explicit and implicit behavioural performance metrics support the generation of a visual percept or a phosphene. Not only that, but evidence suggests that the generated phosphene is similar to a low-contrast visual stimulus (~10% luminance increase) in line with phosphenes generated via microstimulation of V1 (Schiller et al., 2011). The similarities between explicit and implicit performance measurements suggest that both can be helpful in future work identifying the effects of optogenetic stimulation in

the visual cortex. Such implicit measurements might help identify elicited phosphenes that are not reported explicitly by the animals.

Andrei et al. and Chen et al. have reported the lack of phosphene generation through optogenetic stimulation of V1 (Andrei et al., 2019; Chen et al., 2022) but indicated a behaviour effect when stimulation was coupled to visual stimuli. Andrei et al., however, used a different viral vector, lentivirus + CamKII, potentially explaining the difference in findings; furthermore, a weak phosphene could have been induced but ignored by the animal. On the other hand, Chen et al. trained the animals to only respond to visual stimuli as the study's goal was to examine interactions between visual and optogenetically induced responses rather than generate an artificial visual percept.

5.4.3 Neural activity reflects phosphene detection performance

In humans, studies have found high degrees of correlation between neural activity variability in V1 and subjects' performance which was attributed to attentional fluctuations (Ress et al., 2000; Ress & Heeger, 2003). In NHPs, neural correlates for behavioural performance have been found in higher visual areas such as V4 (Luck et al., 1997) and MT (Dezfouli et al., 2018; Newsome et al., 1989; Smith et al., 2015). In V1, choice-related activity variability has been found to correlate to the variability in neural activity especially for population activity compared to single units. This is reflected by multiunit activity that was found to be significantly higher for hits compared to misses (Lamme et al., 2001; Michelson et al., 2017; Nienborg & Cumming, 2014; Roelfsema & Spekreijse, 2001; Seidemann & Geisler, 2018). We found similar variability in the visually evoked MUAe between the successful and failed detection of stimuli with successful trials having overall higher activity prior to the animal's decision or the saccade. Interestingly, while the optogenetically modulated activity was a lot higher than the visually evoked one, we found similar variability in opto trials with successful trials having overall higher activity than failed trials. It is not clear what contributes to the variability in neural activity in V1 and whether

it includes effects from feedback or feedforward connections (Cumming & Nienborg, 2016; Seidemann & Geisler, 2018). This variability in responses could be seen from the onset of the stimulation with a difference in the transient response (Figure 5.7A example). While not the focus of the current study, my results suggest a reflection of the V1 activity variability rather than a modulation of response guided by selective spatial attention; attentional enhancement of neural responses in V1 is well-documented (Reynolds & Chelazzi, 2004), but the modulatory effects have a much later onset >200ms (Hecht et al., 1975; Roelfsema & Spekreijse, 2001; Thiele et al., 2009) than what we observed. Lamme et al. (2001) found earlier modulations, ~120ms, that are also less explained by attention and rather represent variability in the V1 state at the stimulus onset. Interestingly, Lamme and colleagues found that this earlier modulation is only present for more salient stimuli reflecting contextual modulation (Spillmann et al., 2015; Zipser et al., 1996). Additionally, we did not observe any baseline activity differences between correct and failed trials which has been associated with attentional effects (Ress et al., 2000). The variability of optogenetically modulated activity and its effect on performance and perception open the way for future studies developing visual prostheses. Phosphenes generated via electrical microstimulation have been found to vary in appearance (Schmidt et al., 1996; Shepherd et al., 2013) and this variability could be a result of variability in V1 activity itself. With optogenetics, we gain access to neural signals that could be analysed and used to generate more consistent visual percept with a closed-loop prosthesis. It is also worth noting that while the behavioural results indicate a low contrast phosphene, the optogenetically modulated neural response is much higher than the highest contrast visual stimuli. It is not clear why this would be the case. One possibility is the higher modulation recruits suppressive circuits similar to the firmly established visual surround suppression (Bair et al., 2003; Cavanaugh et al., 2012; Cavanaugh et al., 2002); however, we have only observed a positive correlation between neural activity and stimulation power making this unlikely.

Our results show that without the appropriate behavioural testing controls, bias can easily be introduced. However, a more carefully designed paradigm can not only confirm phosphene generation, but also elucidate some of its visual characteristics. We also found that optogenetically generated neural activity reflects behavioural performance similar to visually evoked once indicating that such an artificial drive can drive the local circuitry similar to a typical drive coming along the visual pathway.

Chapter 6: Conclusions and future work

In this study, I have examined the effects of V1 optogenetic stimulation in four macaques. In chapter 3, I confirmed the expression of ChR2 in vivo in two animals; optogenetic modulation was wavelength-specific with short latencies, a characteristic of ChR2. I examined the effects of stimulation light intensities and stimulation frequencies on the modulated activity and found that a higher stimulation frequency, 40Hz, results in a much stronger modulation. To our knowledge, this is one of the few studies to examine stimulation parameters systematically in NHPs. In chapter 4, I explored the laminar effects of optogenetic stimulation; this is the first study to examine the laminar effects of optogenetically stimulating V1 resulting in unique insights. For example, I found that while optogenetic stimulation increases activity across the cortical layers, there was a strong correlation between the modulation strength and opsin expression. Furthermore, my findings suggest that the V1 microcircuit is responsible for the oscillatory signatures observed with static visual stimuli since they can also be observed with the artificial drive of continuous optogenetic stimulation. Additionally, I show the laminar effects of stimulation frequencies and their flow across the layers. In chapter 5, I provide evidence that optogenetic stimulation of V1 can induce a phosphene that is detectable by macaques via the appropriate paradigm. Not only this, but I also shed some light on the visual characteristics of the phosphene using explicit and implicit measures. In this section, I will relate those findings to our knowledge of optogenetics and its use in NHPs and prostheses.

6.1 Optogenetics use in NHPs

In our study, successful and strong optogenetic modulation was observed in the electrophysiological data from only two out of the four animals injected with the same viral vector batch. Those mixed results reflect the findings of the wider NHP community with less than 40% of the labs finding

strong physiological effects of optogenetics (Tremblay et al., 2020). Our injection rates and volume per injection site are akin to the most common values used by other labs as well (Tremblay et al., 2020). Results from monkey Fl, suggest that a more comprehensive viral injection plan might provide better results. Compared to the rest of the animals, injections were made at more depths with less spacing resulting in a larger volume. We also found that while surface light delivery can successfully drive neurons, intracortical light delivery is more reliable in the absence of direct access to the brain surface. For reliable surface stimulation, researchers can surgically remove the dura and use a transparent substitute (Chernov et al., 2018; Ju et al., 2018; Nassi et al., 2015; Ruiz et al., 2013). However, the artificial dura does not offer a long-term solution and will need to be cleaned regularly to restore optical clarity (Ruiz et al., 2013) not to mention the inherent risk in such surgical procedures. In addition, we observed that opsin expression had a larger impact on modulation compared to the precise placement of the fibre. Future studies should put more emphasis on viral targeting in case-specific layer/cell type activation is desired.

Another interesting finding is the laminar effects of stimulation frequencies. Several studies have examined the effects of microstimulation frequency on driving neural activity and signal propagation across cortical areas (Kampe et al., 2000; Logothetis et al., 2010; Murris et al., 2020); however, to my knowledge, there are no similar optogenetic studies. It would be interesting to examine if optogenetic stimulation frequency increase would be proportional to the increase in neural activity or if the benefit observed is tightly related to the gamma frequency range observed in this study. Alternatively, 40Hz stimulation could be enhancing information transmission between neurons and cortical areas by inducing gamma oscillations; coherence in the gamma band is thought to mediate interareal communications (Palmigiano et al., 2017). The frequencies used, however, approach the limits of ChR2 (Grossman et al., 2011). There are alternate faster opsins such as the ChR2 variant, CatCh, that can follow stimulation

up to 100Hz (Wrobel et al., 2018) and the newer Channelrhodopsin, Chronos, that can follow similar frequencies (Hight et al., 2015; Klapoetke et al., 2014). The higher optogenetic stimulation frequencies would allow for comparison to microstimulation studies that typically use higher frequencies than optogenetic stimulation. Additionally, while we found BOLD signal modulation in higher cortical areas such as MT (Ortiz-Rios et al., 2021), electrophysiological recordings in MT would provide vital information about the strength of the propagated signal and provide insight into the oscillatory signatures of feedforward/feedback signals (Bastos et al., 2015) between cortical areas.

In terms of behaviour, our paradigm provided some understanding of the optogenetically elicited phosphene contrast. Variations of the 2AFC paradigm can shed some light on the size and colour of the phosphene as well. Additionally, inter-trial variation of light intensity could reveal the effects of stimulation intensity on those parameters. Pulsed stimulation might also be a preferable alternative to continuous stimulation due to the increased local activation as well as the activation of higher cortical areas. Furthermore, the generated phosphene appears to resemble a weak visual stimulus with low contrast. This could have been a contributing factor in why other studies failed to generate phosphenes using optogenetics since the animals in those studies were not trained to detect weak visual stimuli (Andrei et al., 2019; Chen et al., 2022) and therefore could have ignored any potential phosphenes. Future studies aimed at phosphene generation should expose the animals to a variety of visual stimuli to prepare the expectations of the animals.

6.2 Optogenetic cortical visual prostheses development

There is a great interest in the use of optogenetics in humans and there are already some clinical trials for optogenetic retinal stimulation (Shen et al., 2020); however, the development of optogenetic tools in NHPs has been and remains a vital tool. This study has provided further insight into

the use of optogenetics in the macaque V1. The success of V1 optogenetic stimulation in eliciting sensory percepts in this and previous studies (Jazayeri et al., 2012; Ju et al., 2018; May et al., 2014) makes it an increasingly viable alternative to microstimulation in cortical prostheses. In this section, we explore several important aspects necessary for the development of an optogenetic cortical prosthesis in terms of stimulation.

For an optogenetic cortical prosthesis, bulky light sources such as lasers and LEDs would be impractical; instead, light can be delivered intracortically via a μLED array implant (McAlinden et al., 2019). Alternatively, the μLED array can be placed subdurally or epidurally and connected to optical fibre waveguides (J. Wang & Dong, 2020). Such invasive light delivery methods present challenges to the long-term viability due to gliosis and encapsulation, like intracortical microstimulation. Instead, surface light delivery might be a better solution with μLED arrays placed subdurally or epidurally. We have observed that surface stimulation could drive neural activity not only through the dura but with additional granulation tissue on top. As described earlier, surface, compared to intracortical, electrical stimulation requires higher currents that result in lower visual resolution and possible painful side effects such as headaches. Optogenetic surface stimulation would face fewer issues. To begin with, optogenetic stimulation would likely not affect passing nerves since only the neurons of interest can be targeted with viral vectors. Additionally, compared to electrical surface stimulation, optogenetic surface stimulation does not need to use high light intensities to reach deeper neurons since light intensity is not the only factor that affects light propagation. Longer wavelengths, such as red and infrared wavelengths, demonstrate reduced tissue absorption and scattering compared to blue light resulting in a reduced power drop over the same distance (Acker et al., 2016; Senova et al., 2017). The improved transmission can be harnessed by using red-shifted opsins such as Chrimson and Chronos (Klapoetke et al., 2014) which would result in better light propagation without the use of high light

intensities avoiding harmful heat generation. The use of red-shifted opsins could also be supplemented with advancements in stimulation parameters such as stimulation frequency. We have observed higher neural modulation resulting from pulsed stimulation at 40Hz. Higher stimulation frequencies modulating neural activity more efficiently would require less power. 40Hz stimulation, also, resulted in activation in area MT (Ortiz-Rios et al., 2021) which is involved with motion perception (Anton-Erxleben et al., 2009; Smith et al., 2015); therefore, there is potential for future studies to induce a percept of motion using pulsed optogenetic stimulation. Microstimulation of area MT has been known to modulate motion perception (Murasugi et al., 1993; Nichols & Newsome, 2002). So far, artificial motion perception via V1 stimulation has only been feasible by eliciting different phosphene patterns in sequence (Chen et al., 2020) or more recently by current steering (Beauchamp et al., 2020). In addition to brain stimulation, it is critical to process external images into stimulation patterns is an important step. Traditionally, images obtained from an external video camera would be transformed to extract salient features and objects and then converted into "pixels" corresponding to each stimulating electrode (da Cruz et al., 2013; Zhao et al., 2017). More recent attempts utilised computer vision to extract features (J. Wang et al., 2021). Computer vision techniques are typically used for tasks such as image and text recognition. Bidirectional interface with the brain can also be beneficial for a visual prosthesis since understanding the brain state at the time of stimulation can lead to more efficient stimulation. In this study, I have seen different levels of neural activity for correct compared to incorrect trials that likely reflect the variability of V1 activity. A closed-loop system can produce more consistent percepts. Additionally, this has the potential to use attention to enhance specific regions of the visual field by detecting feedback signals associated with attention (Carrasco, 2011).

We envision a potential optogenetic cortical visual prosthesis using a flexible array of μLEDs (Lee et al., 2018; Rajalingham et al., 2021) placed

epidurally or subdurally to stimulate V1 neurons expressing red-shifted opsins such as Chronos or Chrimson. The μLED array can be used to generate complex shapes and patterns that can be tested in macaques similar to shape generation via microstimulation (Chen et al., 2020). Furthermore, the combination of continuous and pulsed stimulation could open the door for precise shape generation as well as motion perception. Finally, more precise viral targeting and comprehensive delivery would ensure consistent activation that is less affected by the placement and stability of the μLED array. This study has provided further insight into the existing field demonstrating that such a prosthesis is not far off.

6.3 Obstacles for human optogenetic cortical prostheses

The use of animal models, especially NHPs, has been and continues to be crucial to the efforts of vision restoration in humans. To begin with, NHPs have been invaluable in understanding the human visual system and its pathologies due to the shared features across primates (Busskamp & Roska, 2011; Liu et al., 2022; Picaud et al., 2019). Furthermore, animal models have been essential in developing visual protheses; this includes and is not limited to improved biocompatibility of implantable devices (Marin & Fernández, 2010; Nazempour et al., 2018), novel stimulation devices (Chen et al., 2020; Prévot et al., 2020) and novel stimulation techniques such as optogenetics (Gerits & Vanduffel, 2013). While optogenetics has been established earlier in rodents (Aravanis et al., 2007), NHP testing is legally and scientifically required prior to any clinical testing in humans (Sahel et al., 2021) due to the closer genetic similarities between humans and NHPs compared to rodents. Therefore, NHP use is pivotal for the development of such therapeutic solutions.

Since its first use, great advancements have been made to refine optogenetics use; as described in the previous section, great strides have been made in the design and creation of opsins, promoters and light delivery methods making an optogenetic cortical visual prothesis more

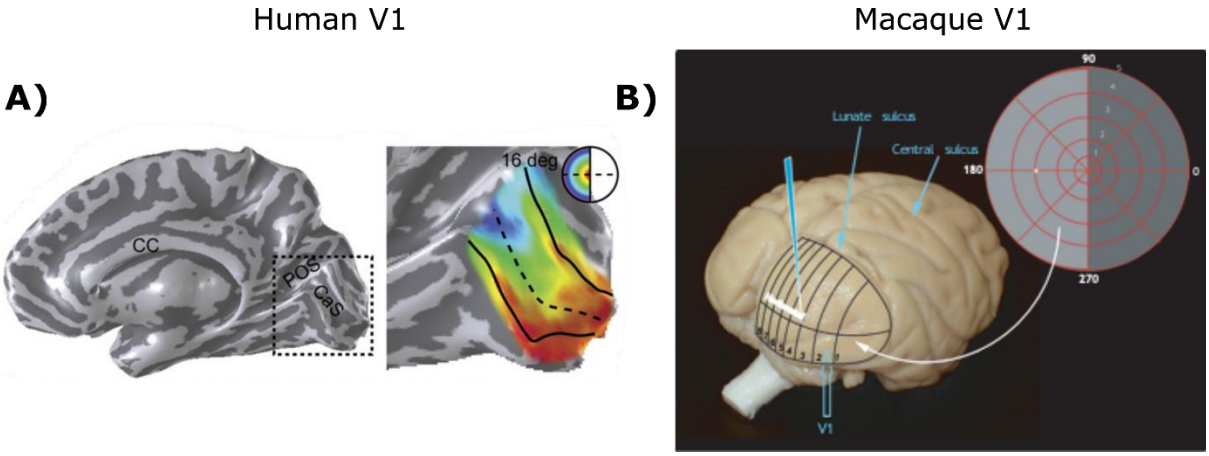

Figure 6.1 V1 location in humans compared to macaques. A. (left) Sagittal view of the human brain indicating the location of V1 inside the calcarine sulcus (CaS). (right) A colour map showing the retinotopic layout of V1 obtained from the response to stimuli at different eccentricities away from the fovea (red). Figure from Wandell et al., 2007.**B.** A posterior view of the macaque brain indicating V1 location and its retinotopic layout. Figure from Schiller & Tehovnik, 2015.

attainable. However, we must consider the challenges of translating such a prothesis to humans. Unlike the flat superficial location in macaques (Figure 6.1B), in humans, V1 is located within the calcarine sulcus on the medial side of the occipital cortex (Figure 6.1A). While the foveal portion of V1 is dorsal and closer to the surface, access is still more challenging requiring more innovative surgical procedures to place stimulating electrodes with few recent successful attempts (Kasdin, 2022; Liu et al., 2022; Pio-Lopez et al., 2021). While optogenetics based prostheses would not require electrodes, the same surgical challenges stand; light sources, such as μLEDs, or waveguides have to be placed at the stimulation sites.

The implantation of the necessary hardware is one piece of the puzzle, another important piece is the choice of the viral vectors necessary for optogenetics. While some combinations of viruses, opsins and promoters have been tested in NHPs, they are an extremely precious resource with each lab dedicating two to four animals for each project (Laurens, 2022); this has resulted in limited systematic testing of viral vectors being undertaken by any research group. Research groups might have explored two or three different viral vectors at most in one study with the majority of groups using more tested and tried viral vectors to ensure success (Tremblay et al., 2020). In chapter 4, we have seen evidence of a

correlation between viral expression and neural activity across the layers; nonetheless, it is the result of one AAV serotype and one promoter. It is unknown whether different expression patterns, resulting from different viral vectors, would result in similar or vastly different activation patterns. As described earlier, V1 is interconnected, and this connectivity might likely be more of a determining factor than the different expression or stimulation patterns; recent findings indicate that the cortical network has a stronger effect on the response to optogenetic stimulation than the stimulation parameters (Bloch et al., 2022). This could potentially mean that a strong enough excitatory drive to V1 would be enough to produce a similar activation pattern regardless of the expression pattern. In parallel, additional studies need to examine if the different viral vectors and expression patterns affect the characteristics of an optogenetically generated phosphene.

While an optogenetic visual cortical prosthesis has great potential, it involves many variables and challenges that need to be examined first before any clinical trials.

References

Acker, L., Pino, E. N., Boyden, E. S., & Desimone, R. (2016). FEF inactivation with improved optogenetic methods. *Proceedings of the National Academy of Sciences of the United States of America*, *113*(46), E7297–E7306. https://doi.org/10.1073/pnas.1610784113

Afraz, A., Boyden, E. S., & DiCarlo, J. J. (2015). Optogenetic and pharmacological suppression of spatial clusters of face neurons reveal their causal role in face gender discrimination. *Proceedings of the National Academy of Sciences of the United States of America*, *112*(21), 6730–6735. https://doi.org/10.1073/pnas.1423328112

Alhourani, A., McDowell, M. M., Randazzo, M. J., Wozny, T. A., Kondylis, E. D., Lipski, W. J., Beck, S., Karp, J. F., Ghuman, A. S., & Richardson, R. M. (2015). Network effects of deep brain stimulation. *Journal of Neurophysiology*, *114*(4), 2105–2117. https://doi.org/10.1152/jn.00275.2015

Andrei, A. R., Pojoga, S., Janz, R., & Dragoi, V. (2019). Integration of cortical population signals for visual perception. *Nature Communications*, *10*(1), 1–13. https://doi.org/10.1038/s41467-019-11736-2

Angelucci, A., & Sainsburry, K. (2006). Contribution of Feedforward Thalamic Afferents and Corticogeniculate Feedback to the Spatial Summation Area of Macaque V1 and LGN. *Journal of Comparative Neurology*, *498*, 330–351. https://doi.org/10.1002/cne

Anton-Erxleben, K., Stephan, V. M., & Treue, S. (2009). Attention reshapes center-surround receptive field structure in macaque cortical area MT. *Cerebral Cortex*, *19*(10), 2466–2478. https://doi.org/10.1093/cercor/bhp002

Aravanis, A. M., Wang, L.-P., Zhang, F., Meltzer, L. A., Mogri, M. Z., Schneider, M. B., & Deisseroth, K. (2007). An optical neural interface: in vivo control of rodent motor cortex with integrated fiberoptic and optogenetic technology. *Journal of Neural Engineering*, *4*(3), S143–S156. https://doi.org/10.1088/1741-2560/4/3/S02

Ayton, L. N., Barnes, N., Dagnelie, G., Fujikado, T., Goetz, G., Hornig, R., Jones, B. W., Muqit, M. M. K., Rathbun, D. L., Stingl, K., Weiland, J. D., & Petoe, M. A. (2020). An update on retinal prostheses. In *Clinical Neurophysiology* (Vol. 131, Issue 6, pp. 1383–1398). https://doi.org/10.1016/j.clinph.2019.11.029

Bair, W., Cavanaugh, J. R., & Movshon, J. A. (2003). Time course and time-distance relationships for surround suppression in macaque V1 neurons. *Journal of Neuroscience*, *23*(20), 7690–7701. https://doi.org/23/20/7690 [pii]

Bair, W., Cavanaugh, J. R., Smith, M. A., & Movshon, J. A. (2002). The timing of response onset and offset in macaque visual neurons. *Journal of Neuroscience*, *22*(8), 3189–3205. https://doi.org/10.1523/jneurosci.22-08-03189.2002

Balaram, P. (2011). VGLUT2 mRNA and protein expression in the visual thalamus and midbrain of prosimian galagos (Otolemur garnetti). *Eye and Brain*, 5. https://doi.org/10.2147/eb.s16998

Balaram, P., & Kaas, J. H. (2014). Towards a unified scheme of cortical lamination for primary visual cortex across primates: Insights from NeuN and VGLUT2 immunoreactivity. *Frontiers in Neuroanatomy*, *8*(AUG), 1–14. https://doi.org/10.3389/fnana.2014.00081

Bamann, C., Kirsch, T., Nagel, G., & Bamberg, E. (2008). Spectral Characteristics of the Photocycle of Channelrhodopsin-2 and Its Implication for Channel Function. *Journal of Molecular Biology*, *375*(3), 686–694. https://doi.org/10.1016/j.jmb.2007.10.072

Barlow, H. B. (1981). Critical Limiting factors in the design of the eye and visual cortex. *Proceedings of the Royal Society of London B: Biological Sciences*, *212*, 1–34.

Barlow, H. B., Blakemore, C., & Pettigrew, J. D. (1967). The neural mechanism of binocular depth discrimination. *The Journal of Physiology*, *193*(2), 327–342. https://doi.org/10.1113/jphysiol.1967.sp008360

Barnett, L., & Seth, A. K. (2014). The MVGC multivariate Granger causality toolbox: A new approach to Granger-causal inference. *Journal of Neuroscience Methods*, *223*, 50–68. https://doi.org/10.1016/j.jneumeth.2013.10.018

Bartlett, J. R., DeYoe, E. A., Doty, R. W., Lee, B. B., Lewine, J. D., Negrão, N., & Overman, W. H. (2005). Psychophysics of electrical stimulation of striate cortex in macaques. *Journal of Neurophysiology*, *94*(5), 3430–3442. https://doi.org/10.1152/jn.00406.2005

Bastos, A. M., Briggs, F., Alitto, H. J., Mangun, G. R., & Usrey, W. M. (2014). Simultaneous Recordings from the Primary Visual Cortex and Lateral Geniculate Nucleus Reveal Rhythmic Interactions and a Cortical Source

for Gamma-Band Oscillations. *Journal of Neuroscience*, *34*(22), 7639–7644. https://doi.org/10.1523/JNEUROSCI.4216-13.2014

Bastos, A. M., Vezoli, J., Bosman, C. A., Schoffelen, J. M., Oostenveld, R., Dowdall, J. R., DeWeerd, P., Kennedy, H., & Fries, P. (2015). Visual areas exert feedforward and feedback influences through distinct frequency channels. *Neuron*, *85*(2), 390–401. https://doi.org/10.1016/j.neuron.2014.12.018

Beauchamp, M. S., Oswalt, D., Sun, P., Foster, B. L., Magnotti, J. F., Niketeghad, S., Pouratian, N., Bosking, W. H., & Yoshor, D. (2020). Dynamic Stimulation of Visual Cortex Produces Form Vision in Sighted and Blind Humans. *Cell*, *181*(4), 774–783. https://doi.org/10.1016/j.cell.2020.04.033.Dynamic

Bijanzadeh, M., Nurminen, L., Merlin, S., Clark, A. M., & Angelucci, A. (2018). Distinct Laminar Processing of Local and Global Context in Primate Primary Visual Cortex. *Neuron*, *100*(1), 259-274.e4. https://doi.org/10.1016/j.neuron.2018.08.020

Bitzenhofer, S. H., Ahlbeck, J., Wolff, A., Wiegert, J. S., Gee, C. E., Oertner, T. G., & Hanganu-Opatz, I. L. (2017). Layer-specific optogenetic activation of pyramidal neurons causes beta-gamma entrainment of neonatal networks. *Nature Communications*, *8*, 1–13. https://doi.org/10.1038/ncomms14563

Blasdel, G. G., Lund, J. S., & Fitzpatrick, D. (1985). Intrinsic connections of macaque striate cortex: axonal projections of cells outside lamina 4C. *Journal of Neuroscience*, *5*(12), 3350–3369.

Bloch, E., Luo, Y., & Cruz, L. da. (2019). Advances in retinal prosthesis systems. *Theraputic Advances in Opthalmology*, *11*, 1–16. https://doi.org/10.1177/https

Bloch, J., Greaves-Tunnell, A., Shea-Brown, E., Harchaoui, Z., Shojaie, A., & Yazdan-Shahmorad, A. (2022). Network structure mediates functional reorganization induced by optogenetic stimulation of non-human primate sensorimotor cortex. *IScience*, *25*(5). https://doi.org/10.1016/j.isci.2022.104285

Bourne, R. R. A., Flaxman, S. R., Braithwaite, T., Cicinelli, M. v., Das, A., Jonas, J. B., Keeffe, J., Kempen, J., Leasher, J., Limburg, H., Naidoo, K., Pesudovs, K., Resnikoff, S., Silvester, A., Stevens, G. A., Tahhan, N., Wong, T., Taylor, H. R., Ackland, P., … Zheng, Y. (2017). Magnitude, temporal trends, and projections of the global prevalence of blindness and distance and near vision impairment: a systematic review and

meta-analysis. *The Lancet Global Health*, *5*(9), e888–e897. https://doi.org/10.1016/S2214-109X(17)30293-0

Bourne, R. R. A., Steinmetz, J. D., Saylan, M., Mersha, A. M., Weldemariam, A. H., Wondmeneh, T. G., Sreeramareddy, C. T., Pinheiro, M., Yaseri, M., Yu, C., Zastrozhin, M. S., Zastrozhina, A., Zhang, Z. J., Zimsen, S. R. M., Yonemoto, N., Tsegaye, G. W., Vu, G. T., Vongpradith, A., Renzaho, A. M. N., … Vos, T. (2021). Causes of blindness and vision impairment in 2020 and trends over 30 years, and prevalence of avoidable blindness in relation to VISION 2020: The Right to Sight: An analysis for the Global Burden of Disease Study. *The Lancet Global Health*, *9*(2), e144–e160. https://doi.org/10.1016/S2214-109X(20)30489-7

Bradley, D. C., Troyk, P. R., Berg, J. A., Bak, M., Cogan, S., Erickson, R., C. Kufta, M. M., McCreery, D., Schmidt, E. M., Towle, V. L., & Xu, H. (2004). Visuotopic Mapping Through a Multichannel Stimulating Implant in Primate V1. *Journal of Neurophysiology*, *93*(3), 1659–1670. https://doi.org/10.1152/jn.01213.2003

Brewer, A. A., Press, W. A., Logothetis, N. K., & Wandell, B. A. (2002). Visual Areas in Macaque Cortex Measured Using Functional Magnetic Resonance Imaging. In *The Journal of Neuroscience* (Vol. 22, Issue 23).

Brindley, G. S. (1971). Sensations Produced by Electrical Stimulation of The Occipital Poles of The Cerebral Hemispheres, and Their Use in Constructing Visual Prostheses. *Visual Prosthesis, The Interdisciplinary Dialogue*, 41–48.

Brindley, G. S., & Lewin, W. S. (1968). The sensations produced by electrical stimulation of the visual cortex. *The Journal of Physiology*, *196*(2), 479–493. https://doi.org/10.1113/jphysiol.1968.sp008519

Brovelli, A., Ding, M., Ledberg, A., Chen, Y., Nakamura, R., & Bressler, S. L. (2004). *Beta oscillations in a large-scale sensorimotor cortical network: Directional influences revealed by Granger causality*. www.pnas.orgcgidoi10.1073pnas.0308538101

Buffalo, E. A., Fries, P., Landman, R., Buschman, T. J., & Desimone, R. (2011). Laminar differences in gamma and alpha coherence in the ventral stream. *Proceedings of the National Academy of Sciences of the United States of America*, *108*(27), 11262–11267. https://doi.org/10.1073/pnas.1011284108

Busskamp, V., & Roska, B. (2011). Optogenetic approaches to restoring visual function in retinitis pigmentosa. In *Current Opinion in*

Neurobiology (Vol. 21, Issue 6, pp. 942–946). https://doi.org/10.1016/j.conb.2011.06.001

Buzsáki, G., & Watson, B. O. (2012). Brain rhythms and neural syntax: Implications for efficient coding of cognitive content and neuropsychiatric disease. *Dialogues in Clinical Neuroscience*, *14*(4), 345–367. https://doi.org/10.31887/dcns.2012.14.4/gbuzsaki

Callaway, E. M. (1998a). Local circuits in primary visual cortex of the macaque monkey. *Annual Review of Neuroscience*, *21*, 47–74. https://doi.org/10.1523/jneurosci.18-04-01505.1998

Cardin, J. A., Carlén, M., Meletis, K., Knoblich, U., Zhang, F., Deisseroth, K., Tsai, L.-H., & Moore, C. I. (2009). Driving fast-spiking cells induces gamma rhythm and controls sensory responses. *Nature*, *459*(7247), 663–667. https://doi.org/10.1038/nature08002

Carrasco, M. (2011). Visual attention : The past 25 years. *Vision Res.*, *51*(13), 1484–1525. https://doi.org/10.1016/j.visres.2011.04.012.Visual

Cavanaugh, J., Joiner, W. M., & Wurtz, R. H. (2012). Suppressive Surrounds of Receptive Fields In Monkey Frontal Eye Field. *Journal of Neuroscience*, *32*(35), 12284–12293. https://doi.org/10.1523/JNEUROSCI.0864-12.2012

Cavanaugh, J. R., Bair, W., & Movshon, J. A. (2002). Nature and Interaction of Signals From the Receptive Field Center and Surround in Macaque V1 Neurons. *Journal of Neurophysiology*, *88*(5), 2530–2546. https://doi.org/10.1152/jn.00692.2001

Cha, K., Horch, K., & Normann, R. A. (1992). Simulation of a phosphene-based visual field: Visual acuity in a pixelized vision system. *Annals of Biomedical Engineering*, *20*(4), 439–449. https://doi.org/10.1007/BF02368135

Chen, S., Benvenuti, G., Chen, Y., Kumar, S., Ramakrishnan, C., Deisseroth, K., Geisler, W. S., & Seidemann, E. (2022). Similar neural and perceptual masking effects of low-power optogenetic stimulation in primate V1. *ELife*, *11*(e68393). https://doi.org/10.1101/2021.02.16.431182

Chen, X., Mihalas, S., Niebur, E., & Stuphorn, V. (2013). Mechanisms underlying the influence of saliency on value-based decisions. *Journal of Vision*, *13*(12), 18. https://doi.org/10.1167/13.12.18

Chen, X., Wang, F., Fernandez, E., & Roelfsema, P. R. (2020). Shape perception via a high-channel-count neuroprosthxesis in monkey visual

cortex. *Science*, *370*(6521), 1191–1196. https://doi.org/10.1126/science.abd7435

Chernov, M. M., Friedman, R. M., Chen, G., Stoner, G. R., & Roe, A. W. (2018). Functionally specific optogenetic modulation in primate visual cortex. *Proceedings of the National Academy of Sciences of the United States of America*, *115*(41), 10505–10510. https://doi.org/10.1073/pnas.1802018115

Christie, I. N., Wells, J. A., Southern, P., Marina, N., Kasparov, S., Gourine, A. v., & Lythgoe, M. F. (2013). FMRI response to blue light delivery in the naïve brain: Implications for combined optogenetic fMRI studies. *NeuroImage*, *66*, 634–641. https://doi.org/10.1016/j.neuroimage.2012.10.074

Chudakov, D. M., Matz, M. v., Lukyanov, S., & Lukyanov, K. A. (2010). Fluorescent proteins and their applications in imaging living cells and tissues. *Physiological Reviews*, *90*(3), 1103–1163. https://doi.org/10.1152/physrev.00038.2009

Clarke, R. J., Zhang, H., & Gamlin, P. D. R. (2003). Characteristics of the pupillary light reflex in the alert rhesus monkey. *Journal of Neurophysiology*, *89*(6), 3179–3189. https://doi.org/10.1152/jn.01131.2002

Corneil, B. D., & Munoz, D. P. (2014). Overt responses during covert orienting. *Neuron*, *82*(6), 1230–1243. https://doi.org/10.1016/j.neuron.2014.05.040

Cumming, B. G., & Nienborg, H. (2016). Feedforward and feedback sources of choice probability in neural population responses. *Current Opinion in Neurobiology*, *37*, 126–132. https://doi.org/10.1016/j.conb.2016.01.009

da Cruz, L., Coley, B. F., Dorn, J., Merlini, F., Filley, E., Christopher, P., Chen, F. K., Wuyyuru, V., Sahel, J., Stanga, P., Humayun, M., Greenberg, R. J., & Dagnelie, G. (2013). The Argus II epiretinal prosthesis system allows letter and word reading and long-term function in patients with profound vision loss. *British Journal of Ophthalmology*, *97*(5), 632–636. https://doi.org/10.1136/bjophthalmol-2012-301525

De, A., El-Shamayleh, Y., & Horwitz, G. D. (2020). Fast and reversible neural inactivation in macaque cortex by optogenetic stimulation of GABAergic neurons. *ELife*, *9*, 1–21. https://doi.org/10.7554/eLife.52658

Deisseroth, K. (2011). Optogenetics. *Nature Methods*, *8*(1), 26–29. https://doi.org/10.1038/nmeth.f.324

Deisseroth, K. (2014). Circuit dynamics of adaptive and maladaptive behaviour. *Nature*, *505*(7483), 309–317. https://doi.org/10.1038/nature12982

Deisseroth, K. (2015). *Optogenetics: 10 years of microbial opsins in neuroscience*. *18*(9), 1213–1225. https://doi.org/10.1038/nn.4091

Desimone, R., & Duncan, J. (1995). Neural Mechanisms of Selective Visual attention. *Annual Review of Neuroscience*, *18*, 193–222. https://doi.org/10.1038/nrn2174

Dezfouli, M. P., Khamechian, M. B., Treue, S., Esghaei, M., & Daliri, M. R. (2018). Neural activity predicts reaction in primates long before a behavioral response. *Frontiers in Behavioral Neuroscience*, *12*(September), 1–11. https://doi.org/10.3389/fnbeh.2018.00207

Diester, I., Kaufman, M. T., Mogri, M., Pashaie, R., Goo, W., Yizhar, O., Ramakrishnan, C., Deisseroth, K., & Shenoy, K. v. (2011). An optogenetic toolbox designed for primates. *Nature Neuroscience*, *14*(3), 387–397. https://doi.org/10.1038/nn.2749.An

Ding, M., Chen, Y., & Bressler, S. L. (2006). Granger Causality: Basic Theory and Application to Neuroscience. In *Handbook of Time Series Analysis: Recent Theoretical Developments and Applications* (pp. 437–460). https://doi.org/10.1002/9783527609970.ch17

Dobelle, W. . H. (2000). Artificial vision for the blind by connecting a television camera to the visual cortex. *ASAIO Journal*, *46*(1), 3–9. https://doi.org/10.1097/00002480-200001000-00002

Dobelle, W. H., & Mladejovsky, M. G. (1974). Phosphenes produced by electrical stimulation of human occipital cortex, and their application to the development of a prosthesis for the blind. *The Journal of Physiology*, *243*(2), 553–576. https://doi.org/10.1113/jphysiol.1974.sp010766

Dobelle, W. H., Mladejovsky, M. G., & Girvin, J. P. (1974). Artificial vision for the blind: Electrical stimulation of visual cortex offers hope for a functional prosthesis. *Science*, *183*(4123), 440–444. https://doi.org/10.1126/science.183.4123.440

Dougherty, K., Cox, M. A., Ninomiya, T., Leopold, D. A., & Maier, A. (2017). Ongoing alpha activity in V1 regulates visually driven spiking responses. *Cerebral Cortex*, *27*(2), 1113–1124. https://doi.org/10.1093/cercor/bhv304

Drebitz, E., Schledde, B., Kreiter, A. K., & Wegener, D. (2019). Optimizing the yield of multi-unit activity by including the entire spiking activity. *Frontiers in Neuroscience*, *13*(FEB). https://doi.org/10.3389/fnins.2019.00083

Duncan, R. O., & Boynton, G. M. (2003). Cortical magnification within human primary visual cortex correlates with acuity thresholds. *Neuron*, *38*(4), 659–671. https://doi.org/10.1016/S0896-6273(03)00265-4

Edell, D. J., Toi, V. van, McNeil, V. M., & Clark, L. D. (1992). Factors Influencing the Biocompatibility of Insertable Silicon Microshafts in Cerebral Cortex. *IEEE Transactions on Biomedical Engineering*, *39*(6), 635–643.

Edwards, T. L., Cottriall, C. L., Xue, K., Simunovic, M. P., Ramsden, J. D., Zrenner, E., & MacLaren, R. E. (2018). Assessment of the Electronic Retinal Implant Alpha AMS in Restoring Vision to Blind Patients with End-Stage Retinitis Pigmentosa. *Ophthalmology*, *125*(3), 432–443. https://doi.org/10.1016/j.ophtha.2017.09.019

EJ, T. (1996). Electrical stimulation of neural tissue to evoke behavioral responses. TL - 65. *Journal of Neuroscience Methods*, *65 VN-r*(1), 1–17. http://www.ncbi.nlm.nih.gov/pubmed/8815302

El-Shamayleh, Y., Ni, A. M., & Horwitz, G. D. (2016). Strategies for targeting primate neural circuits with viral vectors. *Journal of Neurophysiology*, *116*(1), 122–134. https://doi.org/10.1152/jn.00087.2016

Engbert, R., & Kliegl, R. (2003). Microsaccades uncover the orientation of covert attention. *Vision Research*, *43*(9), 1035–1045. https://doi.org/10.1016/S0042-6989(03)00084-1

Fabbrini, F., van den Haute, C., de Vitis, M., Baekelandt, V., Vanduffel, W., & Vogels, R. (2019). Probing the Mechanisms of Repetition Suppression in Inferior Temporal Cortex with Optogenetics. *Current Biology*, *29*(12), 1988-1998.e4. https://doi.org/10.1016/j.cub.2019.05.014

Fallon, J. B., Irvinga, S., Pannud, S. S., Tookerd, A. C., Wise, A. K., Shepherd, R. K., & Irvinea, D. R. F. (2016). Second spatial derivative analysis of cortical surface potentials recorded in cat primary auditory cortex using thin film surface arrays: comparisons with multi-unit data. *Journal of Neuroscience Methods*, *15*(267), 14–20. https://doi.org/10.1016/j.jneumeth.2016.04.004.Second

Farnum, A., & Pelled, G. (2020). New Vision for Visual Prostheses. *Frontiers in Neuroscience*, *14*(February), 1–11. https://doi.org/10.3389/fnins.2020.00036

Fernández, E., & Normann, R. A. (2017). CORTIVIS Approach for an Intracortical Visual Prostheses. *Artificial Vision*, 191–201. https://doi.org/10.1007/978-3-319-41876-6_15

Fitzpatrick, D., Lund, J. S., & Blasdel, G. G. (1985). Intrinsic connections of macaque striate cortex: Afferent and efferent connections of lamina 4C. *Journal of Neuroscience*, *5*(12), 3329–3349. https://doi.org/10.1523/jneurosci.05-12-03329.1985

Fitzpatrick, D., Lund, J. S., Schmechel, D. E., & Towles, A. C. (1987). Distribution of GABAergic neurons and axon terminals in the macaque striate cortex. *Journal of Comparative Neurology*, *264*(1), 73–91. https://doi.org/10.1002/cne.902640107

Fitzpatrick, D., Usrey, W. M., Schofield, B. R., & Einstein, G. (1994). The sublaminar organization of corticogeniculate neurons in layer 6 of macaque striate cortex. *Visual Neuroscience*, *11*(2), 307–315. https://doi.org/10.1017/S0952523800001656

Foroushani, A. N., Pack, C. C., & Sawan, M. (2018). Cortical visual prostheses: From microstimulation to functional percept. *Journal of Neural Engineering*, *15*(2). https://doi.org/10.1088/1741-2552/aaa904

Friedman-Hill, S., Maldonado, P. E., & Gray, C. M. (2000). Dynamics of striate cortical activity in the alert macaque: I. Incidence and stimulus-dependence of gamma-band neuronal oscillations. *Cerebral Cortex*, *10*(11), 1105–1116. https://doi.org/10.1093/cercor/10.11.1105

Frien, A., Eckhorn, R., Bauer, R., Woelbern, T., & Gabriel, A. (2000). Fast oscillations display sharper orientation tuning than slower components of the same recordings in striate cortex of the awake monkey. *European Journal of Neuroscience*, *12*(4), 1453–1465. https://doi.org/10.1046/j.1460-9568.2000.00025.x

Garcia-Marin, V., Kelly, J. G., & Hawken, M. J. (2019). Major feedforward thalamic input into layer 4c of primary visual cortex in primate. *Cerebral Cortex*, *29*(1), 134–149. https://doi.org/10.1093/cercor/bhx311

Gattass, R., Nascimento-Silva, S., Soares, J. G. M., Lima, B., Jansen, A. K., Diogo, A. C. M., Farias, M. F., Botelho, M. M. , E. P., Mariani, O. S., Azzi, J., & Fiorani, M. (2005). Cortical visual areas in monkeys: location, topography, connections, columns, plasticity and cortical dynamics.

Philosophical Transactions of the Royal Society B: Biological Sciences, *360*(1456), 709–731. https://doi.org/10.1098/rstb.2005.1629

Gerits, A., Farivar, R., Rosen, B. R., Wald, L. L., Boyden, E. S., & Vanduffel, W. (2012). Optogenetically induced behavioral and functional network changes in primates. *Current Biology*, *22*(18), 1722–1726. https://doi.org/10.1016/j.cub.2012.07.023

Gerits, A., Vancraeyenest, P., Vreysen, S., Laramée, M.-E., Michiels, A., Gijsbers, R., van den Haute, C., Moons, L., Debyser, Z., Baekelandt, V., Arckens, L., & Vanduffel, W. (2015). Serotype-dependent transduction efficiencies of recombinant adeno-associated viral vectors in monkey neocortex. *Neurophotonics*, *2*(3), 031209. https://doi.org/10.1117/1.nph.2.3.031209

Gerits, A., Vancraeyenest, P., Vreysen, S., Laramée, M.-E., Michiels, A., Gijsbers, R., Van den Haute, C., Moons, L., Debyser, Z., Baekelandt, V., Arckens, L., & Vanduffel, W. (2015). Serotype-dependent transduction efficiencies of recombinant adeno-associated viral vectors in monkey neocortex. *Neurophotonics*, *2*(3), 031209. https://doi.org/10.1117/1.nph.2.3.031209

Gerits, A., & Vanduffel, W. (2013). Optogenetics in primates: A shining future? *Trends in Genetics*, *29*(7), 403–411. https://doi.org/10.1016/j.tig.2013.03.004

Geruschat, D. R., Richards, T. P., Arditi, A., da Cruz, L., Dagnelie, G., Dorn, J. D., Duncan, J. L., Ho, A. C., Olmos de Koo, L. C., Sahel, J. A., Stanga, P. E., Thumann, G., Wang, V., & Greenberg, R. J. (2016). An analysis of observer-rated functional vision in patients implanted with the Argus II Retinal Prosthesis System at three years. *Clinical and Experimental Optometry*, *99*(3), 227–232. https://doi.org/10.1111/cxo.12359

Ghodrati, M., Morris, A. P., & Price, N. S. C. (2015). The (un)suitability of modern liquid crystal displays (LCDs) for vision research. *Frontiers in Psychology*, *6*(MAR), 1–11. https://doi.org/10.3389/fpsyg.2015.00303

Gieselmann, M. A., & Thiele, A. (2020). *Stimulus dependence of directed information exchange between cortical layers in macaque V1*. https://doi.org/10.1101/2020.07.10.197566

Gilbert, C. D. (1977). Laminar differences in receptive field properties of cells in cat primary visual cortex. *The Journal of Physiology*, *268*(2), 391–421. https://doi.org/10.1113/jphysiol.1977.sp011863

Gilja, V., Chestek, C. A., Diester, I., Henderson, J. M., Deisseroth, K., & Shenoy, K. v. (2011). Challenges and opportunities for next-generation

intracortically based neural prostheses. *IEEE Transactions on Biomedical Engineering*, *58*(7), 1891–1899. https://doi.org/10.1109/TBME.2011.2107553

Graziano, M. S. A., Taylor, C. S. R., & Moore, T. (2002). Complex movements evoked by microstimulation of precentral cortex. *Neuron*, *34*(5), 841–851. https://doi.org/10.1016/S0896-6273(02)00698-0

Grosenick, L., Marshel, J. H., & Deisseroth, K. (2015). Closed-loop and activity-guided optogenetic control. *Neuron*, *86*(1), 106–139. https://doi.org/10.1016/j.neuron.2015.03.034

Grossman, N., Nikolic, K., Grubb, M. S., Burrone, J., Toumazou, C., & Degenaar, P. (2011). High-frequency limit of neural stimulation with ChR2. *Proceedings of the Annual International Conference of the IEEE Engineering in Medicine and Biology Society, EMBS*, 4167–4170. https://doi.org/10.1109/IEMBS.2011.6091034

Grossman, N., Poher, V., Grubb, M. S., Kennedy, G. T., Nikolic, K., McGovern, B., Palmini, R. B., Gong, Z., Drakakis, E. M., Neil, M. A. A., Dawson, M. D., Burrone, J., & Degenaar, P. (2010). Multi-site optical excitation using ChR2 and micro-LED array. *Journal of Neural Engineering*, *7*(1). https://doi.org/10.1088/1741-2560/7/1/016004

Gupta, N., Ang, L. C., de Tilly, L. N., Bidaisee, L., & Yücel, Y. H. (2006). Human glaucoma and neural degeneration in intracranial optic nerve, lateral geniculate nucleus, and visual cortex. *British Journal of Ophthalmology*, *90*(6), 674–678. https://doi.org/10.1136/bjo.2005.086769

Gupta, P. R., & Huckfeldt, R. M. (2017). Gene therapy for inherited retinal degenerations: Initial successes and future challenges. *Journal of Neural Engineering*, *14*(5). https://doi.org/10.1088/1741-2552/aa7a27

Gur, M., Kagan, I., & Snodderly, D. M. (2005). Orientation and direction selectivity of neurons in V1 of alert monkeys: Functional relationships and laminar distributions. *Cerebral Cortex*, *15*(8), 1207–1221. https://doi.org/10.1093/cercor/bhi003

Han, X., Qian, X., Bernstein, J. G., Zhou, H., Franzesi, G. T., Stern, P., Bronson, R. T., Graybiel, A. M., Desimone, R., & Boyden, E. S. (2009a). Millisecond-Timescale Optical Control of Neural Dynamics in the Nonhuman Primate Brain. *Neuron*, *62*(2), 191–198. https://doi.org/10.1016/j.neuron.2009.03.011

Hariz, M., Blomstedt, P., & Zrinzo, L. (2013). Future of brain stimulation: New targets, new indications, new technology. *Movement Disorders*, *28*(13), 1784–1792. https://doi.org/10.1002/mds.25665

Hartong, D., Berson, E., & Dryja, T. (2006). Retinitis pigmentosa. *Lancet*, *368*, 1795–1809. https://ac.els-cdn.com/S0140673606697407/1-s2.0-S0140673606697407-main.pdf?_tid=26be6064-c3a4-11e7-b6bd-00000aacb35f&acdnat=1510049725_a881580f76b9dcba337a82cbae60ae14

Hecht, F., McCaw, B. K., Peakman, D., & Robinson, A. (1975). Object-based attention in the primaryvisual cortex of themacaquemonkey. *Nature*, *255*(5505), 243–244.

Hegemann, P. (2008). Algal sensory photoreceptors. *Annual Review of Plant Biology*, *59*, 167–189. https://doi.org/10.1146/annurev.arplant.59.032607.092847

Heitmann, S., Rule, M., Truccolo, W., & Ermentrout, B. (2017). Optogenetic Stimulation Shifts the Excitability of Cerebral Cortex from Type I to Type II: Oscillation Onset and Wave Propagation. *PLoS Computational Biology*, *13*(1), 1–13. https://doi.org/10.1371/journal.pcbi.1005349

Henrie, J. A., & Shapley, R. (2005). LFP power spectra in V1 cortex: The graded effect of stimulus contrast. *Journal of Neurophysiology*, *94*(1), 479–490. https://doi.org/10.1152/jn.00919.2004

Hight, A. E., Kozin, E. D., Darrow, K., Lehmann, A., Boyden, E., Brown, M. C., & Lee, D. J. (2015). Superior temporal resolution of Chronos versus channelrhodopsin-2 in an optogenetic model of the auditory brainstem implant. *Hearing Research*, *322*, 235–241. https://doi.org/10.1016/j.heares.2015.01.004

Histed, M. H., Bonin, V., & Reid, R. C. (2009). Direct Activation of Sparse, Distributed Populations of Cortical Neurons by Electrical Microstimulation. *Neuron*, *63*(4), 508–522. https://doi.org/10.1016/j.neuron.2009.07.016

Horváth, Á. C., Borbély, S., Boros, Ö. C., Komáromi, L., Koppa, P., Barthó, P., & Fekete, Z. (2020). Infrared neural stimulation and inhibition using an implantable silicon photonic microdevice. *Microsystems and Nanoengineering*, *6*(1). https://doi.org/10.1038/s41378-020-0153-3

Hubel, D. H., & Wiesel, T. (1962). Receptive Fields, Binocular Interaction and Functional Architecture in The Cat's Visual Cortex. *Journal of Physiology*, *160*, 106–154.

Hubel, D. H., & Wiesel, T. N. (1977). Functional architecture of macaque monkey visual cortex. *Proceedings of the Royal Society of London B: Biological Sciences*, *198*(July), 1–59. http://www.ncbi.nlm.nih.gov/pubmed/6127704

Humayun, M. S., Prince, M., de Juan, E., Barron, Y., Moskowitz, M., Klock, I. B., & Milam, A. H. (1999). Morphometric analysis of the extramacular retina from postmortem eyes with retinitis pigmentosa. *Investigative Ophthalmology and Visual Science*, *40*(1), 143–148.

Ilker, O., Wang, J., Lu, Y., May, T., Lee, J., Goo, W., O'Shea, D. J. ;, Kalanithi, P. ;, Diester, I., Diagne Mohamed;, Deisseroth, K., Shenoy, K. V. ;, & Nurmikko, A. V. ; (2013). A Coaxial Optrode As Multifunction Write-Read Probe for Optogenetic Studies in Non-Human Primates. *Journal of Neuroscience Methods*, *219*(1), 142–154. https://doi.org/10.1016/j.jneumeth.2013.06.011.A

Iuliano, L., Fogliato, G., Corbelli, E., Bandello, F., & Codenotti, M. (2021). Blind patients in end-stage inherited retinal degeneration: multimodal imaging of candidates for artificial retinal prosthesis. *Eye (Basingstoke)*, *35*(1), 289–298. https://doi.org/10.1038/s41433-020-01188-0

Jackson, A., Mavoori, J., & Fetz, E. E. (2006). Long-term motor cortex plasticity induced by an electronic neural implant. *Nature*, *444*, 56–60. https://doi.org/10.1038/nature05226

Jazayeri, M., Lindbloom-Brown, Z., & Horwitz, G. D. (2012). Saccadic eye movements evoked by optogenetic activation of primate V1. *Nature Neuroscience*, *15*(10), 1368–1370. https://doi.org/10.1038/nn.3210

Jazayeri, M., & Remington, E. (2016). Optogenetics Advances in Primate Visual Pathway. *Neuron*, *90*(1), 8–10. https://doi.org/10.1016/j.neuron.2016.03.024

Jeffries, A. M., Killian, N. J., & Pezaris, J. S. (2014). Mapping the primate lateral geniculate nucleus: A review of experiments and methods. *Journal of Physiology*, *108*(1), 3–10. https://doi.org/10.1016/j.jphysparis.2013.10.001.Mapping

Jia, X., Smith, M. A., & Kohn, A. (2011). Stimulus Selectivity and Spatial Coherence of Gamma Components of the Local Field Potential. *Journal of Neuroscience*, *31*(25), 9390–9403. https://doi.org/10.1523/JNEUROSCI.0645-11.2011

Ju, N., Jiang, R., Macknik, S. L., Martinez-Conde, S., & Tang, S. (2018). Long-term all-optical interrogation of cortical neurons in awake-

behaving non-human primates. *PLoS Biology*, 274308. https://doi.org/10.1101/274308

Kamiński, M., Ding, M., Truccolo, W. A., & Bressler, S. L. (2001). Evaluating causal relations in neural systems: Granger causality, directed transfer function and statistical assessment of significance. *Biological Cybernetics*, *85*, 145–157.

Kampe, K. K. W., Jones, R. A., & Auer, D. P. (2000). Frequency dependence of the functional MRI response after electrical median nerve stimulation. *Human Brain Mapping*, *9*(2), 106–114. https://doi.org/10.1002/(SICI)1097-0193(200002)9:2<106::AID-HBM5>3.0.CO;2-Y

Kasdin, E. (2022, July 29). *A New Frontier – Lion Magazine*. Lion Magazine. https://lionmagazine.org/articles/a-new-frontier/

Kim, C. K., Adhikari, A., & Deisseroth, K. (2017). Integration of optogenetics with complementary methodologies in systems neuroscience. *Nature Reviews Neuroscience*, *18*(4), 222–235. https://doi.org/10.1038/nrn.2017.15.Integration

Kim, H., Ährlund-Richter, S., Wang, X., Deisseroth, K., & Carlén, M. (2016). Prefrontal Parvalbumin Neurons in Control of Attention. *Cell*, *164*(1–2), 208–218. https://doi.org/10.1016/j.cell.2015.11.038

Klapoetke, N. C., Murata, Y., Kim, S. S., Pulver, S. R., Birdsey-Benson, A., Cho, Y. K., Morimoto, T. K., Chuong, A. S., Carpenter, E. J., Tian, Z., Wang, J., Xie, Y., Yan, Z., Zhang, Y., Chow, B. Y., Surek, B., Melkonian, M., Jayaraman, V., Constantine-Paton, M., … Boyden, E. S. (2014). Independent optical excitation of distinct neural populations. *Nature Methods*, *11*(3), 338–346. https://doi.org/10.1038/nmeth.2836

Klein, C., Evrard, H. C. C., Shapcott, K. A. A., Haverkamp, S., Logothetis, N. K. K., & Schmid, M. C. C. (2016a). Cell-Targeted Optogenetics and Electrical Microstimulation Reveal the Primate Koniocellular Projection to Supra-granular Visual Cortex. *Neuron*, *90*(1), 143–151. https://doi.org/10.1016/j.neuron.2016.02.036

Klink, P. C., Dagnino, B., Gariel-Mathis, M. A., & Roelfsema, P. R. (2017). Distinct Feedforward and Feedback Effects of Microstimulation in Visual Cortex Reveal Neural Mechanisms of Texture Segregation. *Neuron*, *95*(1), 209-220.e3. https://doi.org/10.1016/j.neuron.2017.05.033

Kole, M. H. P., Stuart, G. J., Buzsáki, G., Kandel, A., Kipke, D. R., Shain, W., Fetz, E., Henderson, J. M., Hetke, J. F., Belitski, A., Gretton, A., Magri, C., Murayama, Y., Montemurro, M. A., Logothetis, N. K., Panzeri,

S., Cybulski, T. R., Glaser, J. I., Marblestone, A. H., … Koch, C. (2012). Targeted optogenetic stimulation and recording of neurons in vivo using cell-type-specific expression of Channelrhodopsin-2. *Nature Protocols*, *5*(2), 247–254. https://doi.org/10.1038/nprot.2009.228.Targeted

Kozai, T. D. Y., & Vazquez, A. L. (2015). Photoelectric artefact from optogenetics and imaging on microelectrodes and bioelectronics: New Challenges and Opportunities. *Journal of Materials Chemistry B*, *3*(25), 4965–4978. https://doi.org/10.1039/C5TB00108K.Photoelectric

Kujala, J., Jung, J., Bouvard, S., Lecaignard, F., Lothe, A., Bouet, R., Ciumas, C., Ryvlin, P., & Jerbi, K. (2015). Gamma oscillations in V1 are correlated with GABAA receptor density: A multi-modal MEG and Flumazenil-PET study. *Scientific Reports*, *5*(October), 1–12. https://doi.org/10.1038/srep16347

Lamme, V., Supèr, H., & Spekrijse, H. (2001). Two distinct modes of sensory processing observed in monkey primary visual cortex (V1). *Nature Neuroscience*, *4*(3), 304–310.

Laurens, J. (2022). The statistical power of three monkeys. *BioRxiv*, 2022.05.10.491373. https://doi.org/10.1101/2022.05.10.491373

Lee, S. H., Kim, J., Shin, J. H., Lee, H. E., Kang, I. S., Gwak, K., Kim, D. S., Kim, D., & Lee, K. J. (2018). Optogenetic control of body movements via flexible vertical light-emitting diodes on brain surface. *Nano Energy*, *44*(November 2017), 447–455. https://doi.org/10.1016/j.nanoen.2017.12.011

Lerchner, W., Corgiat, B., der Minassian, V., Saunders, R. C., & Richmond, B. J. (2014). Injection parameters and virus dependent choice of promoters to improve neuron targeting in the nonhuman primate brain. *Gene Therapy*, *21*(3), 233–241. https://doi.org/10.1038/gt.2013.75

Lewis, C. M., Ni, J., Wunderle, T., Jendritza, P., Lazar, A., Diester, I., & Fries, P. (2021). Cortical gamma-band resonance preferentially transmits coherent input. *Cell Reports*, *35*(5). https://doi.org/10.1016/j.celrep.2021.109083

Lewis, P. M., Ackland, H. M., Lowery, A. J., & Rosenfeld, J. v. (2015). Restoration of vision in blind individuals using bionic devices: A review with a focus on cortical visual prostheses. *Brain Research*, *1595*, 51–73. https://doi.org/10.1016/j.brainres.2014.11.020

Lewis, P. M., & Rosenfeld, J. v. (2016). Electrical stimulation of the brain and the development of cortical visual prostheses: An historical

perspective. *Brain Research*, *1630*, 208–224. https://doi.org/10.1016/j.brainres.2015.08.038

Lin, J. Y. (2011). A user's guide to channelrhodopsin variants: Features, limitations and future developments. *Experimental Physiology*, *96*(1), 19–25. https://doi.org/10.1113/expphysiol.2009.051961

Lin, J. Y. (2012). A User's Guide to Channelrhodopsin Variants. *Experimental Physiology*, *96*(1), 19–25. https://doi.org/10.1113/expphysiol.2009.051961.A

Liske, H., Qian, X., Anikeeva, P., Deisseroth, K., & Delp, S. (2013). Optical control of neuronal excitation and inhibition using a single opsin protein, ChR2. *Scientific Reports*, *3*, 2–8. https://doi.org/10.1038/srep03110

Liu, X. B., & Jones, E. G. (1996). Localization of alpha type II calcium calmodulin-dependent protein kinase at glutamatergic but not γ-aminobutyric acid (GABAergic) synapses in thalamus and cerebral cortex. *Proceedings of the National Academy of Sciences of the United States of America*, *93*(14), 7332–7336. https://doi.org/10.1073/pnas.93.14.7332

Liu, X., Chen, P., Ding, X., Liu, A., Li, P., Sun, C., & Guan, H. (2022). A narrative review of cortical visual prosthesis systems: the latest progress and significance of nanotechnology for the future. *Annals of Translational Medicine*, *10*(12), 716–716. https://doi.org/10.21037/atm-22-2858

Liu, X., McCreery, D. B., Bullara, L. A., & Agnew, W. F. (2006). Evaluation of the stability of intracortical microelectrode arrays. *IEEE Transactions on Neural Systems and Rehabilitation Engineering*, *14*(1), 91–100. https://doi.org/10.1109/TNSRE.2006.870495

Logothetis, N. K., Augath, M., Murayama, Y., Rauch, A., Sultan, F., Goense, J., Oeltermann, A., & Merkle, H. (2010). The effects of electrical microstimulation on cortical signal propagation. *Nature Neuroscience*, *13*(10), 1283–1291. https://doi.org/10.1038/nn.2631

Logothetis, N. K., Pauls, J., Augath, M., Trinath, T., & Oeltermann, A. (2001). Neurophysiological investigation of the basis of the fMRI signal. *Nature*, *412*(12), 150–157.

Logothetis, N. K., & Wandell, B. A. (2004). Interpreting the BOLD signal. *Annual Review of Physiology*, *66*, 735–769. https://doi.org/10.1146/annurev.physiol.66.082602.092845

Lowery, A. J., Rosenfeld, J. v., Rosa, M. G. P., Brunton, E., Rajan, R., Mann, C., Armstrong, M., Mohan, A., Josh, H., Kleeman, L., Li, W. H., &

Pritchard, J. (2017). Monash Vision Group's Gennaris Cortical Implant for Vision Restoration. *Artificial Vision*, *Hons I*, 215–225. https://doi.org/10.1007/978-3-319-41876-6_17

Lozano-Soldevilla, D., ter Huurne, N., Cools, R., & Jensen, O. (2014). GABAergic modulation of visual gamma and alpha oscillations and its consequences for working memory performance. *Current Biology*, *24*(24), 2878–2887. https://doi.org/10.1016/j.cub.2014.10.017

Lu, Y., Truccolo, W., Wagner, F. B., Vargas-Irwin, C. E., Ozden, I., Zimmermann, J. B., May, T., Agha, N. S., Wang, J., & Nurmikko, A. v. (2015). Optogenetically induced spatiotemporal gamma oscillations and neuronal spiking activity in primate motor cortex. *J Neurophysiol*, *113*, 3574–3587. https://doi.org/10.1152/jn.00792.2014.-Transient

Lu, Y., Yan, Y., Chai, X., Ren, Q., Chen, Y., & Li, L. (2013). Electrical stimulation with a penetrating optic nerve electrode array elicits visuotopic cortical responses in cats. *Journal of Neural Engineering*, *10*(3). https://doi.org/10.1088/1741-2560/10/3/036022

Luck, S. J., Chelazzi, L., Hillyard, S. A., & Desimone, R. (1997). Neural mechanisms of spatial selective attention in areas V1, V2, and V4 of macaque visual cortex. *Journal of Neurophysiology*, *77*(1), 24–42. https://doi.org/10.1152/jn.1997.77.1.24

Lund, J. S. (1973). Organization of neurons in the visual cortex, area 17, of the monkey (Macaca mulatta). *The Journal of Comparative Neurology*, *147*(4), 455–496. https://doi.org/10.1002/cne.901470404

Lund, J. S. (1988). Anatomical organization of macaque monkey striate visual cortex. *Annual Review of Neuroscience*, *11*, 253–288. https://doi.org/10.1146/annurev.ne.11.030188.001345

Lund, J. S., Angelucci, A., & Bressloff, P. C. (2003). Anatomical Substrates for Functional Columns in Macaque Monkey Primary Visual Cortex. *Cerebral Cortex*, *13*(1), 15–24.

Macdougall, M., Nummela, S. U., Coop, S., Disney, A., Mitchell, J. F., & Miller, C. T. (2016). Optogenetic manipulation of neural circuits in awake marmosets. *Journal of Neurophysiology*, *116*(3), 1286–1294. https://doi.org/10.1152/jn.00197.2016

Maier, A., Adams, G. K., Aura, C., & Leopold, D. A. (2010). Distinct Superficial and deep laminar domains of activity in the visual cortex during rest and stimulation. *Frontiers in System Neuroscience*, *4*(August), 1–11. https://doi.org/10.3389/fnsys.2010.00031

Maier, A., Aura, C. J., & Leopold, D. A. (2011). Infragranular sources of sustained local field potential responses in macaque primary visual cortex. *Journal of Neuroscience*, *31*(6), 1971–1980. https://doi.org/10.1523/JNEUROSCI.5300-09.2011

Mamad, O., Agayby, B., Stumpp, L., Reilly, R. B., & Tsanov, M. (2019). Extrafield activity shifts the place field center of mass to encode aversive experience. *ENeuro*, *6*(2). https://doi.org/10.1523/ENEURO.0423-17.2019

Marin, C., & Fernández, E. (2010). Biocompatibility of intracortical microelectrodes: Current status and future prospects. *Frontiers in Neuroengineering*, *3*(MAY). https://doi.org/10.3389/fneng.2010.00008

Marion, R., Li, K., Purushothaman, G., Jiang, Y., & Casagrande, V. A. (2013). Morphological and neurochemical comparisons between pulvinar and V1 projections to V2. *Journal of Comparative Neurology*, *521*(4), 813–832. https://doi.org/10.1002/cne.23203

Matsuo, T., Uchida, T., Sakurai, J., Yamashita, K., Matsuo, C., Araki, T., Yamashita, Y., & Kamikawa, K. (2018). Visual Evoked Potential Recovery by Subretinal Implantation of Photoelectric Dye-Coupled Thin Film Retinal Prosthesis in Monkey Eyes With Macular Degeneration. *Artificial Organs*, *42*(8), E186–E203. https://doi.org/10.1111/aor.13120

Mattis, J., Tye, K. M., Ferenczi, E. a, Ramakrishnan, C., O'Shea, D. J., Prakash, R., Gunaydin, L. a, Hyun, M., Fenno, L. E., Gradinaru, V., Yizhar, O., & Deisseroth, K. (2011). Principles for applying optogenetic tools derived from direct comparative analysis of microbial opsins. *Nature Methods*, *9*(2), 159–172. https://doi.org/10.1038/nmeth.1808

Mattis, J., Tye, K. M., Ferenczi, E. A., Ramakrishnan, C., O'Shea, D. J., Prakash, R., Gunaydin, L. A., Hyun, M., Fenno, L. E., Gradinaru, V., Yizhar, O., & Deisseroth, K. (2012). Principles for applying optogenetic tools derived from direct comparative analysis of microbial opsins. *Nature Methods*, *9*(2), 159–172. https://doi.org/10.1038/nmeth.1808

May, P. J., & Warren, S. (2020). Pupillary light reflex circuits in the Macaque Monkey: the olivary pretectal nucleus. *Brain Structure and Function*, *225*(1), 305–320. https://doi.org/10.1007/s00429-019-02003-7

May, T., Ozden, I., Brush, B., Borton, D., Wagner, F., Agha, N., Sheinberg, D. L., & Nurmikko, A. v. (2014). Detection of optogenetic stimulation in somatosensory cortex by non-human primates - Towards artificial

tactile sensation. *PLoS ONE*, *9*(12), 1–18. https://doi.org/10.1371/journal.pone.0114529

Mazer, J. A., Vinje, W. E., McDermott, J., Schiller, P. H., & Gallant, J. L. (2002). Spatial frequency and orientation tuning dynamics in area V1. *Proceedings of the National Academy of Sciences of the United States of America*, *99*(3), 1645–1650. https://doi.org/10.1073/pnas.022638499

McAlinden, N., Cheng, Y., Scharf, R., Xie, E., Gu, E., Reiche, C. F., Sharma, R., Tathireddy, P., Tathireddy, P., Rieth, L., Blair, S., & Mathieson, K. (2019). Multisite microLED optrode array for neural interfacing. *Neurophotonics*, *6*(03), 1. https://doi.org/10.1117/1.nph.6.3.035010

McFarland, J. M., Bondy, A. G., Saunders, R. C., Cumming, B. G., & Butts, D. A. (2015). Saccadic modulation of stimulus processing in primary visual cortex. *Nature Communications*, *6*, 1–14. https://doi.org/10.1038/ncomms9110

McIntyre, C. C., & Grill, W. M. (2002). Extracellular stimulation of central neurons: Influence of stimulus waveform and frequency on neuronal output. *Journal of Neurophysiology*, *88*(4), 1592–1604. https://doi.org/10.1152/jn.2002.88.4.1592

Mehta, A. D., Ulbert, I., & Schroeder, C. E. (2000a). Intermodal selective attention in monkeys I: Distribution and timing of effects across visual areas. *Cerebral Cortex*, *10*(4), 343–358. https://doi.org/10.1093/cercor/10.4.343

Mehta, A. D., Ulbert, I., & Schroeder, C. E. (2000b). Intermodal selective attention in monkeys. II: Physiological mechanisms of modulation. *Cerebral Cortex*, *10*(4), 359–370. https://doi.org/10.1093/cercor/10.4.359

Mendoza, S. D., El-Shamayleh, Y., & Horwitz, G. D. (2017). AAV-mediated delivery of optogenetic constructs to the macaque brain triggers humoral immune responses. *Journal of Neurophysiology*, *117*(5), 2004–2013. https://doi.org/10.1152/jn.00780.2016

Michalareas, G., Vezoli, J., van Pelt, S., Schoffelen, J. M., Kennedy, H., & Fries, P. (2016). Alpha-Beta and Gamma Rhythms Subserve Feedback and Feedforward Influences among Human Visual Cortical Areas. *Neuron*, *89*(2), 384–397. https://doi.org/10.1016/j.neuron.2015.12.018

Michelson, C. A., Pillow, J. W., & Seidemann, E. (2017). Majority of choice-related variability in perceptual decisions is present in early sensory cortex. *BioRxiv*. https://doi.org/10.1101/207357

Mills, J. O., Jalil, A., & Stanga, P. E. (2017). Electronic retinal implants and artificial vision: Journey and present. *Eye (Basingstoke)*, *31*(10), 1383–1398. https://doi.org/10.1038/eye.2017.65

Mirochnik, R. M., & Pezaris, J. S. (2019). Contemporary approaches to visual prostheses. *Military Medical Research*, *6*(1), 1–9. https://doi.org/10.1186/s40779-019-0206-9

Mohanty, S. K., & Lakshminarayananan, V. (2015). Optical Techniques in Optogenetics. *Journal of Modern Optics*, *62*(12), 949–970. https://doi.org/10.1080/09500340.2015.1010620.Optical

Murasugi, C. M., Salzman, C. D., & Newsome, W. T. (1993). Microstimulation in visual area MT: Effects of varying pulse amplitude and frequency. *Journal of Neuroscience*, *13*(4), 1719–1729. https://doi.org/10.1523/jneurosci.13-04-01719.1993

Murphey, D. K., & Maunsell, J. H. R. (2007). Behavioral detection of electrical microstimulation in different cortical visual areas. *Current Biology*, *17*(10), 862–867. https://doi.org/10.1007/978-3-642-02008-7_22

Murris, S. R., Arsenault, J. T., & Vanduffel, W. (2020). Frequency- And State-Dependent Network Effects of Electrical Stimulation Targeting the Ventral Tegmental Area in Macaques. *Cerebral Cortex*, *30*(8), 4281–4296. https://doi.org/10.1093/cercor/bhaa007

Muthukumaraswamy, S. D., Edden, R. a E., Jones, D. K., Swettenham, J. B., & Singh, K. D. (2009). Resting GABA concentration predicts peak gamma frequency and fMRI amplitude in response to visual stimulation in humans. *Proceedings of the National Academy of Sciences of the United States of America*, *106*(20), 8356–8361. https://doi.org/10.1073/pnas.0900728106

Nagel, G., Ollig, D., Fuhrmann, M., Kateriya, S., Musti, A. M., Bamberg, E., & Hegemann, P. (2002). Channelrhodopsin-1: A Light-Gated Proton Channel in Green Algae. *Science*, *296*(5577), 2395–2398. https://www.science.org

Nagel, G., Szellas, T., Huhn, W., Kateriya, S., Adeishvili, N., Berthold, P., Ollig, D., Hegemann, P., & Bamberg, E. (2003a). Channelrhodopsin-2, a directly light-gated cation-selective membrane channel. *Proceedings*

of the National Academy of Sciences of the United States of America, *100*(24), 13940–13945. https://doi.org/10.1073/pnas.1936192100

Nakamichi, Y., Okubo, K., Sato, T., Hashimoto, M., & Tanifuji, M. (2019). Optical intrinsic signal imaging with optogenetics reveals functional cortico-cortical connectivity at the columnar level in living macaques. *Scientific Reports*, *9*(1), 6466. https://doi.org/10.1038/s41598-019-42923-2

Nassi, J. J., Avery, M. C., Cetin, A. H., Roe, A. W., & Reynolds, J. H. (2015a). Optogenetic activation of normalization in alert macaque visual cortex. *Neuron*, *86*(6), 1504–1517. https://doi.org/10.1016/j.neuron.2015.05.040

Nassi, J. J., & Callaway, E. M. (2007). Specialized Circuits from Primary Visual Cortex to V2 and Area MT. *Neuron*, *55*(5), 799–808. https://doi.org/10.1016/j.neuron.2007.07.037

Nazempour, R., Zhang, Q., Fu, R., & Sheng, X. (2018). Biocompatible and Implantable Optical Fibers and Waveguides for Biomedicine. *Materials*, *11*(8), 1283. https://doi.org/10.3390/ma11081283

Newsome, W. T., Britten, K. H., & Movshon, J. A. (1989). Neuronal correlates of a perceptual decision. *Letters to Nature*, *341*, 52–54. https://doi.org/10.1038/246170a0

Nguyen, H. T., Tangutooru, S. M., Rountree, C. M., Kantzos, A. J. K., Tarlochan, F., Yoon, W. J., & Troy, J. B. (2016). Thalamic visual prosthesis. *IEEE Transactions on Biomedical Engineering*, *63*(8), 1573–1580. https://doi.org/10.1109/TBME.2016.2567300

Nichols, M. J., & Newsome, W. T. (2002). Middle temporal visual area microstimulation influences veridical judgments of motion direction. *Journal of Neuroscience*, *22*(21), 9530–9540. https://doi.org/10.1523/jneurosci.22-21-09530.2002

Nienborg, H., & Cumming, B. G. (2014). Decision-related activity in sensory neurons may depend on the columnar architecture of cerebral cortex. *Journal of Neuroscience*, *34*(10), 3579–3585. https://doi.org/10.1523/JNEUROSCI.2340-13.2014

Niketeghad, S., Muralidharan, A., Patel, U., Dorn, J. D., Bonelli, L., Greenberg, R. J., & Pouratian, N. (2020). Phosphene perceptions and safety of chronic visual cortex stimulation in a blind subject. *Journal of Neurosurgery*, *132*(June), 2000–2007. https://doi.org/10.3171/2019.3.JNS182774.2000

Ohayon, S., Grimaldi, P., Schweers, N., & Tsao, D. Y. (2013). Saccade Modulation by Optical and Electrical Stimulation in the Macaque Frontal Eye Field. *Journal of Neuroscience*, *33*(42), 16684–16697. https://doi.org/10.1523/JNEUROSCI.2675-13.2013

O'Kusky, J., & Colonnier, M. (1982). A laminar analysis of the number of neurons, glia, and synapses in the visual cortex (area 17) of adult macaque monkeys. *Journal of Comparative Neurology*, *210*(3), 278–290. https://doi.org/10.1002/cne.902100307

Oostenveld, R., Fries, P., Maris, E., & Schoffelen, J. M. (2011). FieldTrip: Open source software for advanced analysis of MEG, EEG, and invasive electrophysiological data. *Computational Intelligence and Neuroscience*, *2011*. https://doi.org/10.1155/2011/156869

Ortiz-Rios, M., Agayby, B., Balezeau, F., Haag, M., Rima, S., & Schmid, M. C. (2021). Optogenetic stimulation of primate V1 reveals local laminar and large-scale cortical networks related to perceptual phosphenes. *BioRxiv [Preprint]*, 1–51.

Ortiz-Rios, M., Haag, M., Balezeau, F., Frey, S., Thiele, A., Murphy, K., & Schmid, M. C. (2018). Improved methods for MRI-compatible implants in nonhuman primates. *Journal of Neuroscience Methods*, *308*(May), 377–389. https://doi.org/10.1016/j.jneumeth.2018.09.013

Owen, S. F., Liu, M. H., & Kreitzer, A. C. (2019). Thermal constraints on in vivo optogenetic manipulations. *Nature Neuroscience*, *22*(July), 1061–1065. https://doi.org/10.1038/s41593-019-0422-3

Palmhof, M., Frank, V., Rappard, P., Kortenhorn, E., Demuth, J., Biert, N., Stute, G., Dick, H. B., & Joachim, S. C. (2019). From ganglion cell to photoreceptor layer: Timeline of deterioration in a rat ischemia/reperfusion model. *Frontiers in Cellular Neuroscience*, *13*(May), 1–19. https://doi.org/10.3389/fncel.2019.00174

Palmigiano, A., Geisel, T., Wolf, F., & Battaglia, D. (2017). Flexible information routing by transient synchrony. *Nature Neuroscience*, *20*(7), 1014–1022. https://doi.org/10.1038/nn.4569

Pandey, P., & Ray, S. (2021). Pupil dynamics: A potential proxy of neural preparation for goal-directed eye movement. *European Journal of Neuroscience*, *54*(7), 6587–6607. https://doi.org/10.1111/ejn.15453

Panetsos, F., Sanchez-Jimenez, A., Cerio, E. D. de, Diaz-Guemes, I., & Sanchez, F. M. (2011). Consistent phosphenes generated by electrical microstimulation of the visual thalamus. An experimental approach for

thalamic visual neuroprostheses. *Frontiers in Neuroscience*, *5*(JUL), 1–12. https://doi.org/10.3389/fnins.2011.00084

Peinkhofer, C., Knudsen, G. M., Moretti, R., & Kondziella, D. (2019). Cortical modulation of pupillary function: Systematic review. *PeerJ Computer Science*, *2019*(7). https://doi.org/10.7717/peerj.6882

Perkel, D. J., Bullier, J., & Kennedy, H. (1986). Topography of the afferent connectivity of area 17 in the macaque monkey: A double-labelling study. *Journal of Comparative Neurology*, *253*(3), 374–402. https://doi.org/10.1002/cne.902530307

Peters, A., & Sethares, C. (1991). Organization of pyramidal neurons in area 17 of monkey visual cortex. *Journal of Comparative Neurology*, *306*(1), 1–23. https://doi.org/10.1002/cne.903060102

Pettersen, K. H., Devor, A., Ulbert, I., Dale, A. M., & Einevoll, G. T. (2006). Current-source density estimation based on inversion of electrostatic forward solution: Effects of finite extent of neuronal activity and conductivity discontinuities. *Journal of Neuroscience Methods*, *154*(1–2), 116–133. https://doi.org/10.1016/j.jneumeth.2005.12.005

Pezaris, J. S., & Eskandar, E. N. (2009). Getting signals into the brain: visual prosthetics through thalamic microstimulation. *Neurosurgical Focus*, *27*(1), 1–20. https://doi.org/10.3171/2009.4.FOCUS0986.Getting

Pezaris, J. S., & Reid, R. C. (2007a). Demonstration of artificial visual percepts generated through thalamic microstimulation. *Proceedings of the National Academy of Sciences of the United States of America*, *104*(18), 7670–7675. https://doi.org/10.1073/pnas.0608563104

Pezaris, J. S., & Reid, R. C. (2009). Simulations of electrode placement for a thalamic visual prosthesis. *IEEE Transactions on Biomedical Engineering*, *56*(1), 172–178. https://doi.org/10.1109/TBME.2008.2005973

Picaud, S., Dalkara, D., Marazova, K., Goureau, O., Roska, B., & Sahel, J.-A. (2019). The primate model for understanding and restoring vision. *National Academy of Sciences*, 10. https://doi.org/10.1073/pnas.1902292116ï

Pio-Lopez, L., Poulkouras, R., & Depannemaecker, D. (2021). Visual cortical prosthesis: an electrical perspective. *Journal of Medical Engineering and Technology*, *45*(5), 394–407. https://doi.org/10.1080/03091902.2021.1907468

Pisanello, F., Mandelbaum, G., Pisanello, M., Oldenburg, I. A., Sileo, L., Markowitz, J. E., Peterson, R. E., della Patria, A., Haynes, T. M., Emara, M. S., Spagnolo, B., Datta, S. R., de Vittorio, M., & Sabatini, B. L. (2017). Dynamic illumination of spatially restricted or large brain volumes via a single tapered optical fiber. *Nature Neuroscience*. https://doi.org/10.1038/nn.4591

Pong, M., & Fuchs, A. F. (2000). Characteristics of the Pupillary Light Reflex in the Macaque Monkey: Discharge Patterns of Pretectal Neurons. *Journal of Neurophysiology*, *84*(2), 953–963. https://doi.org/10.1152/jn.2000.84.2.953

Prévot, P. H., Gehere, K., Arcizet, F., Akolkar, H., Khoei, M. A., Blaize, K., Oubari, O., Daye, P., Lanoë, M., Valet, M., Dalouz, S., Langlois, P., Esposito, E., Forster, V., Dubus, E., Wattiez, N., Brazhnikova, E., Nouvel-Jaillard, C., LeMer, Y., … Picaud, S. (2020). Behavioural responses to a photovoltaic subretinal prosthesis implanted in non-human primates. *Nature Biomedical Engineering*, *4*(2), 172–180. https://doi.org/10.1038/s41551-019-0484-2

Qiu, A., Rosenau, B. J., Greenberg, A. S., Hurdal, M. K., Barta, P., Yantis, S., & Miller, M. I. (2006). Estimating linear cortical magnification in human primary visual cortex via dynamic programming. *NeuroImage*, *31*(1), 125–138. https://doi.org/10.1016/j.neuroimage.2005.11.049

Raiguel, S. E., Lagae, L., Guly, B., & Orban, G. A. (1989). Short Communications Response latencies of visual cells in macaque areas V1 , V2 and V5. *Nature*, *493*, 155–159.

Raine, C. (2013). Cochlear implants in the United Kingdom: Awareness and utilization. *Cochlear Implants International*, *14*(SUPPL. 1). https://doi.org/10.1179/1467010013Z.00000000077

Rajalingham, R., Sorenson, M., Azadi, R., Bohn, S., DiCarlo, J. J., & Afraz, A. (2021). Chronically implantable LED arrays for behavioral optogenetics in primates. *Nature Methods*, *18*(9), 1112–1116. https://doi.org/10.1038/s41592-021-01238-9

Ramcharan, E. J., Gnadt, J. W., & Sherman, S. M. (2005). Higher-order thalamic relays burst more than first-order relays. *Proceedings of the National Academy of Sciences of the United States of America*, *102*(34), 12236–12241.

Ramirez, S., Liu, X., Lin, P.-A., Suh, J., Michele Pignatelli, Roger L. Redondo, Tomás J. Ryan, & Susumu Tonegawa. (2012). Creating a

False Memory in the Hippocampus. *Science*, *341*(9), 387–391. https://doi.org/10.1126/science.1238036

Rasch, M. J., Gretton, A., Murayama, Y., Maass, W., & Logothetis, N. K. (2008). Inferring spike trains from local field potentials. *Journal of Neurophysiology*, *99*(3), 1461–1476. https://doi.org/10.1152/jn.00919.2007

Ray, S., Crone, N. E., Niebur, E., Franaszczuk, P. J., & Hsiao, S. S. (2008). Neural correlates of high-gamma oscillations (60-200 Hz) in macaque local field potentials and their potential implications in electrocorticography. *Journal of Neuroscience*, *28*(45), 11526–11536. https://doi.org/10.1523/JNEUROSCI.2848-08.2008

Ray, S., & Maunsell, J. H. R. (2011a). Different Origins of Gamma Rhythm and High-Gamma Activity in Macaque Visual Cortex. *PLoS Biol*, *9*(4), 1000610. https://doi.org/10.1371/journal.pbio.1000610

Ress, D., Backus, B. T., & Heeger, D. J. (2000). Activity in primary visual cortex predicts performance in a visual detection task. *Nature Neuroscience*, *3*(9), 940–945.

Ress, D., & Heeger, D. J. (2003). Neuronal correlates of perception in early visual cortex. *Nature Neuroscience*, *6*(4), 414–420. https://doi.org/10.1038/nn1024

Reynolds, J. H., & Chelazzi, L. (2004). Attentional modulation of visual processing. *Annual Review of Neuroscience*, *27*, 611–647. https://doi.org/10.1146/annurev.neuro.26.041002.131039

Ringach, D. L., Hawken, M. J., & Shapley, R. (2003). Dynamics of orientation tuning in macaque V1: The role of global and tuned suppression. *Journal of Neurophysiology*, *90*(1), 342–352. https://doi.org/10.1152/jn.01018.2002

Ringach, D. L., Shapley, R. M., & Hawken, M. J. (2002). Orientation selectivity in macaque V1: diversity and laminar dependence. *The Journal of Neuroscience : The Official Journal of the Society for Neuroscience*, *22*(13), 5639–5651. https://doi.org/20026567

Roelfsema, P. R., & Spekreijse, H. (2001). The representation of erroneously perceived stimuli in the primary visual cortex. *Neuron*, *31*(5), 853–863. https://doi.org/10.1016/S0896-6273(01)00408-1

Rousche, P. J., & Normann, R. A. (1992). A method for pneumatically inserting an array of penetrating electrodes into cortical tissue. *Annals of Biomedical Engineering*, *20*(4), 413–422. https://doi.org/10.1007/BF02368133

Ruiz, O., Lustig, B. R., Nassi, J. J., Cetin, A., Reynolds, J. H., Albright, T. D., Callaway, E. M., Stoner, G. R., & Roe, A. W. (2013). Optogenetics through windows on the brain in the nonhuman primate. *Journal of Neurophysiology*, *110*(6), 1455–1467. https://doi.org/10.1152/jn.00153.2013

Rushton, D. N., & Brindley, G. S. (1977). Properties of Cortical Electrica! Phosphenes. *Frontiers in Visual Science*, *8*(6), 574–593.

Sachs, H. G., Gekeler, F., Schwahn, H., Jakob, W., Köhler, M., Schulmeyer, F., Marienhagen, J., Brunner, U., & Framme, C. (2005). Implantation of stimulation electrodes in the subretinal space to demonstrate cortical responses in Yucatan minipig in the course of visual prosthesis development. *European Journal of Ophthalmology*, *15*(4), 493–499. https://doi.org/10.1177/112067210501500413

Sahel, J. A., Boulanger-Scemama, E., Pagot, C., Arleo, A., Galluppi, F., Martel, J. N., Esposti, S. D., Delaux, A., de Saint Aubert, J. B., de Montleau, C., Gutman, E., Audo, I., Duebel, J., Picaud, S., Dalkara, D., Blouin, L., Taiel, M., & Roska, B. (2021). Partial recovery of visual function in a blind patient after optogenetic therapy. *Nature Medicine*, *27*(7), 1223–1229. https://doi.org/10.1038/s41591-021-01351-4

Sakaguchi, H., Kamei, M., Fujikado, T., Yonezawa, E., Ozawa, M., Cecilia-Gonzalez, C., Ustariz-Gonzalez, O., Quiroz-Mercado, H., & Tano, Y. (2009). Artificial vision by direct optic nerve electrode (AV-DONE) implantation in a blind patient with retinitis pigmentosa. *Journal of Artificial Organs*, *12*(3), 206–209. https://doi.org/10.1007/s10047-009-0467-2

Saleem, K. S., Avram, A. v., Glen, D., Yen, C. C. C., Ye, F. Q., Komlosh, M., & Basser, P. J. (2021). High-resolution mapping and digital atlas of subcortical regions in the macaque monkey based on matched MAP-MRI and histology. *NeuroImage*, *245*. https://doi.org/10.1016/j.neuroimage.2021.118759

Salin, P.-A., & Bullier, J. (1995). Corticocortical connections in the visual system: structure and function. *Physiological Reviews*, *75*(1), 107–154. https://doi.org/10.1152/physrev.1995.75.1.107

Santos-Ferreira, T. F., Borsch, O., & Ade, M. (2017). Rebuilding the missing Part—A review on photoreceptor transplantation. *Frontiers in Systems Neuroscience*, *10*(January), 1–14. https://doi.org/10.3389/fnsys.2016.00105

Sceniak, M. P., Hawken, M. J., & Shapley, R. (2001). *Visual Spatial Characterization of Macaque V1 Neurons*. www.jn.physiology.org

Scheeringa, R., & Fries, P. (2019). Cortical layers, rhythms and BOLD signals. *NeuroImage*, *197*(October 2017), 689–698. https://doi.org/10.1016/j.neuroimage.2017.11.002

Schiller, P. H., Slocum, W. M., Kwak, M. C., Kendall, G. L., & Tehovnik, E. J. (2011). New methods devised specify the size and color of the spots monkeys see when striate cortex (area V1) is electrically stimulated. *Proceedings of the National Academy of Sciences*, *108*(43), 17809–17814. https://doi.org/10.1073/pnas.1108337108

Schiller, P. H., & Tehovnik, E. J. (2015). *Vision and the Visual System*. Oxford University Press.

Schmidt, E. M., Bak, M. J., Hambrecht, F. T., Kufta, C. v., O'Rourke, D. K., & Vallabhanath, P. (1996). Feasibility of a visual prosthesis for the blind based on intracortical microstimulation of the visual cortex. *Brain*, *119*(2), 507–522. https://doi.org/10.1093/brain/119.2.507

Schoenenberger, P., Grunditz, Å., Rose, T., & Oertner, T. G. (2008). Optimizing the spatial resolution of Channelrhodopsin-2 activation. *Brain Cell Biology*, *36*(1–4), 119–127. https://doi.org/10.1007/s11068-008-9025-8

Schroeder, C. E., Mehta, A. D., & Givre, S. J. (1998). A spatiotemporal profile of visual system activation revealed by current source density analysis in the awake macaque. *Cerebral Cortex*, *8*(7), 575–592. https://doi.org/10.1093/cercor/8.7.575

Schroeder, C. E., Tenke, C. E., Givre, S. J., Arezzo, J. C., & Vaughan, H. G. (1990). Laminar analysis of bicuculline-induced epileptiform activity in area 17 of the awake macaque. *Brain Research*, *515*(1–2), 326–330. https://doi.org/10.1016/0006-8993(90)90617-K

Schroeder, C. E., Tenke, C. E., Givre, S. J., Arezzo, J. C., & VaughanJr, H. G. (1991). Striate cortical contribution to the surface-recorded pattern-reversal vep in the alert monkey. *Vision Research*, *31*(7/8), 1143–1157.

Schütz, A. C., Trommershäuser, J., & Gegenfurtner, K. R. (2012). Dynamic integration of information about salience and value for saccadic eye movements. *Proceedings of the National Academy of Sciences of the United States of America*, *109*(19), 7547–7552. https://doi.org/10.1073/pnas.1115638109

Seidemann, E., & Geisler, W. S. (2018). Linking V1 activity to behavior. *Annual Review of Vision Science*, *4*, 287–310. https://doi.org/10.1146/annurev-vision-102016-061324

Self, M. W., van Kerkoerle, T., Supèr, H., & Roelfsema, P. R. (2013). Distinct Roles of the Cortical Layers of Area V1 in Figure-Ground Segregation. *Current Biology*, *23*(21), 2121–2129. https://doi.org/10.1016/j.cub.2013.09.013

Senova, S., Scisniak, I., Chiang, C. C., Doignon, I., Palfi, S., Chaillet, A., Martin, C., & Pain, F. (2017). Experimental assessment of the safety and potential efficacy of high irradiance photostimulation of brain tissues. *Scientific Reports*, *7*(June 2016), 43997. https://doi.org/10.1038/srep43997

Shapcott, K. A., Schmiedt, J. T., Saunders, R. C., Maier, A., Leopold, D. A., & Schmid, M. C. (2016). Correlated activity of cortical neurons survives extensive removal of feedforward sensory input. *Scientific Reports*, *6*, 1–8. https://doi.org/10.1038/srep34886

Shen, Y., Campbell, R. E., Côté, D. C., & Paquet, M. E. (2020). Challenges for Therapeutic Applications of Opsin-Based Optogenetic Tools in Humans. *Frontiers in Neural Circuits*, *14*(July), 1–11. https://doi.org/10.3389/fncir.2020.00041

Shepherd, R. K., Shivdasani, M. N., Nayagam, D. A. X., Williams, C. E., & Blamey, P. J. (2013). Visual prostheses for the blind. *Trends in Biotechnology*, *31*(10), 562–571. https://doi.org/10.1016/j.tibtech.2013.07.001

Sincich, L. C., Park, K. F., Wohlgemuth, M. J., & Horton, J. C. (2004). Bypassing V1: A direct geniculate input to area MT. *Nature Neuroscience*, *7*(10), 1123–1128. https://doi.org/10.1038/nn1318

Smith, J. E. T., Beliveau, V., Schoen, A., Remz, J., Zhan, C. A., & Cook, E. P. (2015). Dynamics of the functional link between area MT LFPs and motion detection. *Journal of Neurophysiology*, *114*(1), 80–98. https://doi.org/10.1152/jn.00058.2015

Snapp, E. L. (2009). Fluorescent Proteins: A Cell Biologist's User Guide. *Trends Cell Biol.*, *19*(11), 649–655. https://doi.org/10.1016/j.tcb.2009.08.002.Fluorescent

Sohal, V. S., Zhang, F., Yizhar, O., & Deisseroth, K. (2009). Parvalbumin neurons and gamma rhythms enhance cortical circuit performance. *Nature*, *459*(7247), 698–702. https://doi.org/10.1038/nature07991

Spaak, E., Bonnefond, M., Maier, A., Leopold, D. A., & Jensen, O. (2012). Layer-specific entrainment of gamma-band neural activity by the alpha rhythm in monkey visual cortex. *Current Biology*, *22*(24), 2313–2318. https://doi.org/10.1016/j.cub.2012.10.020

Sparks, D. L., & Mays, L. E. (1990). *Signal transformations required for the generation of saccadic eye movements*. www.annualreviews.org

Spillmann, L., Dresp-Langley, B., & Tseng, C. huei. (2015). Beyond the classical receptive field: The effect of contextual stimuli. *Journal of Vision*, *15*(9), 1–23. https://doi.org/10.1167/15.9.7

Strickl, E., & Harris, A. (2022). *Their Bionic Eyes Are Now Obsolete and Unsupported*. https://spectrum.ieee.org/bionic-eye-obsolete

Stujenske, J. M., Spellman, T., & Gordon, J. A. (2015). Modeling the Spatiotemporal Dynamics of Light and Heat Propagation for InVivo Optogenetics. *Cell Reports*, *12*(3), 525–534. https://doi.org/10.1016/j.celrep.2015.06.036

Supèr, H., & Roelfsema, P. R. (2005). Chronic multiunit recordings in behaving animals : advantages and limitations . *Progress in Brain Research*. https://doi.org/10.1016/S0079-6123(04)47020-4

Tantama, M., Hung, Y. P., & Yellen, G. (2012). Optogenetic Reporters: Fluorescent Protein-Based Genetically- Encoded Indicators of Signaling and Metabolism in the Brain. *Progress in Brain Research*, *196*, 235–263. https://doi.org/10.1016/B978-0-444-59426-6.00012-4

Tatler, B. W., Hayhoe, M. M., Land, M. F., & Ballard, D. H. (2011). Eye guidance in natural vision: reinterpreting salience. *Journal of Vision*, *11*(5), 5. https://doi.org/10.1167/11.5.5

Tehovnik, E. J. (1996). Electrical stimulation of neural tissue to evoke behavioral responses. *Journal of Neuroscience Methods*, *65*, 1–17. http://www.ncbi.nlm.nih.gov/pubmed/8815302

Tehovnik, E. J., & Slocum, W. M. (2005). Microstimulation of V1 affects the detection of visual targets: Manipulation of target contrast. *Experimental Brain Research*, *165*(3), 305–314. https://doi.org/10.1007/s00221-005-2306-x

Tehovnik, E. J., & Slocum, W. M. (2007). Phosphene Induction by Microstimulation of Macaque V1. *Brain Research Reviews*, *53*(2), 337–343.

Tehovnik, E. J., & Slocum, W. M. (2009). Depth-dependent detection of microampere currents delivered to monkey V1. *European Journal of*

Neuroscience, *29*(7), 1477–1489. https://doi.org/10.1111/j.1460-9568.2009.06695.x

Tehovnik, E. J., Slocum, W. M., & Carvey, C. E. (2003). Behavioural state affects saccadic eye movements evoked by microstimulation of striate cortex. *European Journal of Neuroscience*, *18*(4), 969–979. https://doi.org/10.1046/j.1460-9568.2003.02798.x

Tehovnik, E. J., Slocum, W. M., Carvey, C. E., & Schiller, P. H. (2005). Phosphene Induction and the Generation of Saccadic Eye Movements by Striate Cortex. *Journal of Neurophysiology*, *93*, 1–19. https://doi.org/10.1152/jn.00736.2004

Tehovnik, E. J., Slocum, W. M., & Schiller, P. H. (2002). Differential effects of laminar stimulation of V1 cortex on target selection by macaque monkeys. *European Journal of Neuroscience*, *16*(4), 751–760. https://doi.org/10.1046/j.1460-9568.2002.02123.x

Tehovnik, E. J., Slocum, W. M., & Schiller, P. H. (2003). Saccadic eye movements evoked by microstimulation of striate cortex. *European Journal of Neuroscience*, *17*(4), 870–878. https://doi.org/10.1046/j.1460-9568.2003.02489.x

Tehovnik, E. J., Slocum, W. M., & Schiller, P. H. (2004). Microstimulation of V1 delays the execution of visually guided saccades. *European Journal of Neuroscience*, *20*(1), 264–272. https://doi.org/10.1111/j.1460-9568.2004.03480.x

Tehovnik, E. J., Slocum, W. M., Smirnakis, S. M., & Tolias, A. S. (2009). Microstimulation of visual cortex to restore vision. *Progress in Brain Research*, *175*(09), 347–375. https://doi.org/10.1016/S0079-6123(09)17524-6

Thiele, A., Delicato, L. S., Roberts, M. J., & Gieselmann, M. A. (2006). A novel electrode-pipette design for simultaneous recording of extracellular spikes and iontophoretic drug application in awake behaving monkeys. *Journal of Neuroscience Methods*, *158*(2), 207–211. https://doi.org/10.1016/j.jneumeth.2006.05.032

Thiele, A., Pooresmaeili, A., Delicato, L. S., Herrero, J. L., & Roelfsema, P. R. (2009). Additive effects of attention and stimulus contrast in primary visual cortex. *Cerebral Cortex*, *19*(12), 2970–2981. https://doi.org/10.1093/cercor/bhp070

Thomson, A. M. (2010). Neocortical layer 6, a review. *Frontiers in Neuroanatomy*, *4*(MARCH), 1–14. https://doi.org/10.3389/fnana.2010.00013

Towle, V. L., Pham, T., McCaffrey, M., Allen, D., & Troyk, P. R. (2021). Toward the development of a color visual prosthesis. In *Journal of Neural Engineering* (Vol. 18, Issue 2). IOP Publishing Ltd. https://doi.org/10.1088/1741-2552/abd520

Tremblay, S., Acker, L., Afraz, A., Albaugh, D. L., Amita, H., Andrei, A. R., Angelucci, A., Aschner, A., Balan, P. F., Basso, M. A., Benvenuti, G., Bohlen, M. O., Caiola, M. J., Calcedo, R., Cavanaugh, J., Chen, Y., Chen, S., Chernov, M. M., Clark, A. M., … Platt, M. L. (2020). An Open Resource for Non-human Primate Optogenetics. *Neuron*, *108*, 1075–1090.

van Kerkoerle, T., Self, M. W., Dagnino, B., Gariel-Mathis, M.-A., Poort, J., van der Togt, C., & Roelfsema, P. R. (2014). Alpha and gamma oscillations characterize feedback and feedforward processing in monkey visual cortex. *Proceedings of the National Academy of Sciences*, *111*(40), 14332–14341. https://doi.org/10.1073/pnas.1402773111

van Kerkoerle, T., Self, M. W., & Roelfsema, P. R. (2017). Layer-specificity in the effects of attention and working memory on activity in primary visual cortex. *Nature Communications*, *8*, 13804. https://doi.org/10.1038/ncomms13804

van Lier, B., Hierlemann, A., & Knoflach, F. (2018). Parvalbumin expression and gamma oscillation occurrence increase over time in a neurodevelopmental model of NMDA receptor dysfunction. *PeerJ*, *2018*(9). https://doi.org/10.7717/peerj.5543

Veraart, C., Wanet-Defalque, M. C., Gérard, B., Vanlierde, A., & Delbeke, J. (2003). Pattern Recognition with the Optic Nerve Visual Prosthesis. *Artificial Organs*, *27*(11), 996–1004. https://doi.org/10.1046/j.1525-1594.2003.07305.x

Verkhratsky, A., Krishtal, O. A., & Petersen, O. H. (2006). From Galvani to patch clamp: The development of electrophysiology. *Pflugers Archiv European Journal of Physiologydn*, *453*(3), 233–247. https://doi.org/10.1007/s00424-006-0169-z

Vinck, M., Huurdeman, L., Bosman, C. A., Fries, P., Battaglia, F. P., Pennartz, C. M. A., & Tiesinga, P. H. (2015). How to detect the Granger-causal flow direction in the presence of additive noise? *NeuroImage*, *108*, 301–318. https://doi.org/10.1016/j.neuroimage.2014.12.017

Volman, V., Margarita Behrens, M., & Sejnowski, T. J. (2011). Downregulation of parvalbumin at cortical GABA synapses reduces

network gamma oscillatory activity. *Journal of Neuroscience*, *31*(49), 18137–18148. https://doi.org/10.1523/JNEUROSCI.3041-11.2011

Waataja, J. J., Tweden, K. S., & Honda, C. N. (2011). Effects of high-frequency alternating current on axonal conduction through the vagus nerve. *Journal of Neural Engineering*, *8*(5). https://doi.org/10.1088/1741-2560/8/5/056013

Wachtler, T., Sejnowski, T. J., & Albright, T. D. (2003). Representation of Color Stimuli in Awake Macaque Primary Visual Cortex. *Neuron*, *37*, 681–691.

Wagenaar, D. A., & Potter, S. M. (2002). Real-time multi-channel stimulus artifact suppression by local curve fitting. *Journal of Neuroscience Methods*, *120*(2), 113–120. https://doi.org/10.1016/S0165-0270(02)00149-8

Wandell, B. A., Dumoulin, S. O., & Brewer, A. A. (2007). Visual field maps in human cortex. In *Neuron* (Vol. 56, Issue 2, pp. 366–383). https://doi.org/10.1016/j.neuron.2007.10.012

Wang, J., & Dong, J. (2020). Optical waveguides and integrated optical devices for medical diagnosis, health monitoring and light therapies. *Sensors (Switzerland)*, *20*(14), 1–33. https://doi.org/10.3390/s20143981

Wang, J., Zhu, H., Liu, J., Li, H., Han, Y., Zhou, R., & Zhang, Y. (2021). The application of computer vision to visual prosthesis. *Artificial Organs*, *45*(10), 1141–1154. https://doi.org/10.1111/aor.14022

Wang, T., Li, Y., Yang, G., Dai, W., Yang, Y., Han, C., Wang, X., Zhang, Y., & Xing, D. (2020). Laminar Subnetworks of Response Suppression in Macaque Primary Visual Cortex. *Journal of Neuroscience*, *40*(39), 7451–7463. https://doi.org/10.1523/JNEUROSCI.1129-20.2020

Watakabe, A., Ohtsuka, M., Kinoshita, M., Takaji, M., Isa, K., Mizukami, H., Ozawa, K., Isa, T., & Yamamori, T. (2015). Comparative analyses of adeno-associated viral vector serotypes 1, 2, 5, 8 and 9 in marmoset, mouse and macaque cerebral cortex. *Neuroscience Research*, *93*, 144–157. https://doi.org/10.1016/j.neures.2014.09.002

Watakabe, A., Sadakane, O., Hata, K., Ohtsuka, M., Takaji, M., & Yamamori, T. (2017). Application of viral vectors to the study of neural connectivities and neural circuits in the marmoset brain. *Developmental Neurobiology*, *77*(3), 354–372. https://doi.org/10.1002/dneu.22459

Watanabe, H., Sano, H., Chiken, S., Kobayashi, K., Fukata, Y., Fukata, M., Mushiake, H., & Nambu, A. (2020). Forelimb movements evoked by

optogenetic stimulation of the macaque motor cortex. *Nature Communications*, *11*(1), 1–9. https://doi.org/10.1038/s41467-020-16883-5

Williams, J. J., Watson, A. M., Vazquez, A. L., & Schwartz, A. B. (2019). Viral-mediated optogenetic stimulation of peripheral motor nerves in non-human primates. *Frontiers in Genetics*, *10*(JUL), 1–16. https://doi.org/10.3389/fnins.2019.00759

Wilschut, T., & Mathôt, S. (2022). Interactions Between Visual Working Memory, Attention, and Color Categories: A Pupillometry Study. *Journal of Cognition*, *5*(1), 1–12. https://doi.org/10.5334/joc.208

Wójcik, D. K. (2014). Current Source Density (CSD) Analysis. *Encyclopedia of Computational Neuroscience*, 1–10. https://doi.org/10.1007/978-1-4614-7320-6

Wrobel, C., Dieter, A., Huet, A., Keppeler, D., Duque-Afonso, C. J., Vogl, C., Hoch, G., Jeschke, M., & Moser, T. (2018). Optogenetic stimulation of cochlear neurons activates the auditory pathway and restores auditory-driven behavior in deaf adult gerbils. *Science Translational Medicine*, *10*(449), eaao0540. https://doi.org/10.1126/scitranslmed.aao0540

Yagi, T., Watanabe, M., Ohnishi, Y., Okuma, S., & Mukai, T. (2005). Biohybrid retinal implant: Research and development update in 2005. *2nd International IEEE EMBS Conference on Neural Engineering*, *2005*, 248–251. https://doi.org/10.1109/CNE.2005.1419603

Yamagishi, S., & Furukawa, S. (2020). Factors Influencing Saccadic Reaction Time: Effect of Task Modality, Stimulus Saliency, Spatial Congruency of Stimuli, and Pupil Size. *Frontiers in Human Neuroscience*, *14*(November), 1–11. https://doi.org/10.3389/fnhum.2020.571893

Yang, X., Pan, X., Blyth, J., & Lowe, C. R. (2008). Towards the real-time monitoring of glucose in tear fluid: Holographic glucose sensors with reduced interference from lactate and pH. *Biosensors and Bioelectronics*, *23*(6), 899–905. https://doi.org/10.1016/j.bios.2007.09.016

Yona, G., Meitav, N., Kahn, I., & Shoham, S. (2016). Realistic numerical and analytical modeling of light scattering in brain tissue for optogenetic applications. *ENeuro*, *3*(1), 420–424. https://doi.org/10.1523/ENEURO.0059-15.2015

Yu, C., Cassar, I. R., Sambangi, J., & Grill, W. M. (2020). Frequency-specific optogenetic deep brain stimulation of subthalamic nucleus improves parkinsonian motor behaviors. *Journal of Neuroscience*, *40*(22), 4323–4334. https://doi.org/10.1523/JNEUROSCI.3071-19.2020

Yu, J., & Ferster, D. (2010). Membrane Potential Synchrony in Primary Visual Cortex during Sensory Stimulation. *Neuron*, *68*(6), 1187–1201. https://doi.org/10.1016/j.neuron.2010.11.027

Zhang, F., Vierock, J., Yizhar, O., Fenno, L. E., Tsunoda, S., Kianianmomeni, A., Prigge, M., Berndt, A., Cushman, J., Polle, J., Magnuson, J., Hegemann, P., & Deisseroth, K. (2011). The microbial opsin family of optogenetic tools. *Cell*, *147*(7), 1446–1457. https://doi.org/10.1016/j.cell.2011.12.004

Zhang, F., Wang, L.-P., Brauner, M., Liewald, J. F., Kay, K., Watzke, N., Wood, P. G., Bamberg, E., Nagel, G., Gottschalk, A., & Deisseroth, K. (2007). Multimodal fast optical interrogation of neural circuitry. *Nature*, *446*(April), 633–639. https://doi.org/10.1038/nature05744

Zhao, Y., Geng, X., Li, Q., Jiang, G., Gu, Y., & Lv, X. (2017). Recognition of a virtual scene via simulated prosthetic vision. *Frontiers in Bioengineering and Biotechnology*, *5*(OCT). https://doi.org/10.3389/fbioe.2017.00058

Zipser, K., Lamme, V. A. F., & Schiller, P. H. (1996). Contextual modulation in primary visual cortex of macaques. *Journal of Neuroscience*, *16*(22), 7376–7389. https://doi.org/21/5/1698 [pii]

Zrenner, E. (2002). Will retinal implants restore vision? *Science*, *295*(5557), 1022–1025. https://doi.org/10.1126/science.1067996

Zrenner, E., Bartz-Schmidt, K. U., Benav, H., Besch, D., Bruckmann, A., Gabel, V. P., Gekeler, F., Greppmaier, U., Harscher, A., Kibbel, S., Koch, J., Kusnyerik, A., Peters, T., Stingl, K., Sachs, H., Stett, A., Szurma, P., Wilhelm, B., & Wilke, R. (2011). Subretinal electronic chips allow blind patients to read letters and combine them to words. *Proceedings of the Royal Society B: Biological Sciences*, *278*(1711), 1489–1497. https://doi.org/10.1098/rspb.2010.1747